VORTICES IN A BEC WITH DIPOLE-DIPOLE INTERACTION

Züleyha ÖZTAŞ

PhD Dissertation

Physics Program

September-2011

JÜRİ VE ENSTİTÜ ONAYI

Züleyha Öztaş'ın **"Vortices in a BEC with Dipole-Dipole Interaction"** başlıklı **Fizik** Anabilim Dalındaki Doktora Tezi 25.08.2011 tarihinde, aşağıdaki jüri tarafından Anadolu Üniversitesi Lisansüstü Eğitim Öğretim ve Sınav Yönetmeliğinin ilgili maddeleri uyarınca değerlendirilerek kabul edilmiştir.

	Adı-Soyadı	İmza
Üye (Tez Danışmanı)	**:Doç. Dr. CEM YÜCE**	**……**
Üye	**:Doç. Dr. HAKAN CEBECİ**	**……**
Üye	**:Doç. Dr. MURAT LİMONCU**	**……**
Üye	**:Yard. Doç. Dr. A. TOLGA TAŞÇI**	**……**
Üye	**:Yard. Doç. Dr. ABDULKADİR ŞENOL**	**……**

Anadolu Üniversitesi Fen Bilimleri Enstitüsü Yönetim Kurulu'nun …… tarih ve …… sayılı kararıyla onaylanmıştır.

Enstitü Müdürü

ABSTRACT

PhD Dissertation

VORTICES IN A BEC WITH DIPOLE-DIPOLE INTERACTION

Züleyha ÖZTAŞ

Anadolu University
Graduate School of Sciences
Physics Program
Supervisor: Assoc. Prof. Dr. Cem YÜCE
2011, 105 pages

Interparticle interactions have fundamental importance in the study of Bose-Einstein condensate (BEC) of dilute gases. In a dipolar BEC, interaction potential includes both s-wave and dipole-dipole interaction term. Dipolar interactions are radically different from s-wave interaction, and they have remarkable consequences for the physics of nonrotating and rotating condensates.

The rotation of BEC leads to the formation of quantized vortex lines. In this thesis, BEC and vortices in BEC are reviewed. Dipolar BEC with a single vortex state is investigated in the Thomas-Fermi approximation. The effects of dipolar interactions on the rotational angular velocity and shape of a dipolar condensate with an off-axis vortex are reported. Vortex dipoles are studied in the low and high dipolar interaction regimes. The dependence of the critical velocity on the dipolar interaction strength and the vortex separation is examined.

Key Words: Bose-Einstein Condensate, Dipole-Dipole Interaction, Rotating Condensate

ÖZET

Doktora Tezi

DİPOL-DİPOL ETKİLEŞİMLİ BEC'DA GİRDAPLAR

Züleyha ÖZTAŞ

Anadolu Üniversitesi
Fen Bilimleri Enstitüsü
Fizik Anabilim Dalı
Danışman: Doç. Dr. Cem YÜCE
2011, 105 sayfa

Atomlar arası etkileşmeler seyreltik gazlardaki Bose-Einstein yoğuşması (BEC) çalışmalarında temel bir öneme sahiptir. Dipolar bir BEC da, etkileşme potansiyeli s-dalga ve dipole-dipole etkileşme terimlerinin her ikisini de içerir. Dipolar etkileşimler s-dalga etkileşimlerinden oldukça farklıdır ve dönen ve dönmeyen yoğuşmalar üzerinde önemli etkilere sahiptir.

Bose-Einstein yoğuşmasının dönmesi kuantize olmuş girdap çizgilerinin oluşmasına neden olur. Bu tezde, BEC ve BEC'da oluşan girdap yapılar gözden geçirildi. Tek girdaplı dipolar BEC Thomas-Fermi yaklaşımında incelendi. Eksenden ötelenmiş tek girdaba sahip bir dipolar yoğuşmanın dönme açısal hızı ve yoğuşma şekli üzerine dipolar etkileşimlerin etkileri bulundu. Girdap çiftleri düşük ve yüksek dipolar etkileşme bölgelerinde çalışıldı. Kritik hızın dipolar etkileşme kuvvetine ve girdaplar arası uzaklığa bağlılığı incelendi.

Anahtar Sözcükler: Bose-Einstein Yoğuşması, Dipole-Dipole Etkileşme, Dönen Yoğuşma

ACKNOWLEDGEMENTS

I would like to express my thanks to my supervisor Assoc. Prof. Dr. Cem YÜCE for directing me in this study. It is a great honour for me to work with him.

I give my thanks to my family and my friends for supporting me on my all life. I also wish to thank to my husband Engin ÖZTAŞ for his patince, understanding, and endless help.

TABLE OF CONTENTS

LIST OF FIGURES

LIST OF SYMBOLS

λ_T : Thermal wavelength

m : Atomic mass

n : Density of particles

h : Planck constant

p : Momentum

k_B : Boltzmann constant

T : Temperature

Δ : Transition frequency

ω : Frequency

ε_0 : Permitivity of space

τ : Lifetime

B : Magnetic field

μ : Magnetic moment

H : Hamiltonian

N : Number of particles

V : Volume

V_{trap} : Trap potential

$\phi(\mathbf{r})$: Potential

a_{ho} : Harmonic oscillator length

g(ε) : Density of states

G(ε) : Number of states

T_c : Lifetime

ξ : Healing length

g : s-wave interaction strength

a_s : Scattering length

U : Interaction potential

Ψ : Wave fuction

R : Radial size

n_0 : Central density

μ_0 : Permeability of space

q_e : Electronic charge

a_0 : Bohr radius

ε_{dd} : Dipolar interaction strength

Φ_{dd} : Mean-field dipolar potential

κ : Condensate aspect ratio

γ : Trap aspect ratio

Ω : Angular velocity

v : Velocity

S : Phase

A : Area

L : Angular momentum

Ω_C : Critical angular velocity

J : Current density

Φ : Velocity potential

c : Speed of sound

β : Vortex core size

v_c : Critical velocity

I : Impulse

ρ_0 : Vortex position

1.INTRODUCTION

Bose-Einstein condensation (BEC) was first predicted by Einstein in 1924: In a system including particles obeying Bose statistics and whose total number is conserved, there should be a temperature below which a finite fraction of all the particles condense into the same single-particle state. The condensation fraction of the particles in the ground state is macroscopic when the system is cooled below a critical temperature. When Einstein made his predictions, quantum theory was not fully developed, and the differences between bosons and fermions were not revealed. After Einstein, important contributions were made by several scientists such as London, Landau, Bogoliubov, Penrose, Onsager, Feynman, Lee, Yang, and Pitaevskii. The relationship between BEC and superfluidity in liquid helium has been an important issue discussed by London and Landau [1]. Bogoliubov, Griffin and others studies showed that BEC gives the microscopic picture behind Landau's quantum hydrodynamics. BEC also relates to superconductivity due to BEC of Cooper pairs. Thus Bose-Einstein condensation is related with several macroscopic quantum phenomena.

Laser techniques, such as laser cooling and magneto-optical trapping, were developed to cool and trap atoms in the 1980s. This led to the successfull achievement of BEC experimentally. BEC was observed in 1995 experimentally on vapours of rubidium [2], sodium [3], and lithium [4]. In these experiments, the atoms were confined in magnetic traps and cooled downto extremely low temperatures. Carl Wieman, Eric Cornell and Wolfgang Ketterle gained the 2001 Nobel prize for their studies on this area. Since then, BEC has gained the growing interest of both experimentalists and theoreticians. BEC is achieved in vapours of hydrogen [5] in 1998, potassium [6] and metastable helium [7] in 2001, and cesium [8] and ytterbium [9] in 2003. Most BEC experiments have been performed using alkali atoms due to their simple ground state electronic structure. For alkali atoms, all electrons except one occupy closed shells and the remaining electron is in an s orbital in a higher shell. The optical transitions of these atoms can be excited by available lasers and the internal energy-level structure is favorable for cooling to very low temperatures. To reach temperatures and densities to observe BEC, laser and evaporative cooling techniques are used

together [10]. The atoms are expanded by switching off the confining trap and the condensate is imaged with optical methods. A sharp peak in the velocity distribution below a certain critical temperature is observed. It is a clear signature for BEC.

2. BOSE EINSTEIN CONDENSATE

Bose-Einstein condensation is based on the indistinguishability and wave nature of particles. Consider a uniform gas of particles with mass m and number density n. The mean thermal energy of the gas is $k_B T \approx p^2/2m$. The well known relation $\lambda_T \sim h/p$ gives the mean thermal wavelength

$$\lambda_T = \left(\frac{h^2}{2\pi m k_B T} \right)^{\frac{1}{2}} \tag{2.1}$$

where T is the temperature. In the classical limit (high temperatures, short wavelengths), the thermal de Broglie wavelength is small compared to $n^{-1/3}$. Hence quantum effects are negligible in this regime. It is convenient to define the dimensionless parameter $n\lambda^3$, which is phase-space density. This parameter is small in the classical limit since $\lambda_T \to 0$ when $T \to \infty$. When atoms are cooled downto the temperature where λ_T is comparable to the interatomic separation $n^{-1/3}$, the atomic wavepackets begins to overlap and the indistinguishability of particles becomes important. This temperature is called the critical temperature T_C, which is the onset of BEC. In an ideal gas, all particles occupy the single-particle ground state at T =0 K. The density of the condensed gas is of the order of n ~10^{13}-10^{14} cm^{-3}. The corresponding critical temperature given by the relation $k_B T_c \approx \hbar^2 n^{2/3}/m$ is approximately 10^{-6} K. The typical particle number of BEC is between 10^4 -10^7.

2.1. Trapping and Cooling of Atoms

There are several steps in the condensation of atoms experimentally. The first step is laser cooling which is achieved by three pairs of laser beams along six directions – front and back, left and right, up and down. Subsequently the lasers are turned off and the atoms are confined by a magnetic trap described typically by a harmonic potential. In this stage, the temperature is approximately 100 μK, with 10^9 atoms. In this trap, the atoms are trapped by the Zeeman interaction of

the electron spin with an inhomogeneous magnetic field. If the complications caused by the nuclear spin is neglected, an atom with its electron spins parallel to the magnetic field are attracted to the minimum of the magnetic field (low-field seeking state), while ones with electron spin antiparallel are repelled (high-field seeking state). Laser cooling alone is not enough to produce sufficiently high densities and low temperatures for condensation. The cloud of atoms is cooled further by evaporative cooling which is similar to blowing on coffee to cool it. It allows the removal of more energetic atoms, therefore the cloud gets further cooling. At the end of this step, the final temperature is of the order of 100 nK and about 10^4-10^7 atoms remain.

2.1.1 Laser Created Potentials

Atoms in a laser field experience a force because of the interaction of the laser field with the electric dipole moment induced in the atoms. The force on atoms in a laser field is used by different ways in BEC experiments. The detuning of the transition frequency between ground and excited states is given by [11, 12]

$$\Delta \equiv \hbar\omega_{las} - \left(E_e - E_g\right) \tag{2.2}$$

It is also convenient to define the saturation intensity I_0 , since the force also depends on the intensity. It is given by

$$I_0 = \varepsilon_0 c\Gamma^2 / d^2 \tag{2.3}$$

where ε_0 is the dielectric constant, c the speed of light, d an appropriately defined dipole matrix element for the transition in question, and $\Gamma \equiv \hbar/\tau$ with the lifetime of the excited state τ [11, 12]. A value of I_0 is typically of order 100 W/m^2. The change in energy of the atom in the laser field is, in the limit $\Gamma << \Delta$

$$\Delta E_{laser}(\mathbf{r}) = \left(\frac{I(\mathbf{r})}{I_0} \right) \frac{\Gamma^2}{\Delta} \tag{2.4}$$

Provided $<< (\Delta/\Gamma)^2$, I/I_0 can be larger than 1. A region of high laser intensity supplies an attractive potential for $\Delta < 0$ (''red detuning'') and a repulsive potential for $\Delta > 0$ (''blue detuning''). A red-detuned potential is used as an optical trap. A blue-detuned potential creates a potential barrier. This barrier separates a condensate and an impurity potential. The interference pattern created by counter-propagating laser beams is called an optical lattice giving a periodic potential for atoms.

2.1.2. Magnetic traps

Magnetic field configurations with either a local minimum in the magnitude of the magnetic field, or a local maximum is constructed by a magnetic trap. Various techniques can be used to provide a local minimum. The most widely used methods are *Time-Orbiting Potential* (TOP) and *Ioffe-Pritchard* traps [12]. Magnetic traps used in BEC experiments have axial symmetry and a finite offset field. With an appropriate choice of cylindrical polar coordinate system the *magnitude* of the field has the form [11]

$$|B(\mathbf{r})| = B_0 + \frac{1}{2}\alpha\rho^2 + \frac{1}{2}\beta z^2 \tag{2.5}$$

Magnetic trapping of neutral atoms occurs because of the Zeeman effect. The energy of an atomic state is dependent on the magnetic field. Thus, an atom in an inhomogeneous field experiences a spatially-varying potential. For simplicity, the energy of a state can be assumed linear in the magnetic field. This is true generally for the doubly polarized states. For other states it is a good approximation when the level shifts produced by the magnetic field are either very small or very large compared with the hyperfine splitting. Thus the energy of an atom in a particular state *i* may be written as [13]

$$E_i = C_i - \mu_i B \tag{2.6}$$

where μ_i is the magnetic moment of the state and C_i is a constant. Potential energy $-\mu_i B$ is the contribution to the energy of atom. If the magnetic moment is positive, the atom experiences a force driving it to higher field regions. If it is negative, the force is towards lower field regions. Therefore, states with a positive magnetic moment are called as *high-field seekers*, and those with a negative magnetic moment as *low-field seekers*.

2.1.3. Hyperfine state

An atomic BEC have internal degrees of freedom due to the hyperfine spin of atoms. A hyperfine-Zeeman sublevel of an atom with total electronic angular momentum **J** and nuclear spin **I** may be labeled by the projection m_F of total atomic spin **F = I + J** on the axis of the field **B**. The value of total **F** can take a value between |I − J| to |I + J|. Therefore, the hyperfine coupling is much larger than the typical temperature of an ultra-cold atomic system. The hyperfine state is shown by $|F, m_F\rangle$ with $m_F = -F, -F+1, \cdots, F-1, F$.

Experiments on BEC have been made typically with states having total electronic spin 1⁄2, and most of them have been made with states having nuclear spin I = 3⁄2 (^{87}Rb, ^{23}Na, and ^{7}Li). Successful experiments with hydrogen (I = 1⁄2) and ^{85}Rb atoms (I = 5⁄2) have also been carried out. In the ground-state electronic structure of alkali atoms, one electron is in an s orbital in a higher shell while other electrons occupy closed shells. The nuclear and electronic spins are coupled by the hyperfine interaction. Since the electrons have no orbital angular momentum (L = 0), no magnetic field produce at the nucleus. Therefore, the coupling arises only due to the magnetic field produced by the electronic spin. When there is no external magnetic field the atomic levels are split by the hyperfine interaction. The coupling is represented by a term H_{hf} in the Hamiltonian of the form

$$H_{hf} = A\mathbf{I}.\mathbf{J} \tag{2.7}$$

where A is a constant.

The internal sublevels of the atom can couple when an external field is applied. To take into account the effect of this field on the energy levels the Zeeman energies are added to Eq.(2.7). Zeeman energies arises from the interaction of the magnetic moments of the electron and the nucleus with the magnetic field. Taken the magnetic field **B** in the z direction, the total Hamiltonian is thus

$$H_{spin} = A\mathbf{I}.\mathbf{J} + CJ_z + DI_z \tag{2.8}$$

The constants C and D are given by [13]

$$C = g\mu_B B \tag{2.9}$$

and

$$D = -\frac{\mu}{I} B \tag{2.10}$$

In writing Eq. (2.9) it is assumed that the electronic orbital angular momentum L is zero and its spin S is 1/2. Generally, D maybe neglected because $|C/D| \sim m_p/m_e \approx 2000$. g factor of the electron maybe put equal to 2.

2.1.4. Detection

After BEC has been created, time-of-flight (TOF) or in situ techniques can be used to probe its properties. The TOF technique is more often used in vortex experiments. In the TOF technique the magnetic or optical field is switched off at time t = 0 and an image of the BEC is taken a few milliseconds later. When the trap is switched off the sample begins to expand. Then the sample is imaged with optical methods such as a CCD camera.

2.1.5 Evaporative cooling

The temperatures reached by laser cooling are not low enough to produce BEC. The technique of evaporative cooling is employed to achieve a further decrease in the temperature of the gas. In this technique atoms with an energy higher than the average energy of particles in the system are removed. If one makes a hole near high sides of the trap, atoms with an energy at least equal to the trap energy at the hole can escape. In practice one can make such a hole by applying radio-frequency (rf) radiation. The radio-frequency magnetic field changes the electronic spin state of an atom from a low-field seeking one to a high-field seeking one.

2.2 Ideal Bose Gas

The ideal Bose gas is an ideal Boltzmann gas at high temperatures and low densities. Thus, the largest deviations in thermodynamic properties occur if the condition

$$n\lambda_T{}^3 = \frac{N}{V}\left(\frac{h^2}{2\pi m k_B T}\right)^{\frac{3}{2}} << 1 \qquad (2.11)$$

is no longer satisfied. $n\lambda^3$ must not become too large in real systems, since the interactions are not negligible. Therefore, the ideal Bose gas is a model system which can only approximately describe real systems.

For an ideal Bose gas in thermodynamic equilibrium at temperature T, the mean occupation number of the vth state is given by the Bose distribution

$$f(\varepsilon_v) = \frac{1}{e^{(\varepsilon_v-\mu)/k_B T} - 1} \qquad (2.12)$$

where ε_v is the energy of the single-particle state for the particular trapping potential. Since the number of particles is conserved, the chemical potential μ which is determined as a function of N and T enters the distribution function

(2.12). The mean total number of particles and the mean total energy are given by [14, 15]

$$N(T,\mu)=\sum_{v} f(\varepsilon_v) \tag{2.13}$$

$$E(T,\mu)=\sum_{v} \varepsilon_v f(\varepsilon_v) \tag{2.14}$$

For $(\varepsilon_v-\mu)/k_BT\to 0$, the mean occupation number N becomes divergent. Since this case is unphysical, the chemical potential of the system has to be smaller than the ground state energy of the single particle Hamiltonian with the potential V_{trap}.

2.2.1 Ideal Bose Gas in a Harmonic Trap

An important property characterizing the magnetic traps is that the confining potential can be approximated with the quadratic form

$$V_{trap}(\mathbf{r})=\frac{1}{2}\left(\omega_x^2x^2+\omega_y^2y^2+\omega_z^2z^2\right) \tag{2.15}$$

where ω_x, ω_y and ω_z are trap frequencies. This potential refers to a harmonic trap. Neglecting interatomic interactions, the many-body Hamiltonian is the sum of single-particle Hamiltonians whose eigenvalues are

$$\varepsilon(n_x,n_y,n_z)=\left(n_x+\frac{1}{2}\right)\hbar\omega_x+\left(n_y+\frac{1}{2}\right)\hbar\omega_y+\left(n_z+\frac{1}{2}\right)\hbar\omega_z \tag{2.16}$$

Here the numbers n_i assume all integers greater than or equal to zero. The ground state $\Psi(\mathbf{r_1},...\mathbf{r_N})$ of non-interacting bosons confined by the trap potential is obtained by putting all the particles into the lowest single particle state

$$\Psi(\mathbf{r_1},...\mathbf{r_N}) = \prod_i \varphi_0(\mathbf{r}_i) \tag{2.17}$$

where

$$\varphi_0(\mathbf{r}) = \left(\frac{m\omega_{ho}}{\pi\hbar}\right)^{3/4} \exp\left[-\frac{m}{2\hbar}\left(\omega_x x^2 + \omega_y y^2 + \omega_z z^2\right)\right] \tag{2.18}$$

and ω_{ho} is the geometric average of the oscillator frequencies given by

$$\omega_{ho} = \left(\omega_x \omega_y \omega_z\right)^{1/3} \tag{2.19}$$

The density distribution becomes $n(\mathbf{r}) = N|\varphi_0(\mathbf{r})|^2$. The size of the cloud does not depend on N and is characterised by the harmonic oscillator length:

$$a_{ho} = \sqrt{\frac{\hbar}{m\omega_{ho}}} \tag{2.20}$$

This length is also the average width of the Gaussian given by Eq. (2.18). The harmonic oscillator length is typically of the order of $1\,\mu m$ in experiments. At finite temperature some atoms occupy the ground state while other atoms are thermally distributed in the excited states. The size of the thermal cloud is larger than the harmonic oscillator length.

Assuming that the level spacing becomes smaller and smaller when $N \to \infty$, the summation in Eq.(2.13)-(2.14) can be replaced by an integral and the density of states is used. For energies large compared with $\hbar\omega_i$, n_i may be taken as continuous variables and the zero-point motion can be neglected. A coordinate system defined by three variables $\varepsilon_i = \hbar\omega_i n_i$ can be used to find density of states. In terms of these variables, a surface of constant energy (2.16) is the plane $\varepsilon = \varepsilon_1 + \varepsilon_2 + \varepsilon_3$ [13]. The number of states $G(\varepsilon)$ is proportional to the volume in the first octant bounded by this plane [13]

$$G(\varepsilon)=\frac{1}{\hbar^3\omega_x\omega_y\omega_z}\int_0^{\varepsilon}d\varepsilon_1\int_0^{\varepsilon-\varepsilon_1}d\varepsilon_2\int_0^{\varepsilon-\varepsilon_1-\varepsilon_2}d\varepsilon_3=\frac{\varepsilon^3}{6\hbar^3\omega_x\omega_y\omega_z} \tag{2.21}$$

The density of the states can be found by using the relation $g(\varepsilon)=dG(\varepsilon)/d\varepsilon$

$$g(\varepsilon)=\frac{\varepsilon^2}{2\hbar^3\omega_x\omega_y\omega_z} \tag{2.22}$$

The density of states generally changes with the power of the energy [13]

$$g(\varepsilon)=C_\alpha\varepsilon^{\alpha-1} \tag{2.23}$$

where C_α is a constant. The coefficient for a three-dimensional harmonic-oscillator potential with $\alpha=3$ is [13]

$$C_3=\frac{1}{2\hbar^3\omega_x\omega_y\omega_z} \tag{2.24}$$

2.2.2 The Critical Temperature

Below a given temperature the population of the lowest state becomes macroscopic. It corresponds to the onset of Bose-Einstein condensation. To calculate this critical temperature, the condensate fraction, and the other thermodynamic quantities, one can start from Eqs. (2.13) and (2.14). If the number of particles is sufficiently large, the zero-point energy in Eq.(2.16) can be neglected. Therefore, the lowest energy ε_0 is equal to zero. The number of particles in excited states is given by

$$N_{ex}=\int_0^{\infty}d\varepsilon g(\varepsilon)f(\varepsilon) \tag{2.25}$$

The number of particles has its greatest value for $\mu = 0$, and the transition temperature T_c is determined by the condition that the total number of particles can be accommodated in excited states, that is

$$N = N_{ex}(T_c, \mu = 0) = \int_0^\infty d\varepsilon g(\varepsilon) \frac{1}{e^{\varepsilon/kT_c} - 1} \tag{2.26}$$

Eq. (2.26) can be rewritten using dimensionless variable $x = \varepsilon / kT_c$

$$N = C_\alpha (kT_c)^\alpha \int_0^\infty dx \frac{x^{\alpha-1}}{e^x - 1} = C_\alpha \Gamma(\alpha)\zeta(\alpha)(kT_c)^\alpha \tag{2.27}$$

where $\Gamma(\alpha)$ is the gamma function and $\zeta(\alpha) = \sum_{n=1}^{\infty} n^{-\alpha}$ is the Riemann zeta function. In Eq. (2.27), the integrand is expanded in powers of e^{-x}, and the integral $\int_0^\infty dx x^{\alpha-1} e^{-x} = \Gamma(\alpha)$ is used. The result is

$$\int_0^\infty dx \frac{x^{\alpha-1}}{e^x - 1} = \Gamma(\alpha)\zeta(\alpha) \tag{2.28}$$

From Eq.(2.27) it is found that

$$N = (kT_c)^3 [C_\alpha \Gamma(\alpha)\zeta(\alpha)] \tag{2.29}$$

Therefore, the transition temperature for Bose-Einstein condensation is obtained as ($\alpha = 3$)

$$kT_c = \hbar\omega_{ho} \left(\frac{N}{\zeta(3)} \right)^{1/3} \approx 0.94 \hbar\omega_{ho} N^{1/3} \tag{2.30}$$

where Riemann zeta function is $\zeta(3) \approx 1.212$. For temperatures higher than T_c the chemical potential is less than the energy of the lowest state and becomes N dependent. The result (2.30) maybe written in the useful form [13]

$$T_c \approx 4.5\left(\frac{\bar{f}}{100Hz}\right)N^{1/3} \text{ nK} \tag{2.31}$$

where $\bar{f} = \omega_{ho}/2\pi$.

The existence of BEC in an harmonic oscillator potential is a result of the assumption that the separation of single-particle energy levels is much less than kT. For an isotropic harmonic oscillator with frequencies $\omega_x = \omega_y = \omega_z = \omega_0$, the energy quantum $\hbar\omega_0$ should be much less than kT_c. It means the condition is $N^{1/3} >> 1$ according to Eq.(2.30). Considering the finiteness of the particle number, the transition becomes smooth. N typically changes from 10^4-10^6 in the system, so the transition temperature is 20 to 200 times larger than $\hbar\omega_0$. The frequency $\omega_{ho}/2\pi$ is between typically from tens to hundreds of Hertz. Thus, $\hbar\omega_0$ of the order of a few nK. [13, 16]

2.2.3 Condensate fraction

Below the transition temperature, the number N_{ex} of particles in excited states is given by Eq. (2.25) with $\mu = 0$,

$$N_{ex}(T) = \int_0^\infty d\varepsilon g(\varepsilon)\frac{1}{e^{\varepsilon/kT_c} - 1} = C_\alpha \int_0^\infty d\varepsilon \varepsilon^{\alpha-1}\frac{1}{e^{\varepsilon/kT} - 1} \tag{2.32}$$

For $\alpha > 1$, Eq. (2.29) may be used to find the result

$$N_{ex} = C_\alpha \Gamma(\alpha)\zeta(\alpha)(kT)^\alpha \tag{2.33}$$

This result does not depend on the total number of particles. Using Eq. (2.30) for T_c, the number of excited states in a three-dimensional harmonic-oscillator potential is found as

$$N_{ex} = N\left(\frac{T}{T_c}\right)^3 \tag{2.34}$$

The number of condensated particle N_0 equals the total number of particles N minus the number of particles N_{ex} in excited states:

$$N_0(T) = N - N_{ex}(T) \tag{2.35}$$

or

$$N_0 = N\left(1 - \left(\frac{T}{T_c}\right)^3\right) \tag{2.36}$$

2.3 Effects of Interparticle Interactions

Interparticle interactions have fundamental importance in the study of BEC of dilute gases. At very low temperatures the de Broglie wavelengths of the atoms are very large compared to the range of the interatomic potential. The density and energy of the atoms are so low that they are usually away from each other. Thus, interatomic interactions are effectively weak and dominated by *s*-wave scattering. One can only consider binary collisions in the theoretical model neglecting three-body processes. The scattering is characterised by the *s*-wave scattering length, a_s. The sign of the scattering length depends on the details of the interatomic potential, it is higher than zero for repulsive interactions while smaller than zero for attractive interactions. With the conditions above, the interaction potential can be approximated by

$$U = g\delta(\mathbf{r} - \mathbf{r}') \tag{2.37}$$

where g is the interaction strength given by $g = 4\pi\hbar^2 a_s / m$, and $\mathbf{r}$ and $\mathbf{r}'$ are the positions of the two particles, m is atomic mass.

2.3.1 The Gross–Pitaevskii equation

In a BEC with weakly-interacting atoms, almost all the atoms occupy the same quantum state and the condensate may be described very well in terms of mean-field theory. To determine the energy of many-body states, a Hartree or mean-field approach is used. The wave function is a symmetrized product of single-particle wave functions in these approaches. All bosons occupy the same single-particle state, $\phi(\mathbf{r})$, in a completely condensed state. Thus. the wave function of the N particle system can be written as

$$\Psi(\mathbf{r_1}, \mathbf{r_2}, ..., \mathbf{r}_N) = \prod_{i=1}^{N} \phi(\mathbf{r}_i) \tag{2.38}$$

The single-particle wave function $\phi(\mathbf{r}_i)$ is normalized as

$$\int d\mathbf{r} |\phi(\mathbf{r})|^2 = 1 \tag{2.39}$$

The effective Hamiltonian of the system maybe written

$$H = \sum_{i=1}^{N} \left[\frac{\mathbf{p}_i^2}{2m} + V(\mathbf{r}_i) \right] + g \sum_{i<j} \delta(\mathbf{r_i} - \mathbf{r_j}) \tag{2.40}$$

$V(\mathbf{r})$ being the external potential. The Hamiltonian of the system of weakly interacting bosons confined in a trap potential is

$$E = N \int d\mathbf{r} \left[\frac{\hbar^2}{2m} |\nabla \phi(\mathbf{r})|^2 + V_{trap}(\mathbf{r}) |\phi(\mathbf{r})|^2 + \frac{(N-1)}{2} g |\phi(\mathbf{r})|^4 \right] \tag{2.41}$$

The first term in the integral Eq (2.41) is the kinetic energy of the condensate, E_{kin} , the second is the harmonic oscillator energy, E_{trap} , while the last one is the mean field interaction energy, E_{int} .

Considering a uniform Bose gas, the interaction energy of an atom pair is g/V . The energy of a state with N bosons all in the same state is given by

$$E = \frac{N(N-1)}{2V} g \approx \frac{1}{2} V n^2 g \tag{2.42}$$

where $n = N/V$, and $N(N-1)/2$ is the number of possible ways of making pairs of bosons. It is assumed that $N >> 1$ in the last expression. The wave function of the condensed state is related with particle number N ,

$$\psi(\mathbf{r}) = N^{1/2} \phi(\mathbf{r}) \tag{2.43}$$

The density of particles is given by

$$n(\mathbf{r}) = |\psi(\mathbf{r})|^2 \tag{2.44}$$

Neglecting the terms which are of order $1/N$, the energy of the system may be written as

$$E(\psi) = \int d\mathbf{r} \left[\frac{\hbar^2}{2m} |\nabla \psi(\mathbf{r})|^2 + V_{trap}(\mathbf{r}) |\psi(\mathbf{r})|^2 + \frac{1}{2} g |\psi(\mathbf{r})|^4 \right] \tag{2.45}$$

In the limit of a nearly ideal Bose gas at $T = 0$ K, the spatial form of the condensate wave function $\psi(\mathbf{r})$ follows by minimizing the total energy E , with the constraint that the total number of particles N is conserved

$$N = \int d\mathbf{r} |\psi(\mathbf{r})|^2 \tag{2.46}$$

The constraint is conveniently determined by the method of Lagrange multipliers. One can write $\delta E - \mu \delta N = 0$, where the chemical potential μ is the Lagrange multiplier. The chemical potential ensures constancy of the particle number and the variations of ψ and ψ^* may thus be taken to be arbitrary. This is equivalent to minimizing the quantity $E - \mu N$ at fixed μ [17]. By equating to zero, the variation of $E - \mu N$ with respect to $\psi^*(\mathbf{r})$ gives the time-independent Gross–Pitaevskii equation

$$-\frac{\hbar^2}{2m}\nabla^2\psi(\mathbf{r}) + V_{trap}(\mathbf{r})\psi(\mathbf{r}) + g|\psi(\mathbf{r})|^2\psi(\mathbf{r}) = \mu\psi(\mathbf{r}) \qquad (2.47)$$

GP equation is essentially a nonlinear Schrödinger equation that includes a nonlinear term $g|\psi(\mathbf{r})|^2$. For non-interacting particles all in the same state the chemical potential is equal to the energy per particle, but for interacting particles the situation is different.

The validity of GP equation is based on the condition that a_s be much smaller than the average distance between atoms and that the number of atoms in the condensate be much larger than 1. The GP equation can be used, at low temperature, to explore the macroscopic behavior of the system. The dimensionless parameter controlling the validity of the dilute-gas approximation is $\bar{n}|a_s|^3$. The scattering length for the atomic species used in the experiments, for example, are $a_s = 2.75$ nm for ^{23}Na [17], and $a_s = -1.45$ nm for ^{7}Li [18]. Typical values of density range are between 10^{13} to 10^{15} cm^{-3}, so that $\bar{n}|a_s|^3$ is always less than 10^{-3}.

2.3.2 The ground state for trapped bosons

If the atoms in BEC are interacting, the shape of the condensate can change significantly with respect to the Gaussian. The central density is lowered (raised) by a repulsive (attractive) interaction and the radius of the atomic cloud

consequently increases (decreases). This affects both the structure of the ground state and the dynamics and thermodynamics of the system [16].

Neglecting the anisotropy of the trap potential, consider the potential which has the form $V = m\omega_0^2 r^2/2$. If the size the cloud is $\sim R$, the potential energy of a particle confined in the trap is $\sim m\omega_0^2 R^2/2$. A typical particle density is $n \approx N/R^3$, and the interaction energy of is of order $ng \approx gN/R^3$. The effect of an additional contribution to the energy varying as R^{-3} shifts the minimum of the total energy to larger values of R for repulsive interactions. Therefore, for increasing values of Na_s, the kinetic energy term becomes less important. The equilibrium size is found by minimizing the sum of the potential and interaction energies. By equating the two energies, the equilibrium radius is found as [13]

$$R \sim a_{ho}\left(\frac{Na_s}{a_{ho}}\right)^{1/5} \tag{2.48}$$

and the energy per particle is

$$\frac{E}{N} \sim \hbar\omega_0\left(\frac{Na_s}{a_{ho}}\right)^{2/5} \tag{2.49}$$

When $\bar{n}|a_s|^3 << 1$ the system is said to be dilute or weakly interacting, but the smallness of this parameter does not imply necessarily that the interaction effects are small. Interaction and kinetic energies have to be compared. The ratio Na_s/a_{ho} in Eq. (2.49) is a dimensionless measure of the strength of the interaction. This ratio is much larger than unity in most experiments (with repulsive interactions) . Hence, the radius R is somewhat larger than a_{ho}. In equilibrium, the trap and interaction energies are both proportional to R^2 while the kinetic energy varies with R^{-2}. Therefore the ratio between the kinetic energy, and the potential or interaction energy is proportional to $(a_{ho}/Na_s)^{4/5}$. It

means that the kinetic energy can be neglected for clouds containing a sufficiently large number of particles.

If interatomic forces are attractive ($a_s < 0$), the gas tends to increase its density in the center of the trap in order to lower the interaction energy. The zero-point kinetic energy balance the interaction energy and stabilize the system. When the central density grows too much, the kinetic energy is no longer able to stabilize the system, and the system undergoes to the collapse. The collapse occurs when the number of particles in the condensate exceeds a critical value N_{cr} , wich is of the order of $a_{ho}/|a_s|$ [16].

The balance between the kinetic and the interaction energies of the condensate fixes a typical length scale which is called the healing length ξ . This is the minimum distance over which the order parameter can heal. If the condensate density grows from 0 to *n* within a distance ξ , the kinetic and the interaction energies are $\sim \hbar^2/(2m\xi^2)$ and $\sim 4\pi\hbar^2 a_s n/m$, respectively. The expression for the healing length found by equating these energies is

$$\xi = (8\pi n a_s)^{-1/2} \tag{2.50}$$

In a trapped BEC, the central density, or the average density, can be used to get an order of magnitude of the healing length [16].

Direct integration of the GP equation gives a useful expression for the chemical potential

$$\mu = (E_{kin} + E_{trap} + 2E_{sw})/N \tag{2.51}$$

in terms of the different contributions to the energy. Using the virial theorem yields the relation

$$\langle p_x^2 \rangle / 2m - (m/2)\omega_x \langle x^2 \rangle + \frac{1}{2} E_{sw} = 0 \tag{2.52}$$

and similarly for y and z. Summing over three dimensions yields [13, 16]

$$2E_{kin} - 2E_{trap} + 3E_{sw} = 0 \tag{2.53}$$

These results are exact within Gross-Pitaevskii theory.

2.3.3 The Thomas–Fermi approximation

As mentioned in the previous subsection dimensionless parameter Na_s/a_{ho} characterizes the importance of the interaction in a trapped condensate. In the usual situation with the particle number $N \approx 10^6$, the scattering length is of order of a few nm, and harmonic oscillator length is of order of a few μm. Thus, the dimensionless parameter Na_s/a_{ho} is large in this case, and the resulting regime is known as the Thomas-Fermi (TF) limit. In TF limit, the repulsive interactions dominate and expand the cloud to a mean radius R that greatly exceeds the mean oscillator length approximately by a factor of 10. The radial gradient of the density is decreased due to this expansion, and the related kinetic energy becomes negligible compared with the trap and the interaction energies. From Eq. (2.47) one finds

$$\left[V(\mathbf{r}) + g|\psi(\mathbf{r})|^2\right]\psi(\mathbf{r}) = \mu\psi(\mathbf{r}) \tag{2.54}$$

where μ is the chemical potential. This equation can be solved directly for the equilibrium density

$$n(\mathbf{r}) = |\psi(\mathbf{r})|^2 = \left[\mu - V_{trap}(\mathbf{r})\right]/g \tag{2.55}$$

in the region where the right hand side is positive, while $\psi = 0$ outside this region. The boundary of the cloud is therefore given by

$$V_{trap}(\mathbf{r}) = \mu \tag{2.56}$$

The physical meaning of this approximation is that the energy to add a particle at any point in the cloud is the same every point. Eq.(2.55) yields a simple expression for the case of a quadratic harmonic trap

$$n(r) = n_0\left(1 - \frac{x^2}{R_x^2} - \frac{y^2}{R_y^2} - \frac{z^2}{R_z^2}\right) \tag{2.57}$$

Here $n_0 = \mu/g$ is the central density and $R_j^2 = 2\mu/m\omega_j^2$ are the squared condensate lengths in the three dimensions. This density has a parabolic form and fills the interior of an ellipsoid. From the normalization condition one can find $N = 8\pi n_0 R_0^3/15$, where $R_0^3 = R_x R_y R_z$ depends on the chemical potential μ. After some calculations the central density is valculated as $n_0 = \mu/g = R_0^2/8\pi a_s a_{ho}^4$. A combination of these results gives an important relation

$$\frac{R_0^5}{a_{ho}^5} = 15\frac{Na_s}{a_{ho}} \tag{2.58}$$

which is large in TF limit. Correspondingly, the TF chemical potential becomes

$$\mu_{TF} = \frac{1}{2}m\omega_0^2 R_0^2 = \frac{1}{2}\hbar\omega_0 \frac{R_0^2}{a_{ho}^2} \tag{2.59}$$

so that $\mu_{TF} >> \hbar\omega_0$ in the TF limit. The chemical potential depends on $N^{2/5}$. From the thermodynamic relation $\mu = \partial E/\partial N$, the TF energy for a trapped condensate reads

$$E_{TF} = \frac{5}{7}\mu_{TF} N \tag{2.60}$$

It is also common to use the central density n_0 to define the healing length in a non-uniform trapped condensate, which gives

$$\xi^2 = \frac{1}{8\pi a_s n_0} \tag{2.61}$$

Inserting n_0 in the above equation gives an important result

$$\frac{\xi}{a_{ho}} = \frac{a_{ho}}{R_0} \tag{2.62}$$

Thus the TF oscillator length a_{ho} is the geometric mean of ξ and R_0, and Eq. (2.62) then yields a clear separation of TF length scales, with $\xi << a_{ho} << R_0$.

3. DIPOLAR BOSE EINSTEIN CONDENSATION

Significant experimental progress was made in recent years in the cooling and trapping of dipolar atoms. BEC of chromium atoms was achieved in 2004 [19]. Chromium atoms possess a large magnetic moment. Thus the effects of dipolar interactions can be observed in the BEC of chromium atoms. The relative contribution of the dipolar interaction can be also made larger compared with s-wave interaction using Feshbach resonance. Chromium atoms have an extraordinarily large magnetic moment of $6\mu_B$. Since the dipolar interaction scales with the square of the magnetic moment, dipolar interaction between two chromium atoms is a factor of 36 higher than in alkali BECs. The large magnetic moment is due to the unique electronic structure. While the alkali atoms have a simple electronic configuration with only one valence electron, chromium has six valence electrons. An extraordinary large magnetic moment is not always of advantage. The dipole–dipole interaction induces new loss mechanisms. The probability of inelastic collisions due to dipolar relaxation [20] leads to very large loss rates of magnetically trapped chromium atoms. This excessive dipolar relaxation rate causes standard condensation techniques to fail in a magnetic trap.

Dipolar interactions introduce new physical effects on BEC since they are radically different from the contact interaction. The applied magnetic field is expected to align the magnetic dipoles of the atoms in BEC and the dipolar interactions lead to an anisotropic change of the shape of the gas. This effect may be considered as dipole-dipole induced magnetostriction. The stability of the condensate is significantly modified by the presence of dipolar interactions. In particular, a dipolar BEC is unstable in a spatially homogeneous case like a condensate with $a_s < 0$. Such a condensate can be stabilized by confinement in a trap. Modifications of the groundstate wavefunction [21, 22] and the stability criteria of dipolar condensates in different trap geometries were studied [21, 23, 24].

Dipolar BECs are also discussed in the context of spinor condensates [25, 26]. Large spin and magnetic moment together lead to interesting new effects such as the conversion of spin into angular momentum [27]. The influence of

dipolar interactions on the formation of vortex lattices in rotating dipolar BECs has been studied [28, 29]. The existence of 2D solitons is expected when the dipolar interaction is strong enough. Tuning of the dipolar interactions is possible by spinning the quantization axis of the atomic dipoles [30] together with the Feshbach tuning of the contact interaction. All effects of dipolar and nondipolar cases can be investigated by these adjustments. The various physical effects that are predicted for dipolar BEC and the growing number of theoretical work on these effects make dipolar quantum gases one of the most exciting fields of atom optics.

3.1. Dipolar Interaction

Atoms or molecules having a permanent dipole moment (either magnetic or electric) interact via dipolar interaction beside short-range interaction [31]. For two particles with dipole moments along the unit vectors $\mathbf{e_1}$ and $\mathbf{e_2}$, and with relative position r (Fig.3.1), the energy due to the dipole-dipole interaction is [32]

$$U_{dd}(\mathbf{r}) = \frac{C_{dd}}{4\pi}\frac{(\mathbf{e_1}.\mathbf{e_2})r^2 - 3(\mathbf{e_1}.\mathbf{r})(\mathbf{e_2}.\mathbf{r})}{r^5} \tag{3.1}$$

where the coupling constant C_{dd} is equal to $\mu_0\mu^2$ for particles having a permanent magnetic dipole moment μ, where μ_0 is the permeability of vacuum, and d^2/ε_0 for particles having a permanent electric dipole moment d, where ε_0 is the permittivity of vacuum. For a polarized gas where all dipoles are directed in the z direction (Fig.3.1), this expression gives

$$U_{dd}(\mathbf{r}) = \frac{C_{dd}}{4\pi}\frac{1-3\cos 2\theta}{r^3} \tag{3.2}$$

where θ is the angle between the direction of polarization and the relative position of the particles. From Eq.(3.1) and Eq.(3.2), two main properties of the dipole-dipole interaction is understood. First of them is the long range character of interaction. Contrast to short-range character of the contact interaction, dipolar

interaction is long-range. In systems with short-range interactions, the energy is extensive in the thermodynamic limit. On the contrary, in a system of particles interacting by long-range interactions, the energy per particle both depend on the density and the total number of particles. The necessary condition for obtaining an extensive energy is that the integral of the interaction potential $U(\mathbf{r})$

$$U(\mathbf{r}) = \int_{r_0}^{\infty} U(\mathbf{r}) d^D r \tag{3.3}$$

where D is the dimensionality of the system and r_0 some short-distance cut off [32]. For interactions decaying at large distances as $1/r^n$, $D < n$ is the condition for short-range interaction. Hence, the dipolar interaction $(n = 3)$ is long-range in three dimensions, and short range in one and two dimensions [32].

The second property of dipolar interaction is its anisotropic character. The dipolar interaction has the angular symmetry of the Legendre polynomial of second order $P_2(\cos\theta)$ [32]. As θ varies between 0 and $\pi/2$, the factor $1 - 3\cos 2\theta$ varies between -2 and 1. Therefore, the dipolar interaction is repulsive for side to side configuration, while it is attractive for head-to-tail configuration (Fig.3.1). For a special value of θ ($\theta_m = \arccos(1/\sqrt{3}) \cong 54.7^\circ$), the dipole-dipole interaction vanishes.

It is convenient to use the Fourier transform of the dipolar interaction in the study of the elementary excitations. The Fourier transform

$$\tilde{U}_{dd}(\mathbf{k}) = \int U_{dd}(\mathbf{r}) e^{-i\mathbf{k}.r} d^3 r \tag{3.4}$$

of Eq.(3.2) is

$$\tilde{U}_{dd}(\mathbf{k}) = C_{dd}\left(\cos^2\alpha - 1/3\right) \tag{3.5}$$

where α is the angle between **k** and the polarization direction [32]. The Fourier transform of the dipolar interaction does not depend on the modulus of the wavevector **k** in three dimensions. This property is same for contact interaction whose Fourier trnsform is g.

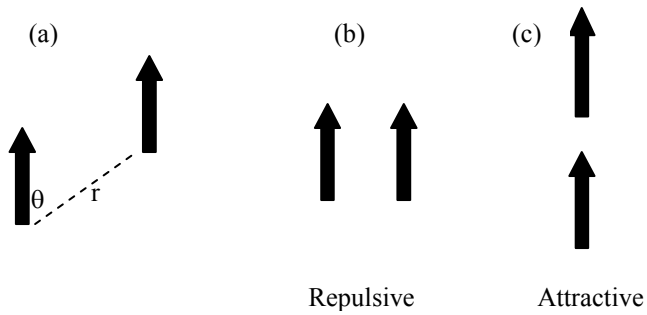

Fig. 3.1. Configuration of two dipoles. (a) Notations for the dipolar interaction. (b) Side-to-side configuration. (c) Head-to-tail configuration.

Fig.3.1 shows the arrangement of dipoles. Dipoles placed side-to side repel each other, while dipoles in a head to tail configuration attract. The dipoles in a prolate trap (side-to side configuration) causes to a mainly attractive gas, and it may exhibit collapse. Locating the dipoles in a oblate trap (head to tail configuration) causes to a mainly repulsive gas. It leads to partially stabile system. Due to the partial attractiveness of dipolar interaction, a dipolar Bose gas is similar to a Bose gas with a short-range interaction with a negative scattering length [33]. If the number of particles N is smaller than a critical value N_c, the collapse of the gas can be prevented. The attractive forces compress the gas to a smaller volume in order to lower the interaction energy in a confined gas, but the zero-point kinetic energy opposes these forces. For a small number of particles this can create an energy barrier and leads to a metastable condensate.

Consider prolate $(\omega_x \geq \omega_z)$ and oblate traps with $(\omega_x \leq \omega_z)$. There is a quantum phase transition as a function of the trap aspect ratio $\lambda^* = (\omega_x / \omega_z)^{1/2} \cong 0.4$ [34]. Above this value the sign of the mean dipolar interaction energy changes from positive to increasingly negative, and it remains increasingly negative for $\lambda > 1$. The condensate becomes more and more prolate,

until it undergoes a collapse. It is similar to BEC with negative scattering length in s-wave interaction case. [33]

For hard oblate traps with $\lambda < \lambda^*$, dipolar interaction grows as $N\mu^2$ increases and the gas is dominantly repulsive [34]. There is no collapse and the gas having much larger values of N is stable. The condensate aspect ratio κ, which is equal to R_x/R_z decreases with $N\mu^2$. For $\omega_x << \omega_z$, one can distinguish two regimes: i) for $\hbar\omega_x << U_{dd} << \hbar\omega_z$, a quasi two dimensional Bose gas with repulsive interactions, which has radially a parabolic TF profile is examined. ii) for $U_{dd} \geq \hbar\omega_z$, a three dimensional gas in the TF regime is considered. The gas feels the attractive dipolar interactions and subjects to a short wavelength instability, which leads to a roton-maxon minimum and then instability in the excitations spectrum [34].

3.2. Tunability

One of the important properties of dipolar interaction is its tunability. For electric dipoles this can be achieved by changing the applied external electric field. Even in the case of polar molecules, the presence of an external electric field is necessary to create permanent dipole moments of the molecules. The field matches the spherically symmetric rotational ground state of the molecule to the excited rotational state with different parity. Thus, it creates a non-zero average dipole moment. The strength of the external field indicates the degree of polarization and the magnitude of the dipole moment. The effective dipolar interaction may be tuned by the competition between an orienting electric field and the quantum or thermal rotation of the molecule [35]. This method works for values of the field up to the saturation limit. At the saturation limit the molecule is completely polarized (typically 10^4 V/cm). The dipole moment still grows at higher values of the field, but this is a much smaller effect.

In general the dipolar interaction U_{dd} can be tuned by using a time-dependent field to align the dipoles [36]

$$B(t) = B\left(\cos\varphi \mathbf{e}_z + \sin\varphi\left(\cos(\Omega t)\mathbf{e}_x + \sin(\Omega t)\mathbf{e}_y\right)\right) \tag{3.6}$$

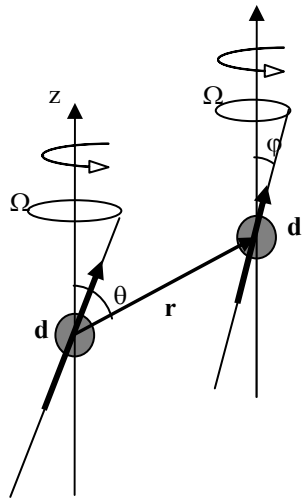

Fig. 3.2. Tunability of the dipolar interaction.

where $\mathbf{e}_x$, $\mathbf{e}_y$ and $\mathbf{e}_z$ are unit vectors defining the x, y and z axis, respectively. This field is a combination of a static field along the z-axis and a fast rotating field in the xy-plane. The ratio of the amplitudes of the static and rotating fields determines the angle φ, $0 \le \varphi < \pi/2$. In this situation, the atoms fell a time-averaged dipolar interaction [35]. The rotation frequency Ω of the magnetic field around the z-axis has to be chosen such that the magnetic moments can follow the rotation adiabatically. Ω also should be fast enough for the atomic motion on the time scale of one rotation to be negligible. This is obtained by the condition $\omega_{Larmor} >> \Omega >> \omega_{trap}$ and puts a constraint on the minimum field to be used since the Larmor frequency of the atomic precession is $\omega_{Larmor} = \mu_m B/\hbar$ [36]. Then the effective dipolar interaction between atoms is given by

$$U_{dd}(\mathbf{r},\varphi) = -\frac{\mu_0 \mu_m^2}{4\pi}\left(\frac{3\cos^2\varphi - 1}{2}\right)\left(\frac{3\cos^2\theta - 1}{r^3}\right) \qquad (3.7)$$

where φ is the angle between the magnetic field direction and the z-axis and Θ is the angle between the vector r and the z-axis [36]. Eq.(3.2) differs from Eq.(3.7),

by a factor $\alpha(\varphi) = (3\cos^2\varphi - 1)/2$. This factor can be changed continuously from 1 to $-1/2$ varying the angle φ.

3.3. Creation of dipolar gas

In order to study a quantum gas with significant dipolar interactions, one can use particles having either an electric dipole moment d, or a magnetic dipole moment μ. The typical order of magnitude of d for an atomic or molecular system is $d \propto q_e a_0$, where q_e is the electron charge and a_0 the Bohr radius. On the other hand the magnetic moments are on the order of the Bohr magneton μ_B. Using the identitites of a_0 and μ_B in terms of fundamental constants, the ratio of magnetic to electric dipolar coupling constants is

$$\frac{\mu_0 \mu^2}{d^2/\varepsilon_0} \propto \alpha^2 \propto 10^{-4} \tag{3.8}$$

where $\alpha \cong 1/137$ is the fine structure constant. The different systems that can be used to study experimentally for dipolar condensate are given below [32].

Polar molecules: Polar molecules are good candidates for dipolar condensate because of their strong electric dipole moment. Three conditions need to be satisfied for a molecule to have a significant dipole moment [32]:

a) A heteronuclear molecule which have a permanent dipole moment is necessary.

b)The molecule must be in a low vibrational state in order to have a dipole moment .

c) An external electric field which is on the order of 10^4 V/cm must be applied to orient the molecule. In fact, the ground state J = 0 is rotationally symmetric and therefore the average dipole moment is zero. Only by a mixing with higher rotational levels, induced by the electric field, the average dipole moment become non-zero.

Heteronuclear molecules in their ground state have a large electric dipole moment which is on the order of one Debye (1D ≃ 3.3×10^{-30} C·m). The

properties of such a gas is dominated by the dipolar interactions if the scattering length is of the order of that of the atoms used in experiments (typically around $100a_0$, where a_0 is the Bohr radius).

Rydberg atoms: Rydberg atoms is another system in which large electric dipole moments can be attained [31, 32]. They are highly excited atoms which have large principal quantum number n and a dipole moment scaling like n^2. The mutual interaction is dependent on the atomic states. With an electric field, states with different electron orbital angular momentum can be mixed. Thus, the atoms get a dipole moment and can interact to first order by dipolar interaction. Due to the very large dipole moments, the dipolar interaction is very strong, and it is felt over very long distances such as many tens of microns.

Light-induced dipoles: Atoms in their ground state, which is a parity eigenstate, do not have an electric dipole moment. Their electric polarizability is usually very small. Hence, extreme electric field strengths are necessary to induce a large dipolar interaction [22, 37]. Following G. Kurizki and coworkers, resonant excitation of a dipole optical allowed transition to induce an AC dipole moment on the order of one atomic unit ea_0 can be used [33]. Since the dipole moment also couples to the vacuum modes of the radiation field, the spontaneous light forces scale just like the light induced dipolar interactions. The anisotropic nature of the dipolar interaction might be used for a proof of principle experiment allowing to discriminate the spontaneous light forces from the dipolar forces. This kind of interactions have the same form as retarded interactions between two dipoles. They include $1/r^3$, $1/r^2$ and radiative $1/r$ terms multiplied by the suitable factors oscillating with the spatial period of the laser wavelength. Using an order of several laser fields all anisotropic $1/r^3$ terms have been proposed to cancel, leaving an effective isotropic, gravity-like $1/r$ potential.

Paramagnetic atoms with large magnetic moments μ: Some atoms like Cr, Eu, Dy have a large magnetic moment in their ground state. The only quantum gas to

reveal measurable dipolar effects is the chromium, and its condensation was obtained in 2004 [19]. The magnetic dipole moment of chromium atom is $6\mu_B$, and its scattering length is about $100a_0$ (a_0 is the Bohr radius). These values allows to observe a perturbative effect of the dipolar interaction.

3.4. GP Equation for Dipolar BEC

Consider a BEC with the dipoles aligned in the *z* direction by an external field. The mean-field potential depends on the whole density distribution of a condensate because of the long-range character of the dipole–dipole interaction. For a density distribution $n(\mathbf{r})$, the mean-field potential is [21, 38]

$$\Phi_{dd} = \int U_{dd}(\mathbf{r}-\mathbf{r}')n(\mathbf{r}')d^3r' = \int U_{dd}(\mathbf{r}-\mathbf{r}')|\psi(\mathbf{r}')|^2 d^3r' \tag{3.9}$$

With this interaction term, the Gross–Pitaevskii equation (2.47) gets the form

$$i\hbar\frac{\partial}{\partial t}\Psi(\mathbf{r},t) = \left(-\frac{\hbar}{2m}\nabla^2 + V_{trap}(\mathbf{r}) + g\Psi^2(\mathbf{r},t) + \int U_{dd}(\mathbf{r}-\mathbf{r}')|\psi(\mathbf{r}')|^2 d^3r'\right)\Psi(\mathbf{r},t) \tag{3.10}$$

and $\Phi_{dd}(\mathbf{r})$ is the mean-field potential due to dipole-dipole interactions [39]:

$$\Phi_{dd}(\mathbf{r}) \equiv \int d^3r' U_{dd}(\mathbf{r}-\mathbf{r}')\, n(\mathbf{r}') \tag{3.11}$$

It is convenient to introduce a dimensionless parameter which characterises the relative strength of the dipolar and contact interactions [39],

$$\varepsilon_{dd} \equiv \frac{C_{dd}}{3g} \tag{3.12}$$

The BEC is stable as long as $-0.5 < \varepsilon_{dd} < 1$, but loses that stability in the TF limit when $\varepsilon_{dd} > 1$ [40]. In the presence of a strong electric field the *s*-wave scattering length can be modified. Thus, g and ε_{dd} are effective quantities when dealing with electrically induced dipoles. For the alkalis used in BEC experiments, the value of ε_{dd} is extremely small (for ^{87}Rb, $\varepsilon_{dd} \cong 0.007$), hence dipolar interactions are negligible.

In the presence of the nonlocal dipolar mean-field potential $\Phi_{dd}(\mathbf{r})$, TF equation is give by an integral equation

$$\mu = \frac{1}{2} m(\omega_x^2 \rho^2 + \omega_z^2 z^2) + gn(\mathbf{r}) + \Phi_{dd}(\mathbf{r}) \tag{3.13}$$

It is straightforward to show that this equation gets an inverted parabola as a self-consistent solution. The dipolar interaction can be analysied by using the mathematical identity

$$\frac{(\delta_{ij} - 3\mathbf{r}_i \mathbf{r}_j)}{r^3} = -\nabla_i \nabla_j \frac{1}{r} - \frac{4\pi}{3} \delta_{ij} \delta(\mathbf{r}) \tag{3.14}$$

It can be written

$$\Phi_{dd}(\mathbf{r}) = -C_{dd} \mathbf{e}_i \mathbf{e}_j \left(\nabla_i \nabla_j \phi(\mathbf{r}) + \frac{\delta_{ij}}{3} n(\mathbf{r}) \right) \tag{3.15}$$

with

$$\phi(\mathbf{r}) = \frac{1}{4\pi} \int \frac{d^3 r' n(\mathbf{r}')}{|\mathbf{r} - \mathbf{r}'|} \tag{3.16}$$

The problem reduces to an analogy with electrostatics, and the potential $\phi(\mathbf{r})$ arising from the static charge distribution $n(\mathbf{r})$ needs to be calculated. $\phi(\mathbf{r})$ given by Eq. (3.16) must obey Poisson's equation $\nabla^2 \phi = -n(\mathbf{r})$ [39]. Proceeding from

the TF Eq. (3.13), an exact solution for the density $n(\mathbf{r})$ of a condensate with dipolar interactions was calculated in [38] for cylindrically symmetric trap with $\omega_x = \omega_y$. O'Dell *et al* have shown in [38] that even under the influence of the dipolar mean-field potential $\Phi_{dd}(\mathbf{r})$, the wavefunction has the shape of an inverted parabola in the TF limit:

$$n(r) = n_0\left[1 - \frac{\rho^2}{R_x^2} - \frac{z^2}{R_z^2}\right] \quad \text{for } n(r) \geq 0, \tag{3.17}$$

with radii $R_x = R_y$ and R_z and where $\rho^2 = x^2 + y^2$, and the central density n_0 is constrained by normalization to be

$$n_0 = \frac{15N}{8\pi R_x^2 R_z} \tag{3.18}$$

Then Poisson's equation is satisfied by an electrostatic potential of the form

$$\phi(\mathbf{r}) = a_0 + a_1\rho^2 + a_2 z^2 + a_3\rho^4 + a_4 z^4 + a_5\rho^2 z^2 \tag{3.19}$$

Hence the TF equation contains only parabolic and constant terms in the presence of dipolar interactions a parabolic density profile is also an exact solution of the TF problem in a harmonic trap. However, this time it is expected that the condensate aspect ratio differs from that of the trap. It is difficult to calculate the integral (3.16) for a density of the form (3.17), because the domain of integration is bounded by and has the symmetry of a spheroid or an ellipsoid. Evaluating this integral is possible taking explicit account of this symmetry [38]. One way of calculating the integral is to transform it into spheroidal coordinates and to use Green's function of Poisson's equation in these coordinates [41]. Finally, The results are transformed back into Cartesian coordinates [39].

3.4.1. Green's Function in Spheroidal Coordinates

For prolate spheroidal coordinates (ξ,η,φ), trasformation between between cartesian and prolate spheroidal coordinates are $x = q\sqrt{(\xi^2-1)(1-\eta^2)}\cos\varphi \quad y = q\sqrt{(\xi^2-1)(1-\eta^2)}\sin\varphi$, $z = q\xi\eta$. Surfaces of constant ξ are confocal spheroids, and their eccentricityis is $1/\xi$. ξ is between 1 and ∞. Surfaces of constant η are confocal two-sheet hyperboloids of revolution. η changes from -1 and 1. For $R_z > R_x$ the boundary of the density profile (3.17) is a prolate spheroid and its semimajor axis is R_z, semiminor axis is R_x, and eccentricity is $\sqrt{1-R_x^2/R_z^2}$. To make the spheroidal coordinate system confocal to that boundary the scaling constant $q = \sqrt{R_z^2 - R_x^2}$ must be chosen. Then using the Green's function in prolate spheroidal coordinates [41] to find the potential (3.16) as

$$\phi(\xi,\eta,\varphi) = \frac{R_z^2 - R_x^2}{2}\left[\int_1^{\xi} d\xi' \int_{-1}^{1} d\eta' (\xi'^2 - \eta'^2) n(\xi' - \eta') \sum_{\ell=0}^{\infty} (2\ell+1) P_\ell(\eta) P_\ell(\eta') Q_\ell(\xi) P_\ell(\xi')\right]$$
$$+ \frac{R_z^2 - R_x^2}{2}\left[\int_{\xi}^{1/\sqrt{1-R_x^2/R_z^2}} d\xi' \int_{-1}^{1} d\eta' (\xi'^2 - \eta'^2) n(\xi', \eta') \sum_{\ell=0}^{\infty} (2\ell+1) P_\ell(\eta') P_\ell(\xi) Q_\ell(\xi')\right] \tag{3.20}$$

where P_ℓ, are Legendre functions of the first and Q_ℓ, of the second kind. Performing the η' integration first it can be seen that the only contributing , ℓ are 0, 2, and 4. To transform the result for $\phi(\xi,\eta,\varphi)$ in Cartesian coordinates one need to make the substitutions $\xi = (r_1 + r_2)/2q$ and $\eta = (r_1 - r_2)/2q$ with $r_1 = \left[x^2 + y^2 + (z+q)^2\right]^{\frac{1}{2}}$ and $r_2 = \left[x^2 + y^2 + (z-q)^2\right]^{\frac{1}{2}}$. The potential of the form predicted by Eq. (3.19) is calculated as follows

$$\phi(\mathbf{r}) = \frac{n_0 R_x^2}{192(1-\kappa^2)^2}\left\{24\Xi(1-\kappa^2)^2 + 48(1-\kappa^2)(2-\Xi)\left(\frac{z}{R_z}\right)^2 - 24(1-\kappa^2)(2-\kappa^2\Xi)\left(\frac{\rho}{R_x}\right)^2\right.$$
$$\left. 8(2\kappa^2 - 8 + 3\Xi)\left(\frac{z}{R_z}\right)^4 + 3\left[2(2-5^2) + 3\kappa^4\Xi\right]\left(\frac{\rho}{R_x}\right)^4 + 24(2 + 4\kappa^2 - 3\kappa^{2}\Xi)\left(\frac{\rho}{R_x}\right)^2\left(\frac{z}{R_z}\right)^2\right\}$$

(3.21)

where $\kappa \equiv R_x / R_z$ is the aspect ratio of the BEC and

$$\Xi \equiv \frac{1}{\sqrt{1-\kappa^2}} In \frac{1+\sqrt{1-\kappa^2}}{1-\sqrt{1-\kappa^2}} \qquad \text{for} \quad \kappa < 1 \quad \text{(prolate)} \tag{3.22}$$

For $R_x > R_z$, then the boundary of the density profile (3.17) is an oblate spheroid, and oblate spheroidal coordinates $x = q\sqrt{(\xi^2+1)(1-\eta^2)}\cos\varphi$, $y = q\sqrt{(\xi^2+1)(1-\eta^2)}\sin\varphi$, $z = q\xi\eta$ are used. Surfaces of constant ξ are confocal spheroids with eccentricity $1/\sqrt{\xi+1}$, and ξ is between 0 and ∞. $q = \sqrt{R_x^2 - R_z^2}$ is choosen to make the coordinate system confocal to the boundary of $n(\mathbf{r})$. Using the Green's function in oblate spheroidal coordinates [41] the potential is found as

$$\phi(\xi,\eta,\varphi) = \frac{R_x^2 - R_z^2}{2}\left[\int_0^{\xi} d\xi' \int_{-1}^{1} d\eta' (\xi'^2 - \eta'^2) n(\xi' - \eta') i \sum_{\ell=0}^{\infty} (2\ell+1) P_\ell(\eta) P_\ell(\eta') Q_\ell(i\xi) P_\ell(i\xi')\right]$$
$$+ \frac{R_x^2 - R_z^2}{2}\left[\int_{\xi}^{1/\sqrt{1-R_x^2/R_z^2}} d\xi' \int_{-1}^{1} d\eta' (\xi'^2 - \eta'^2) n(\xi',\eta') i \sum_{\ell=0}^{\infty} (2\ell+1) P_\ell(\eta') P_\ell(i\xi) Q_\ell(i\xi')\right]$$

(3.23)

To return to Cartesian coordinates one need to make the substitutions $\xi = \left(\sqrt{x^2 + y^2 + (z+iq)^2} + \sqrt{x^2 + y^2 + (z-iq)^2}\right)\Big/(2q)$ and

$\eta = \left(\sqrt{x^2 + y^2 + (z+iq)^2} - \sqrt{x^2 + y^2 + (z-iq)^2} \right) \Big/ (2iq)$. Then it is found that the result for the potential is the same as in Eq. (3.20) but with

$$\Xi \equiv \frac{2}{\sqrt{\kappa^2 - 1}} \arctan \sqrt{\kappa^2 - 1} \qquad \text{for } \kappa > 1 \quad \text{(oblate)} \qquad (3.24)$$

3.4.2. Solution of the Thomas-Fermi Equation

Taking the external field to be along the z axis and using Eq.(3.15) and (3.20), the parabolic dipolar potential is found as

$$\Phi_{dd} = \frac{n_0 C_{dd}}{3} \left[\frac{\rho^2}{R_x^2} - \frac{2z^2}{R_z^2} - f(\kappa) \left(1 - \frac{3}{2} \frac{\rho^2 - 2z^2}{R_x^2 - R_z^2} \right) \right] \qquad (3.25)$$

where $f(\kappa)$ is:

$$f(\kappa) \equiv \frac{2 + \kappa^2 [4 - 3\Xi(\kappa)]}{2(1 - \kappa^2)} \qquad (3.26)$$

$f(\kappa)$ is a monotonically decreasing function of κ and vanishes for $\kappa = 1$. It means that for an isotropic density distribution the dipole-dipole mean-field potential averages to zero [32]. $f(\kappa)$ has values in the range $1 \geq f(\kappa) \geq -2$. Substituting $\Phi_{dd}(\mathbf{r})$ into the Thomas-Fermi equation and comparing the coefficients of ρ^2 , z^2, and 1 yields three equations [39]. The first equation, related with the constant terms, gives the chemical potential

$$\mu = g n_0 [1 - \varepsilon_{dd} f(\kappa)] \qquad (3.27)$$

It is understood from this equation that the effect of dipole-dipol interactions is to lower the chemical potential of a prolate $(\kappa < 1)$ condensate, while raising that of

an oblate $(\kappa > 1)$ condensate. The radii $R_x (= R_y)$ and R_z of the exact parabolic solution are obtained from the coefficients of ρ^2 and z^2 as follows

$$R_x = R_y = \left[\frac{15gN\kappa}{4\pi m \omega_x^2} \left\{ 1 + \varepsilon_{dd} \left(\frac{3}{2} \frac{\kappa^2 f(\kappa)}{1-\kappa^2} - 1 \right) \right\} \right]^{\frac{1}{5}} \tag{3.28}$$

and $R_z = R_x / \kappa$. The aspect ratio κ is evaluated by solving a transcendental equation

$$3\kappa^2 \varepsilon_{dd} \left[\left(\frac{\gamma^2}{2} + 1 \right) \frac{f(\kappa)}{1-\kappa^2} - 1 \right] + (\varepsilon_{dd} - 1)(\kappa^2 - \gamma^2) = 0 \tag{3.29}$$

where $\gamma = \omega_z / \omega_x$ is the ratio of the harmonic trapping frequencies. The effect of dipolar forces polarized along the *z* axis is to make the condensate more oblate along z axis. If $\varepsilon_{dd} = (5/2)(\gamma^2 - 1)/(\gamma^2 + 2)$, the condensate becomes exactly spherical for an oblate trap $(\gamma > 1)$.

In order to illustrate the static properties of the Thomas-Fermi solution for a dipolar BEC, an experiment has a large number of atoms and a particular aspect ratio g is imagined, and the value of ε_{dd} is adiabatically increased from zero [39]. For electrically induced dipoles this would involve increasing the electric field. For magnetic dipoles this can be done by either rotate the external magnetic field, gradually changing the angle of rotation [30], or reduce the *s*-wave scattering length using a Feshbach resonance. In the absence of the external field, the condensate aspect ratio matches the trap aspect ratio, $\kappa = \gamma$. When the dipole-dipole interactions are switched on the condensate becomes more prolate than the trap so that one always has $\kappa < \gamma$. As long as $0 \le \varepsilon_{dd} \le 1$, the equation (3.29) has a single solution κ for any value of trap γ.

4.VORTICES IN A BEC

One of the most fascinating properties of BEC is its behaviour under rotation. Like superfluid helium, BEC does not rotate in the manner of an ordinary fluid which undergoes rigid body rotation. When an ordinary fluid is put into a rotating container, the steady state corresponds to a rotation of the fluid as a whole together with the container. The velocity of an ordinary fluid is the same as the velocity of a rigid rotating body $\mathbf{v} = \mathbf{\Omega} \times \mathbf{r}$. [42] The superfluid is not joined by the walls of the rotating bucket for a low enough rotation frequency so it stays at rest in the laboratory frame. In this state, rotational motion does not occur. The condensate phase is constant over the whole volume. However above a critical frequency Ω_C, a vortex line appears. The condensate density drops to zero on the vortex line. In this case, the phase of the condensate wave function is given by $S(\mathbf{r}) = \theta$, and θ is the azimuthal angle around the vortex axis (along z axis). For frequencies considerably higher than Ω_C, a single vortex line with a quantum number q larger than 1 would appear $(S(\mathbf{r}) = q\theta)$. Nevertheless this state is unstable, and it fragments into q vortices each having a unit circulation [42].

The rotation of a superfluid leads to the formation of quantized vortex lines. Fritz London suggested the connection between the superfluidity of liquid ^{4}He and BEC in 1938 [43]. Superfluid liquid ^{4}He plays an important role in the development of physical concepts since it is the first example of BEC. Onsager is the first scientist who proposed that quantized vortex lines were related with superfluid liquid ^{4}He [44]. Feynman independently proposed quantization of circulation in liquid ^{4}He. He investigated its consequences for flow experiments [45]. Madison et al. succeeded in observing a vortex and a vortex lattice in a trapped BEC [42]. They used a similar method that used in the observation of superfluid helium in a rotating bucket [46].

While classical vortices can take any value of circulation, superfluids are irrotational, and vortices are formed with quantized circulation. Quantized vortices have been observed in several forms such as single vortices [47, 48], vortex lattices [42, 49-51] and vortex pairs and rings [52-54] in BEC.

These phenomenon are similar to observed in liquid helium, but the atomic Bose-Einstein condensates differ fundamentally from the helium BEC in some ways. A dilute Bose gas is a dilute system where the interactions are characterized by s-wave scattering length. Superfluid ^4He has relatively high density and strong repulsive interactions are present in the system. Atomic BEC have a nonuniform density because of the confining potential contrary to uniform helium. Measurements of the momentum distribution showed that low-temperature condensate fraction is ~0.1 in bulk superfluid ^4He [55-57]. However, in the low-temperature atomic condensates all atoms participates in BEC.

4.1. Quantized vortices

Quantized vortices represent phase defects in the topology of the superfluid systems. When a superfluid is subjected to rotational motion, vortices will be formed in it. This situation is true for dilute BEC. A conventional fluid rotating with angular frequency Ω has the velocity field of rigid body rotation $\mathbf{v} = \mathbf{\Omega} \times \mathbf{r}$ as mentioned above. Hence the "vorticity" of the flow is uniform $\nabla \times \mathbf{v} = \mathbf{2\Omega}$. However, Onsager and Feynman noted that superfluid helium could not rotate as a conventional fluid. In the presence of the vortex along the *z*-axis, the condensate wavefunction $\Psi(\mathbf{r},t)$ can be expressed in terms of a fluid density $n(\mathbf{r},t)$ and a macroscopic phase $S(\mathbf{r},t)$ via

$$\Psi(\mathbf{r},t) = \sqrt{n(\mathbf{r},t)}\exp[iS(\mathbf{r},t)] \tag{4.1}$$

Then the superfluid velocity becomes

$$v = \frac{\hbar}{m}\nabla S \tag{4.2}$$

Note that the flow of the condensate is irrotational wherever S is not singular. It means that the condensate can be rotated only by the generation of vortices such that the condensate density vanishes at the vortex cores. The vorticity apparently vanishes:

$$\nabla \times v = \frac{\hbar}{m} \nabla \times \nabla S = 0 \tag{4.3}$$

Since the wave function is single-valued, the change in phase around any closed contour C must be an integer multiple of 2π ,

$$\int_C \nabla S . d\mathbf{l} = 2\pi q \,, \tag{4.4}$$

where q is an integer. From Eq.(4.2) and Eq.(4.4), it is found that the circulation of the velocity flow around a closed contour which encircles the vortex is quantized in units of $(\hbar/m)$,

$$\Gamma = \int_C \mathbf{v} . d\mathbf{l} = q\left(\frac{\hbar}{m}\right) \tag{4.5}$$

The velocity of the superfluid is given by

$$\mathbf{v} = \frac{\hbar}{mr} q\boldsymbol{\varphi} \tag{4.6}$$

The velocity diverges as $r \to \infty$. The angular momentum along z is $L_z = N\hbar q$. As the angular velocity increases, one can create vortex states with q values 2, 3,... In a harmonically-confined condensate, the configuration of singly-charged vortices is energytically favorable compared to the multiply-charged vortex with $q > 1$. A q-fold vortex with $\Psi \propto e^{iq\theta}$ satisfies the GP equation, but the corresponding energy increases like q^2. As a result, a multiply quantized vortex is expected to be unstable compared to the formation of singly quantized vortices. Thus a $q > 1$ vortex can decay into singly-quantized vortices via dynamical instability. A rotating BEC generally consists of an array of singly charged vortices in the form of a triangular Abrikosov lattice.

Each quantized vortex line in rotating superfluid ^4He has a uniform localized vorticity. Although the flow is strictly irrotational away from the cores, Feyman argued that a uniform array of vortices can mimic solid-body rotation on average [45]. The integral of the vorticity of a uniformly rotating body over an area A is $2A_v$, where A_v is the area enclosed by the contour C. Thus the circulation should be $\Gamma = 2\Omega A_v$. The areal vortex density in a rotating superfluid becomes

$$n_v = \frac{N_v}{A_v} = \frac{2\Omega}{q} \tag{4.7}$$

The area per vortex, $1/n_v = q/2\Omega$, decreases with increasing rotation speed.

4.2. Vortex Generation

Vortices can be formed by different ways such as rotation, a moving obstacle, or phase imprinting methods [58]. These ways are explained brifley below.

Rotation: Vortices can be nucleated only when the stirring frequency Ω of the container is higher than a critical value Ω_C. Experiments related with the vortex formation usually have used a smooth rotating potential created by a laser or magnetic field which allows a small transverse anisotropy to rotate the condensate. This rotating potential causes a low-energy collective oscillation or shape deformation of the condensate. A vortex may be detected by the imaging of the density profile of the condensate since the density vanishes at the vortex core. The stirring potential is turned off in an adiabatic way and the condensate density along the rotating axis is imaged to detect the presence of a vortex. The healing length is so small that it cannot be observed optically in the experiments. The vortices approach the surface of the condensate as the rotation frequency increases.

The energetic criterion for vortex formation is a necessary, but not sufficient, condition. There must also be a dynamic condition for vorticity to be introduced into the condensate.

The generation of vortices in rotating trapped condensate seems to be related with the instabilities of collective excitations. Instability can be induced resonantly exciting a surface mode by addition of a rotating deformation to the trap potential. For small perturbations, this resonance occurs near to a rotation frequency $\Omega = \omega_\ell / \ell$, where ω_ℓ is the frequency of a surface mode with multipolarity ℓ. The surface modes satisfy the relation $\omega_\ell = \sqrt{\ell}\omega_r$, where ω_r is radial trap frequency [59] for TF approximation. So $\Omega = \omega_r / \sqrt{\ell}$. A similar way to vortex nucleation is revealed by considering stationary states of the BEC in a rotating elliptical trap, which excites the $\ell = 2$ quadrupole mode. Thus, it generates vortices when stirred at $\Omega \approx \omega_r / \sqrt{2}$. This value is in agrrement with experiments [42, 50, 60] and numerical simulations [61, 62]. For low rotation frequencies, only one solution is found. For higher rotations $\left(\Omega > \omega_r / \sqrt{2}\right)$ a bifurcation occurs and up to three solutions are exist. Above the bifurcation point one or more of the solutions become dynamically unstable. This leads to vortex formation.

Surface mode instabilities can also be observed at finite temperature by a rotating noncondensed thermal cloud. If $\Omega > \omega_\ell / \ell$ condition is satisfied for the thermal cloud such instabilities occur [63]. All modes can be excited in this way. Hence, the criterion for vortex nucleation is $\Omega_C > \min\left(\omega_\ell / \ell\right)$, similar to the Landau criterion. Such a minimum exists at $\Omega_C > 0$ since the exactness of the TF result $\omega_\ell = \sqrt{\ell}\omega_r$ decreases for high ℓ [64].

Nucleation by a moving object: In trapped BEC vortices can also be nucleated through the optical dipole force from a laser, providing a localized repulsive Gaussian potential. This laser beam repels atoms from its focus generating a moving macroscopic hole in the condensate. When the potential is subjected to a

linear motion, vortex pair formation occurs providing that the potential is moved at a velocity above a critical value.

An alternative way to vortex formation is to move the laser beam potential in a circular path around the trap center. One or more vortices can be generated by stirring the condensate in this way. Vortices can be experimentally generated even at low stirring frequencies by this technique Ref. [65].

Other mechanisms and structures: Other ways of vortex formation have been also proposed in several studies. Williams and Holland [66] offered a combination of rotation and coupling between two hyperfine levels to generate a condensate with two components. One of these state is a vortex state. The non-vortex state can be retained or removed with a resonant laser pulse. Phase imprinting method also has been used to experimentally generate multiply-quantized vortices [67]. Vortex rings which are the decay product of dynamically unstable dark solitary waves in 3D geometries have also been the subject of interest [68, 69].

4.3. Theoretical Background

The solution of the GP equation in the rotating frame is used to determine the rotation frequency of vortex formation. Consider a single vortex in a condensate trapped by an axisymmetric trap with frequencies ω_z and $\omega_\perp = \omega_x = \omega_y$, and the trap aspect ratio $\gamma = \dfrac{\omega_z}{\omega_\perp}$. Radial and axial lengths are equal to each other for this trap: $R_x = R_y = R_\perp$. The axisymmetric harmonic potential is $V_{trap}(r,z) = \dfrac{m\omega_\perp^2}{2}\left(\rho^2 + \gamma^2 z^2\right)$. When the system rotates, it is convenient to consider the corresponding rotating frame. Supposing the rotation is about z-axis, the integrand of the GP with the additional term $-\Psi^* \Omega L_z \Psi$, where $L_z = xp_y - yp_x = -i\hbar\left(x\partial_y - y\partial_x\right)$ is the z-component of the angular momentum operator, is given by [12]

$$E' = \int dr \Psi(\mathbf{r},t)^* \left(-\frac{\hbar^2 \nabla^2}{2m} + V_{trap} + \frac{g}{2}\left|\Psi(\mathbf{r},t)\right|^2 - \Omega L_z \right) \Psi(\mathbf{r},t) \qquad (4.8)$$

The variables in the integrand are those in the rotating frame. The corresponding GP equation becomes

$$i\hbar \frac{\partial \Psi(\mathbf{r},t)}{\partial t} = \left[-\frac{\hbar^2 \nabla^2}{2m} + V_{trap} + g\left|\Psi(\mathbf{r},t)\right|^2 - \Omega L_z \right] \Psi(\mathbf{r},t) \qquad (4.9)$$

Eq. (4.9) gives the structure of the vortex. In many cases, Eq. (4.9) is an accurate microscopic description of an atomic BEC, because of the small condensate depletion $\bar{n}|a_s|^3 << 1$. In the TF limit $Na_s/a_{ho} >> 1$, the repulsive interactions significantly expand the condensate, thus the kinetic energy related with the density variation becomes negligible compared to the trap and interaction energies. Then, the density can be obtained approximately as

$$n(r,z) \approx n_0 \left(1 - \frac{\xi^2}{r^2} - \frac{r^2}{R_\perp^2} - \frac{z^2}{R_z^2} \right) \Theta\left(1 - \frac{\xi^2}{r^2} - \frac{r^2}{R_\perp^2} - \frac{z^2}{R_z^2} \right) \qquad (4.10)$$

where $n_0 = \mu/g$ is the centeral density of the non-vortex condensate. The TF radiuses are $R_\perp^2 = 2\mu/m\omega_\perp^2$ and $R_z^2 = 2\mu/m\omega_z^2$ and the healing length is $\xi = \left(\hbar^2/2mgn_0\right)^{1/2} = \left(8\pi a_s n_0\right)^{-1/2}$. The healing length is an important quantitiy for a superfluid. The healing length ξ characterizes the vortex core size, and is very small ($\xi/R_\perp = \hbar\omega_\perp/2\mu = \left(15Na_s/a_{ho}\right)^{-2/5} << 1$) in the TF limit [12]. The core radius increases away from the trap center. The healing length is typically of order 0.5 μm for an atomic condensate, and is large compared to the typical particle separation. For the case of superfluid helium in which interactions are strong, the healing length is very short. Thus, the vortex core size is of order the inter-particle spacing .

Increasing the quantum number q widens the core radius because of the centrifugal effects. For a $q = 1$ vortex at the center of an axially-symmetric potential, each particle carries $\hbar$ of angular momentum. However, if the vortex is off-center, the angular momentum per particle becomes a function of position. The vortex affects the density only in the neighborhood of the vortex core. The chemical potential of vortex state μ differs from that of nonvortex state μ_0 in TF limit by small fractional corrections of order $(a_{ho}/R_0)^4 In(R_0/a_{ho})$, where $R_0 = (R_x R_y R_z)^{1/3}$ [55].

A vortex created at the centre of a stationary trap is not thermodynamically stable. The vortex state corresponds to a maximum of the energy functional and will tend to spiral out of the trap in a finite time. The instability of the vortex solution is also seen in the excitation spectrum, which shows modes of positive norm and negative frequency corresponding to a precession of the vortex line around the centre of the trap . The vortex state can be stabilized by setting the trap into rotation, when it becomes a minimum of the energy functional. A mechanism to transfer angular momentum to the vortex state is also needed. It can be achieved by a rotating non-axisymmetric perturbation.

The energy associated with a single vortex line determines the stability of the vortex state. The kinetic energy of the superfluid provides a dominant contribution to this energy. This energy is

$$E_1 = \int \frac{1}{2} m n v_s^2 dr = \frac{m\bar{n}}{2} R_z \int_{\xi}^{R_\perp} v_s^2 2\pi r dr = q^2 R_z \frac{\pi\hbar^2 \bar{n}}{m} In\left(\frac{R_\perp}{\xi}\right) \qquad (4.11)$$

where we assume the spatially uniform density $\bar{n}$. Since Eq. (4.9) is directly proportional to q^2, vortices with $q > 1$ are energetically not favorable.

Experiments in rotating trapped BEC generally occur in the TF regime. The mean condensate radius R is large relative to the mean oscillator length a_{ho} because of dominant repulsive interactions. The vortex core size is smaller than a_{ho} with the ratio a_{ho}/R_0. Hence, the presence of a few vortices does not

significantly affect the density. In most cases, the condensates are axisymmetric with radial and axial trap frequencies $\omega_\perp$ and ω_z, so that the nonrotating TF density depends only on $\rho = \sqrt{x^2 + y^2}$ and z.

The trap with different radial and axial radiuses $\left(R_x \neq R_y\right)$ is a nonaxisymmetric trap. When a singly quantized vortex is formed along the z-axis of a nonaxisymmetric trap the condensate wave function is not an eigenfunction of the angular momentum operator L_z. The phase of the condensate wave function near the trap centre has the form [32]

$$S \approx \varphi - \frac{1}{4}\left(\frac{1}{R_x^2} - \frac{1}{R_y^2}\right) r_\perp^2 In\left(\frac{r_\perp}{R_\perp}\right)\sin(2\varphi) \tag{4.12}$$

in the TF approximation and the condensate velocity is

$$v \approx \frac{\hbar}{m}\left\{\frac{\hat{\varphi}}{r_\perp} - \frac{1}{2}\left(\frac{1}{R_x^2} - \frac{1}{R_y^2}\right) r_\perp In\left(\frac{r_\perp}{R_\perp}\right)\left(\cos(2\varphi)\hat{\varphi} + \sin(2\varphi) r_\perp^2\right)\right\} \tag{4.13}$$

where $R_\perp^2 = 2R_x^2 R_y^2 / \left(R_x^2 + R_y^2\right)$. The condensate wave function and the condensate velocity possess cylindrical symmetry in the vicinity of the vortex core. This situation is different far from the vortex core where the condensate velocity adjusts to the anisotropy of the trap and becomes asymmetric [55].

4.4. Critical Rotational Velocity

The energy of a nonvortex state $E_0'(\Omega)$ in the rotating frame is numerically equal to the energy E_0 in the laboratory frame since the corresponding angular momentum vanishes. The corresponding energy of the system with the angular momentum L_z is $E_1'(\Omega) = E_1 - N\hbar\Omega$. The difference between these two energies is the excess energy given by

$$\Delta E'(\Omega) = E_1'(\Omega) - E_0'(\Omega) = E_1 - E_0 - N\hbar\Omega \tag{4.14}$$

In the laboratory frame, E_1 is higher than E_0 because of the kinetic energy of the circulating flow. If the condensate is in equilibrium in the rotating frame, the excess energy of the vortex vanishes at a thermodynamic critical angular velocity Ω_C determined by $\Delta E'(\Omega_C) = 0$. Thus, the critical rotation frequency Ω_C above which the vortex state is energytically favorable is given by

$$\Omega_C = \frac{E_1 - E_0}{N\hbar} \tag{4.15}$$

in terms of the energy of the vortex and non-vortex states evaluated in the laboratory frame. The ground state energy is equivalent to the minimum of the thermodynamic free energy. Therefore, the rotation frequency is also called the thermodynamic frequency of vortex nucleation since it is evaluated by minimizing the thermodynamic free energy.

For a noninteracting trapped gas, the difference $E_1 - E_0 = N\hbar\omega_\perp$ follows immediately from the excitation energy for the singly quantized vortex relative to the stationary ground state. In the noninteracting gas, the critical angular velocity is equal to the radial trap frequency. This critical angular velocity is also valid for a q-fold vortex in a noninteracting condensate, due to the special form of the noninteracting excitation energy $E_q - E_0 = Nq\hbar\omega_\perp$ and the corresponding angular momentum $Nq\hbar$. Hence, the noninteracting condensate becomes degenerate as $\Omega \to \omega_\perp$ [32]. This degeneracy states the cancellation between the centrifugal potential $-\frac{1}{2}M\Omega^2 r_\perp^2$ and the radial trap potential $-\frac{1}{2}M\omega^2 r_\perp^2$ as $\Omega \to \omega_\perp$ [55].

For small and middle values of Na_s/a_{ho}, $\Omega_C/\omega_\perp$ decreases with increasing particle numbers [55]. For a weakly interacting system, this ratio is $\Omega_C/\omega_\perp \approx 1 - \left(1/2\sqrt{2\pi}\right)\left(Na_s/d_z\right)$ for small values of the interaction parameter Na_s/a_{ho} [34]. In the strongly interacting TF limit, $E_1(N)$ can be found by the

equation $\mu_1 = \partial E_1 / \partial N$, where the chemical potential $\mu_1(N)$ for a condensate containing a singly quantized vortex can be evaluated with Eq. (4.14). With the corresponding expressions of the vortex-free condensate gives the approximate expression [70, 71]

$$\Omega_C \approx \frac{5}{2}\frac{\hbar^2}{MR_\perp^2} In\left(\frac{0.67R_\perp}{\xi}\right) \tag{4.16}$$

The total angular momentum of the trap gas with nonuniform density is lower than the that of a uniform fluid. This expression exceeds the usual estimate $\Omega_C \approx (\hbar/MR_\perp^2) In(1.46\,R_\perp/\xi)$ for uniform superfluid in a rotating cylinder of radius $R_\perp$ because. Eq. (4.16) is equivalent to

$$\frac{\Omega_C}{\omega_\perp} \approx \frac{5}{2}\frac{d_\perp^2}{R_\perp^2} In\left(\frac{0.67R_\perp}{\xi}\right) \tag{4.17}$$

where $d_\perp$ is the harmonic oscillator length of the trap along the radial direction Since $d_\perp^2/R_\perp^2 \propto \xi/R_\perp << 1$, this ratio is small in the TF limit. For an axisymmetric condensate, Eq. (4.17) depends on N and γ because of the TF relation $d_\perp^2/R_\perp^2 = (d_\perp/15Na_s\gamma)^{2/5}$ .The critical angular frequency decreases as the number of atoms in the trap increases.

Nearly the same functional relationship is true for the thermodynamic critical frequency Ω_C and the number of atoms in the condensate N_0 for nonzero temperatures. The difference between these relationships is that the number of atoms in the condensate depends on temperature:

$$\frac{N_0}{N} = 1 - \left(\frac{T}{T_C}\right)^3 \tag{4.18}$$

where T_C is the critical temperature of condensate. The distribution function of the thermal atoms changes because of the centrifugal force in a rotating trap. The critical temperature decreases as

$$\frac{T_C(\Omega)}{T_C^0} = \left(1 - \frac{\Omega^2}{\omega_\perp^2}\right)^{1/3} \tag{4.19}$$

where T_C^0 is the critical temperature without rotation. The critical temperature $T_C(\Omega)$, below which the vortex corresponds to a thermodynamically stable configuration in a trap rotating with frequency Ω is calculated with Equations (4.17)–(4.19). The gas shows Bose–Einstein condensation for temperatures below $T_C(\Omega)$. The critical temperature for the creation of stable vortices exhibits a maximum as a function of Ω.

4.5 Vortex in an Attractively Interacting BEC

Attractive interactions in BEC are characterized by a negative s-wave scattering length $a_s < 0$. Vortices in such a condensate have also received theoretical interest. A homogenous BEC with $a_s < 0$ is not stable because of collapse. However, an inhomogeneous BEC is stable as long as the number of condensed atoms N is smaller than a critical value. A central vortex state decreases the peak density so it may help stabilization of a trapped condensate with $a_s < 0$. For $\Omega < \omega_\perp$ excitation of a vortex in a harmonically trapped BEC with $a_s < 0$ is prohibited by the center-of-mass motion, which is the lowest energy state for a given angular momentum [72].

The critical angular velocity of BEC with attractive interactions is larger than that with noninteracting particles. For repulsive interaction, the situation is opposite. The generation of a vortex in a trapped BEC with repulsive interactions is more energetically favorable than for attractive interactions since more internal potential energy is needed to lower the average density for attractive interactions.

The vortex state is more stable than the state without vortex. More atoms can be put into the rotating gas before attaining the critical density for the collapse.

4.6 Precession of a Vortex

Precession of a off-axis vortex in a condensate is a simple example of vortex motion. A vortex may be formed slightly away from the centre instead of the centre of the condensate. In this situation a lateral force arising from the density gradient in the condensate affects the vortex. This lateral force induces a Magnus force effect which may be thought of as a sort of effective buoyancy. The total buoyancy force is usually towards the condensate surface and the result is a precession of the core around the condensate axis due to the Magnus effect. Besides the vortex may be subjected to a damping force which causes radial drag. The vortex spirals core towards the condensate surface due to energy dissipation and damping processes.

Consider a vortex line with a single quantum circulation in a condensate confined by a cylindrical container whose cross section is a circle of radius *R*. The density is constant everywhere except a small region in the core of the vortex. The angular momentum per unit length about the axis of the cylinder is

$$\mathrm{L} = \mathrm{nm}\int \rho d\rho d\varphi v\rho \tag{4.20}$$

If the vortex is at a distance *b* from the axis of the cylinder, the angular momentum per unit length is given by [13]

$$\mathrm{L} = \mathrm{nh}\int_{\mathrm{b}}^{\mathrm{R}} \rho \mathrm{d}\rho = \pi n R^2 \hbar\left(1 - \frac{b^2}{R^2}\right) \tag{4.21}$$

The vortex and its image vortex interact each other. The azimuthal angle of their positions changes, but their radial coordinates remains constant. The angular velocity can be determined by the equation [13]

$$\dot{\varphi} = \Omega = \frac{\partial E}{\partial L} = \frac{\partial E/\partial b}{\partial L/\partial b} \tag{4.22}$$

Since the energy and the angular momentum both depend parametrically on *b,* the frequency also depends on *b*. The velocity at which the vortex advances is precisely the flow velocity of the fluid at the position of the vortex. It is in agreement with Kelvin's theorem.

4.7 Hydrodynamic Theory of the Condensate

The hydrodynamic equations of BEC defines the time evolution of the density and the velocity of the condensate. Vortex nucleation is a dynamic process in a trapped gas. In TF limit these hydrodynamic equations are the same as the Euler equations of the classical hydrodynamics. A linear stability analysis of the hydrodynamic equations gives a description of the collective excitations. One actually gets an analytical description of this collective excitations using this classical hydrodynamic theory. There is a relation between hydrodynamic theory and the Bogoliubov theory which also describes the collective excitations. It was shown by Sinha [73] that the dispersion law [74] for the collective excitations obtained under classical hydrodynamic approximation can be derived by applying the TF approximation directly to the Bogoliubov equations [75]. The hydrodynamic theory of the condensate has been discussed in several papers and reviewed in [13, 76, 77].

To enable the construction of a hydrodynamic theory of the condensate, the wavefunction $\Psi(\mathbf{r})$ can be split into a modulus and a phase $\Psi(\mathbf{r}) = \sqrt{n(\mathbf{r},t)}e^{iS(\mathbf{r})}$ where $n(\mathbf{r},t) = |\Psi(\mathbf{r},t)|^2$ is the particle density. The corresponding current density is

$$\mathbf{J} = \left(\frac{\hbar}{2mi}\right)\left(\Psi^*\nabla\Psi - (\nabla\Psi^*)\Psi\right) = |\Psi|^2\,\frac{\hbar\nabla S}{m} \tag{4.23}$$

The hydrodynamic equation $\mathbf{J} = n\mathbf{v}$ identifies the local velocity as

$$\mathbf{v}(\mathbf{r},t) = \nabla\Phi(\mathbf{r},t) \tag{4.24}$$

where $\Phi = \hbar S/m$ is the velocity potential which was proposed proposed by Feynman (1955) about the vortices in superfluid Helium. Substituting the wave function into the time-dependent GP equation and seperating its imaginary and real parts one can find the following continuity and Bernoulli equations, respectively [75]

$$\frac{\partial n}{\partial t} + \nabla.(n\mathbf{v}) = 0 \tag{4.25}$$

$$\frac{1}{2}mv^2 + V_{trap}(\mathbf{r}) - \frac{\hbar^2}{2m}\frac{\nabla^2\sqrt{n}}{\sqrt{n}} + gn + m\frac{\partial\Phi}{\partial t} = 0 \tag{4.26}$$

Equations (4.25) and (4.26) exhibit all the hydrodynamic behaviour found for classical irrotational compressible isentropic flow. Taking the gradient of both sides of the equation (4.26), the time derivative of the velocity field is obtained as

$$\begin{aligned} m\frac{\partial\mathbf{v}}{\partial t} &= -\left(\frac{1}{2}mv^2 + V_{trap}(\mathbf{r}) + gn - \frac{\hbar^2}{2m}\frac{\nabla^2\sqrt{n}}{\sqrt{n}}\right) \\ &= -\nabla\left(\frac{1}{2}mv^2 + \mu\right) \end{aligned} \tag{4.27}$$

where the chemical potential is given by

$$\mu = V_{trap}(\mathbf{r}) + gn - \frac{\hbar^2}{2m}\frac{\nabla^2\sqrt{n}}{\sqrt{n}} = \mu_{TF} - \frac{\hbar^2}{2m}\frac{\nabla^2\sqrt{n}}{\sqrt{n}} \tag{4.28}$$

For a uniform condensate in which $V_{trap} = 0$ at T = 0, the chemical potential $\mu = gn_0$ and the pressure $P = \left(-\frac{\partial E}{\partial V}\right)_T = \frac{g}{2}n_0^2$. Using this expression for

pressure after replacing n_0 by n, Eq. (4.27) can be rewritten in the form

$$m\frac{\partial \mathbf{v}}{\partial t} = -\nabla\left(\frac{1}{2}mv^2 + V_{trap}(\mathbf{r}) + \frac{\nabla P}{n} - \frac{\hbar^2}{2m}\frac{\nabla^2\sqrt{n}}{\sqrt{n}}\right) \tag{4.29}$$

Eq. (4.29) is very similar to the Euler equation

$$m\frac{\partial \mathbf{v}}{\partial t} = -\nabla\left(m(\mathbf{v}.\nabla)\mathbf{v} + V_{trap}(\mathbf{r}) + \frac{\nabla P}{n}\right) \tag{4.30}$$

where $\nabla\left(\frac{1}{2}mv^2\right) = m(\mathbf{v}.\nabla)\mathbf{v}$.

The last term in Eq.(4.29) drops in TF limit. In TF approximation, neglecting the term $\frac{\hbar^2}{2m}\frac{\nabla^2\sqrt{n}}{\sqrt{n}}$ in Eq. (4.29), one can get the classical hydrodynamic equation

$$m\left(\frac{\partial}{\partial t} + \mathbf{v}.\nabla\right)\mathbf{v} = -\nabla\left(V_{trap}(\mathbf{r}) + gn\right) \tag{4.31}$$

and the chemical potential μ becomes μ_{TF}. In the case of rotation, the hydrodynamic equations in TF limit take the form

$$\frac{\partial n}{\partial t} + \nabla\left(n(\mathbf{v} - \mathbf{\Omega}\times\mathbf{r})\right) = 0 \tag{4.32}$$

$$m\frac{\partial \mathbf{v}}{\partial t} + \nabla\left(\frac{1}{2}mv^2 + V_{trap}(\mathbf{r}) + \frac{\nabla p}{n} - \mathbf{v}(\mathbf{\Omega}\times\mathbf{r})\right) = 0 \tag{4.33}$$

where Ω is the angular velocity. Since the only degrees of freedom are those of the condensate wave function, which has a magnitude and a phase, motions of the condensate maybe specified in terms of a local density and a local velocity. Ordinary liquids and gases have many more degrees of freedom. Therefore, it is

usually necessary to use a microscopic description, such as the distribution function for the particles. However, a hydrodynamic description is possible for ordinary fluids in which collisions between particles are sufficiently frequent so that thermodynamic equilibrium is established locally. The state of the liquid or gas may then be given completely in terms of the local particle density, the local velocity, and the local temperature. The temperature is not a related variable at zero temperature, and the motion may be described in terms of the local density and the local velocity like a condensate. The equations of motion for a condensate and for a perfect fluid are similar. They are expressions of the conservation laws for particle number and for total momentum. However, the physical reasons for a description in terms of a local density and a local velocity are considerably different for the two cases.

4.8. Elementary Excitations

Elementary excitations maybe examined by taking into account small deviations of the state of the gas from equilibrium and finding periodic solutions of the time-dependent GP equation. Using the hydrodynamic equations is an equivalent approach. The density can be written as $n = n_{eq} + \delta n$, where n_{eq} is the equilibrium density and δn the deviation of the density from its equilibrium value. Linearizing Eqs. (4.25), (4.27), and (4.28) by treating the velocity $\mathbf{v}$ and δn as small quantities, one finds [13]

$$\frac{\partial \delta n}{\partial t} = -\nabla.\left(n_{eq}\mathbf{v}\right) \tag{4.34}$$

$$m\frac{\partial \mathbf{v}}{\partial t} = -\nabla \delta\mu \tag{4.35}$$

where $\delta\mu$ is found by linearizing Eq.(4.28). Taking the time derivative of Eq.(4.23) and eliminating the velocity by means of (4.24) one finds the equation of motion describing the excitations of a Bose gas [13]

$$m\frac{\partial^2 \delta n}{\partial t^2} = \nabla.\left(n_{eq}\nabla \delta\tilde{\mu}\right) \tag{4.36}$$

n_{eq} is the density of the condensate neglecting the zero-temperature depletion of the condensate. In the undisturbed state, the density n is the same everywhere in a uniform gas and therefore may be taken outside the spatial derivatives. From Eq. (4.28) the change in $\tilde{\mu}$ is equal to [13]

$$\delta\tilde{\mu} = \left(gn + \frac{\hbar^2 q^2}{4mn}\right)\delta n \tag{4.37}$$

The equation of motion becomes

$$m\omega^2 \delta n = \left(ngq^2 + \frac{\hbar^2 q^4}{4m}\right)\delta n \tag{4.38}$$

Non-vanishing solutions of Eq.(4.38) are possible if the frequency is given by $\omega = \pm\varepsilon_q/\hbar$, where ε_q is the energy of an excitation

$$\varepsilon_q = \sqrt{2ng\varepsilon_q^0 + \left(\varepsilon_q^0\right)^2} \tag{4.39}$$

and ε_q^0 is the free particle energy. The zero-temperature excitation spectrum was first derived by Bogoliubov from microscopic theory [78]. For small q, ε_q is a linear function of q,

$$\varepsilon_q \approx c\hbar q \tag{4.40}$$

Phonons are the linear part of this excitation spectrum. The sound velocity c is given by

$$c = \sqrt{ng/m} \tag{4.41}$$

The Bogoliubov theory is valid as long as the wavelength of the excitation is much greater than the s-wave scattering length. The repulsive interaction has turned the energy spectrum linear in q at long wavelengths. At short wavelengths the leading contributions to the spectrum are the free-particle spectrum and a mean-field contribution

$$\varepsilon_q \approx \varepsilon_q^0 + ng \tag{4.42}$$

The transition between the linear spectrum and the quadratic one occurs when the kinetic energy, becomes large compared with the potential energyof a particle. This occurs at a wave number $\approx (2mgn)^{\frac{1}{2}}/\hbar$. It is the inverse of the coherence length. The relation between the coherence length and the sound velocity is $\xi = \hbar/\sqrt{2}\,mc$. Atoms behave like free particles on length scales longer than the healing length. The spectrum of elementary excitations in superfluid ^4He is different from that of a dilute gas due to the strong short-range correlations.

Eq.(4.38) does not precisely apply to a parabolic trap, since the density is not homogeneous. However, the form of $\omega(q)$ is very similar to that of Eq.(4.38). The speed of sound, and therefore the excitation spectrum Eq.(4.38), can be defined at each point $\mathbf{r}$ in the local density approximation, where $c = \sqrt{n(\mathbf{r})g/m}$ [79]. This approximation is true when TF radius of the condensate in the $\mathbf{q}$ direction is much larger than the wavelength of the excitation. The central density varies with the square of the condensate radius in the TF limit. Thus, the speed of sound in a trapped condensate increases linearly with TF radius.

4.9 Elliptical Trap

One way of rotating the condensate is to use a rotating elliptical harmonic trap. In an elliptical trap, the presence of vortices predicted to create with rotation angular velocities above $\Omega \approx 0.3\omega_\perp$ [80]. However, experimentally vortices are

generated at much higher velocities since only at higher velocities a dynamical route to vortex nucleation appears [50, 81]. In ENS group experiments a harmonic rotating potential with adjustable anisotropy λ and rotation frequency Ω is created [82]. A striking result of the ENS experiments is that, for a very weak anisotropy λ, nucleation of vortices occur in the interval of rotation frequencies around $0.7\omega_{\perp}$.

In the rotating frame, the static solutions in an elliptical trap are quadrupole solutions with elliptical density profiles. These solutions, and their stability characters, are examined by the classical hydrodynamic equation in the rotating frame [83, 84]. Experimentally, these solutions can be achieved by two procedures. Procedure I involves increasing the rotation frequency from zero for a fixed elliptical trap. Procedure II involves increasing the trap ellipticity from zero while rotating at a fixed frequency. If these procedures are employed adiabatically, the condensate have the stationary states in the rotating frame. This has been observed experimentally [50, 85]. The onset of the instability has been examined theoretically based on classical hydrodynamics [83, 84] and is in excellent agreement with experimental results [50, 85]. If the rotating elliptical trap is introduced non-adiabatically, the condensate undergoes shape oscillations which can be unstable and lead to vortex lattice formation. These non-adiabatic dynamics have been also observed experimentally [85] and explained theoretically [86, 87].

For large systems, the equations of motion are described by the hydrodynamic theory of superfluids in TF limit. If the trapping potential rotates with angular velocity Ω, it is convenient to write these equations in the rotating frame:

$$\frac{\partial n}{\partial t} + \nabla\left(n\left(\mathbf{v} - \mathbf{\Omega} \times \mathbf{r}\right)\right) = 0 \tag{4.43}$$

$$m\frac{\partial \mathbf{v}}{\partial t} + \nabla\left(\frac{1}{2}mv^2 + V_{trap}\left(\mathbf{r}\right) + ng - m\mathbf{v}\left(\mathbf{\Omega} \times \mathbf{r}\right)\right) = 0 \tag{4.44}$$

These equations are studied by Recati *et. al.* in the case of a dilute BEC in a rotating harmonic trap with the frequencies ω_x, ω_y, ω_z [83]. The oscillator potential is $V_{trap}(\mathbf{r}) = m/2\left(\omega_x^2 x^2 + \omega_y^2 y^2 + \omega_z^2 z^2\right)$, where $\omega_x > \omega_y$. The trap is almost elliptical in the rotating xy plane in the experiments [50, 85]. Therefore, an ellipticity parameter λ defines the x, y trap frequencies to be $\omega_x = \sqrt{1-\lambda}\omega_\perp$ and $\omega_y = \sqrt{1+\lambda}\omega_\perp$, where $\omega_\perp^2 = \left(\omega_x^2 + \omega_y^2\right)/2$ is the geometric mean of the frequencies. $V_{trap}(\mathbf{r})$ does not depend on time in the rotating frame. The x and y axes rotate at the frequency Ω around the z axis. The wavefunction is given by

$$\Psi = \sqrt{n}\exp\left(\frac{m}{\hbar} i\alpha xy\right) \tag{4.45}$$

The elliptical trap causes to excite a quadrupolar mode in the condensate while rotating. The irrotational quadrupolar flow in the condensate defined by the velocity field [88],

$$\mathbf{v} = \alpha\nabla(xy) \tag{4.46}$$

where α is the velocity field amplitude and proportional to the ellipticity of the condensate density profile. Substituting expression (4.46) into Eq. (4.44), the density is given by the parabolic shape

$$n(\mathbf{r}) = \frac{1}{g}\left(\tilde{\mu} - \frac{m}{2}\left(\tilde{\omega}_x^2 x^2 + \tilde{\omega}_y^2 y^2 + \omega_z^2 z^2\right)\right) \tag{4.47}$$

in the presence of the rotation. The effective oscillator frequencies are [83]

$$\tilde{\omega}_x^2 = \omega_x^2 + \alpha^2 - 2\alpha\Omega \tag{4.48}$$

$$\tilde{\omega}_y^2 = \omega_y^2 + \alpha^2 - 2\alpha\Omega \tag{4.49}$$

which fix the average square radii of the atomic cloud through the relationships [83]

$$\widetilde{\omega}_x^2\left\langle x^2\right\rangle = \widetilde{\omega}_y^2\left\langle y^2\right\rangle = \omega_z^2\left\langle z^2\right\rangle = \frac{2\widetilde{\mu}}{7m} \tag{4.50}$$

where

$$\widetilde{\mu} = \frac{\hbar\widetilde{\omega}_{ho}}{2}\left(\frac{15Na}{\widetilde{a}_{ho}}\right)^{2/5} \tag{4.51}$$

is the chemical potential in the rotating frame. This chemical potential provides the proper normalization of the density (4.47). The rotation of the trap with α which is different from zero causes a modification in the shape of the density profile due to the change of the effective frequencies $\widetilde{\omega}_x$ and $\widetilde{\omega}_y$.

The equation of continuity (4.43) takes the form $\left(\mathbf{v}-\boldsymbol{\Omega}\times\mathbf{r}\right).\nabla n = 0$ at equilibrium, and gives the expression for α [83]:

$$\alpha = -\Omega\left(\frac{\widetilde{\omega}_x^2 - \widetilde{\omega}_y^2}{\widetilde{\omega}_x^2 + \widetilde{\omega}_y^2}\right) \tag{4.52}$$

From (4.50) and (4.52) , the expectation value of the angular momentum is found to be

$$\left\langle L_z\right\rangle = m\int\left(\mathbf{r}\times\mathbf{v}\right)_z n(\mathbf{r})d\mathbf{r} \equiv \Omega\Theta \tag{4.53}$$

where $\Theta = Nm\left\langle x^2 - y^2\right\rangle^2 \Big/ \left\langle x^2 + y^2\right\rangle$ of the moment of inertia. The ratio between Θ and the classical rigid value $\Theta_{rig} = Nm\left\langle x^2 + y^2\right\rangle$ takes the expression [83]

$$\frac{\Theta}{\Theta_{rig}} = \left(\frac{\widetilde{\omega}_x^2 - \widetilde{\omega}_y^2}{\widetilde{\omega}_x^2 + \widetilde{\omega}_y^2}\right)^2 \tag{4.54}$$

Θ and Θ_{rig} depend on the value of Ω since $\langle x^2 \rangle$ and $\langle y^2 \rangle$ are modified by the rotation. By inserting Eqs. (4.48) and (4.49) into Eq.(4.52) the following equation for α [83] is found

$$2\alpha^3 + \alpha\left(\omega_x^2 + \omega_y^2 - 4\Omega^2\right) + \Omega\left(\omega_x^2 - \omega_y^2\right) = 0 \tag{4.55}$$

which defines the stationary condensate solutions in a harmonic trap with ellipticity λ rotating at frequency Ω. Depending on the value of Ω and ellipticity

$$\lambda = \frac{\omega_x^2 - \omega_y^2}{\omega_x^2 + \omega_y^2} \tag{4.56}$$

of the trap, either 1 or 3 solutions can be derived in analytic form. The physical solutions should satisfy the conditions $\tilde{\omega}_x^2 > 0$ and $\tilde{\omega}_y^2 > 0$. These conditions provides the normalizability of the density and except some of the solutions of (4.55).

Eq. (4.55) defines static solutions, but they are not necessarily stable solutions. Small perturbations in density δn and phase $\delta\varphi$ to the static solutions are considered to examine their dynamical stability [84, 89]. Taking the variational derivatives of Eqs. (4.43) and (4.44) yields the time-evolution equations

$$\frac{\partial}{\partial t}\begin{bmatrix}\delta\phi \\ \delta n\end{bmatrix} = -\begin{bmatrix}\mathbf{v}_c.\nabla & g/\hbar \\ \nabla.\left(n\frac{\hbar}{m}\nabla\right) & \mathbf{v}_c.\nabla\end{bmatrix}\begin{bmatrix}\delta\phi \\ \delta n\end{bmatrix} \tag{4.57}$$

where $\mathbf{v}_c = \mathbf{v} - \mathbf{\Omega}\times\mathbf{r}$ is the velocity field in the rotating frame. A polynomial ansatz which consists of terms of the form $x^i y^j$, where $i, j \geq 0$ and $i + j \leq 7$, is taken for the perturbations δn and $\delta\varphi$, and inserted into Eq.(4.57). If the eigenvalues of Eq.(4.57) are purely imaginary or have a negative real part, the

perturbations are stable oscillations which decay over time. If they have a real positive component, the perturbations grows exponentially. These solutions are dynamically unstable. Thus, they lead to vortex lattice formation [84, 89].

5. VORTICES IN DIPOLAR BEC

Dipolar interaction has remarkable consequences for the physics of rotating dipolar gases in TF limit. The principal effect of dipolar interactions on the equilibrium properties of a condensate is to cause distortion of its aspect ratio so that it is elongated along the direction of the dipoles. This feature affects the stability of a vortex in a dipolar BEC. The stability of vortices in dipolar condensates has been recently addressed. The theoretical investigations have shown that the stability of dipolar gases depends on the trap geometry [23, 90]. In Ref. [91], the authors have studied the stability and excitations of singly and doubly quantized vortices in dipolar BECs, while in Ref. [92] a phase transition has been predicted between straight and twisted vortex lines. Also, the transverse instability of vortex lines has been studied in Ref. [93].

It has been shown that the critical angular frequency for vortex creation may be significantly affected by the dipolar interaction [94]. In an axially symmetric traps with the axis along the dipole orientation, the critical angular velocity, above which a vortex is energetically favorable, is decreased in oblate traps due to the dipolar interaction [94, 95]. The effect of the dipole-dipole interaction is the lowered precession velocity of an off-center straight vortex line in an oblate trap [96]. In addition, dipolar gases under fast rotation develop vortex lattices, which due to the dipolar interaction may be severely distorted [97], and even may change their configuration from the usual triangular Abrikosov lattice into other arrangements [28, 29]. The experimental way towards unstable dynamics which may lead to vortex lattice formation was examined in [40] .

In the Thomas–Fermi (TF) limit, the dipolar interactions change the possibility of vortex lattice formation for a rotating dipolar BEC in an elliptical trap [40]. Rotating BEC with dipolar interactions was analyzed theoretically in elliptical traps and discussed the regimes of stability and instability [38, 98].

5.1 Dipolar Condensate in an Elliptical Trap

Hydrodynamic equations in the dipolar BEC are obtained by adding dipolar interaction to Eqs. (4.32) and (4.33)

$$\frac{\partial n}{\partial t}+\nabla\left(n\left(\mathbf{v}-\mathbf{\Omega}\times\mathbf{r}\right)\right)=0 \tag{5.1}$$

$$m\frac{\partial \mathbf{v}}{\partial t}+\nabla\left(\frac{1}{2}mv^2+V_{trap}\left(\mathbf{r}\right)+\Phi_{dd}\left(\mathbf{r}\right)+ng-m\mathbf{v}\left(\mathbf{\Omega}\times\mathbf{r}\right)\right)=0 \tag{5.2}$$

$$\mu=\frac{m}{2}\left(\widetilde{\omega}_x^2x^2+\widetilde{\omega}_y^2y^2+\omega_z^2z^2\right)+gn\left(\mathbf{r}\right)+\Phi_{dd}\left(\mathbf{r}\right) \tag{5.3}$$

The dipolar potential with an inverted parabola density is found to be [40]

$$\frac{\Phi_{dd}}{3g\varepsilon_{dd}}=\frac{n_0\kappa_x\kappa_y}{2}\left[\beta_{001}-\frac{x^2\beta_{101}+y^2\beta_{011}+3z^2\beta_{002}}{R_z^2}\right]-\frac{n}{3} \tag{5.4}$$

where the coefficients β_{ijk} are [40]

$$\beta_{ijk}=\int_0^\infty\frac{ds}{\left(\kappa_x^2+s\right)^{i+1/2}\left(\kappa_y^2+s\right)^{j+1/2}\left(1+s\right)^{k+1/2}} \tag{5.5}$$

where i, j, and k are integers. For the cylindrically symmetric case with $\kappa_x=\kappa_y=\kappa$, the integrals β_{ijk} are

$$\beta_{ijk}=2\frac{{}_2F_1\left(k+\frac{1}{2},1;i+j+k+\frac{3}{2};1-\kappa^2\right)}{\left(1+2i+2j+2k\right)\kappa^{2(i+j)}} \tag{5.6}$$

where ${}_2F_1$ denotes the Gauss hypergeometric function [40]. Therefore, rearranging Eq. (5.3) gives an expression for the density profile

$$\rho = \frac{\mu - \frac{m}{2}\left(\widetilde{\omega}_x^2 x^2 + \widetilde{\omega}_y^2 y^2 + \omega_z^2 z^2\right)}{g\left(1-\varepsilon_{dd}\right)} + \frac{3g\varepsilon_{dd}\frac{n_0\kappa_x\kappa_y}{2R_z^2}\left(x^2\beta_{101} + y^2\beta_{011} + 3z^2\beta_{002} - R_z^2\beta_{001}\right)}{g\left(1-\varepsilon_{dd}\right)} \tag{5.7}$$

Comparing the x^2, y^2, and z^2 terms in Eqs. (5.3) and (5.7), three equations which define the size and the shape of the condensate are found [40]

$$\kappa_x^2 = \left(\frac{\omega_z}{\widetilde{\omega}_x}\right)^2 \frac{1+\varepsilon_{dd}\left(\frac{3}{2}\kappa_x^3\kappa_y\beta_{101} - 1\right)}{\zeta} \tag{5.8}$$

$$\kappa_y^2 = \left(\frac{\omega_z}{\widetilde{\omega}_y}\right)^2 \frac{1+\varepsilon_{dd}\left(\frac{3}{2}\kappa_y^3\kappa_x\beta_{011} - 1\right)}{\zeta} \tag{5.9}$$

$$R_z^2 = \frac{2gn_0}{m\omega_z^2}\zeta \tag{5.10}$$

where $\zeta = 1-\varepsilon_{dd}\left(1-\left(9\kappa_x\kappa_y/2\right)\beta_{002}\right)$. Furthermore, by inserting Eq.(5.7) into Eq. (5.1) we find that stationary solutions satisfy the condition [40]

$$\begin{aligned} 0 = &\left(\alpha+\Omega\right)\left(\widetilde{\omega}_x^2 - \frac{3}{2}\varepsilon_{dd}\frac{\omega_\perp^2\kappa_x\kappa_y\gamma^2}{\zeta}\beta_{101}\right) \\ &+\left(\alpha-\Omega\right)\left(\widetilde{\omega}_y^2 - \frac{3}{2}\varepsilon_{dd}\frac{\omega_\perp^2\kappa_x\kappa_y\gamma^2}{\zeta}\beta_{011}\right) \end{aligned} \tag{5.11}$$

Eq. (5.11) can be solved for velocity field amplitude α for a given ε_{dd}, and trap geometry [40]. For $\varepsilon_{dd} = 0$, α does not depend on the s-wave interaction strength and the trap ratio. However, α becomes dependent on both g and γ for $\varepsilon_{dd} \neq 0$. For fixed ε_{dd} and trap geometry, Eq. (5.11) leads to branches of α. These

branches are significantly different between circular traps $(\lambda = 0)$ or elliptical traps $(\lambda > 0)$ in the x-y plane [40].

$\lambda = 0$ **case:**

For this case, only one solution exists corresponding to $\alpha = 0$ up to a critical rotation frequency. Two more solutions with $\alpha > 0$ and $\alpha < 0$ exist at this critical frequency. This frequency at which the solution bifurcates is called bifurcation frequency Ω_b. For nondipolar condensate the bifurcation point is $\Omega_b = \omega_\perp / \sqrt{2}$. In this case, the system becomes energetically unstable to the spontaneous excitation of quadrupole modes for $\Omega \geq \omega_\perp / \sqrt{2}$. For $\Omega > \Omega_b$, solutions are given by $\alpha = \pm\sqrt{2\Omega^2 - \omega_\perp^2}/\omega_\perp$ [13, 20]. In the TF regime, a general surface excitation with angular momentum $\hbar\ell = \hbar q_\ell R$ obeys the classical dispersion relation $\omega_\ell^2 = (q_\ell / m)\nabla_R V_{trap}$ Ref [13] . Consequently, for the nonrotating and nondipolar BEC, $\omega_\ell = \sqrt{\ell}\omega_\perp$. The mode frequency is shifted by $-\ell\Omega$ due to rotation. Thus, the frequency of the $\ell = 2$ quadrupole surface excitation becomes $\omega_2(\Omega) = \sqrt{2}\omega_\perp - 2\Omega$ in the rotating frame [13] The bifurcation frequency thus coincides with the vanishing of the energy of the quadrupolar mode in the rotating frame. Two more solutions derive from excitation of the quadrupole mode for $\Omega \geq \omega_\perp / \sqrt{2}$. Ω_b does not depend on the interactions for nondipolar condensate since the mode frequencies ω_ℓ themselves are independent of g.

For dipolar condensate the potential Φ_{dd} gives nonlocal contributions and breaks the dependence of the force $-\nabla V$ on R [38, 40]. Therefore, the resonant condition for exciting the quadrupolar mode changes with ε_{dd}. The solutions change in the presence of dipolar interactions and the bifurcation point Ω_b moves to lower (higher) frequencies for $\varepsilon_{dd} > 0$ $(\varepsilon_{dd} < 0)$ [40].

$\alpha = 0$ solutions have zero ellipticity in the *x*-*y* plane. $|\alpha| > 0$ solutions have an elliptical density profile. The condensate is elongated in *x* direction for $\alpha > 0$ and it is elongated in *y* direction for $\alpha < 0$.

The bifurcation point can be calculated analytically. For $\alpha = 0$ the condensate is cylindrically symmetric with $\kappa_x = \kappa_y = \kappa$. For small $\alpha \to 0_+$, the first-order corrections to κ_x and κ_y with respect to κ can be calculated from Eqs. (5.8) and (5.9). Using $\Omega \to \Omega_b$ when $\alpha \to 0$ and inserting these aspect ratios in Eq. (5.11) , one can find [40]

$$\frac{\Omega_b}{\omega_\perp} = \sqrt{\frac{1}{2} + \frac{3}{4}\kappa^2 \varepsilon_{dd} \gamma^2 \frac{\kappa^2 \beta_{201} - \beta_{101}}{1 - \varepsilon_{dd}\left(1 - \frac{9}{2}\kappa^2 \beta_{002}\right)}} \tag{5.12}$$

It is found in Ref [40] that for nondipolar condensate the bifurcation point remains unaltered at $\Omega_b = \omega_x / \sqrt{2}$ as γ is changed [83, 84]. As dipolar interactions are increased the shape of the condensate changes from oblate to prolate. For a fixed γ they found that as ε_{dd} increases the bifurcation frequency decreases monotonically [40].

$\lambda > 0$:

The solutions for $\lambda > 0$ have an upper branch of $\alpha > 0$ solutions which exists over the whole range of Ω and a lower branch of $\alpha < 0$ solutions which back-bends and is double valued for a weak ellipticity of $\lambda = 0.025$. The frequency at which the lower branch back-bends is called the back-bending frequency Ω_b. No $\alpha = 0$ solution exists with $\Omega \neq 0$. The backbending frequency Ω_b increases with increasing trap ellipticity in nondipolar condensates. The presence of dipolar interactions reduces Ω_b for $\varepsilon_{dd} > 0$, and increases Ω_b for $\varepsilon_{dd} < 0$ [20]. The back-bending of the lower branch can show an instability.

For $\lambda \neq 0$, with increasing ε_{dd} the BEC becomes more prolate like zero ellipticity case. This deformation is due to the anisotropic character of dipolar interactions. The dipolar interactions are isotropic in the $x - y$ plane. Thus, they increase the deformation of the BEC in that plane.

The solutions derived in the previous subsections are static solutions in the rotating frame, but they are not necessarily stable. To analys their dynamical instabilities consider small perturbations in the BEC density and phase of the form $\rho = \rho_0 + \delta\rho$ and $S = S_0 + \delta S$. By linearizing the Eqs.(5.1) and (5.2), the dynamics of these perturbations can be described as [40]

$$\frac{\partial}{\partial t}\begin{bmatrix}\delta S\\ \delta n\end{bmatrix} = -\begin{bmatrix}\mathbf{v_C}.\nabla & g\left(1+\varepsilon_{dd}K\right)/m\\ \nabla.\rho_0\nabla & \left[(\nabla.v)+\mathbf{v_c}.\nabla\right]\end{bmatrix}\begin{bmatrix}\delta S\\ \delta\rho\end{bmatrix} \tag{5.13}$$

where $\mathbf{v_C} = \mathbf{v} - \boldsymbol{\Omega}\times\mathbf{r}$ and the integral operator K is defined as [40]

$$\left(K\delta\rho\right)(\mathbf{r}) = -3\frac{\partial^2}{\partial z^2}\int\frac{\delta\rho(\mathbf{r}')dr'}{4\pi|\mathbf{r}-\mathbf{r}'|} - \delta\rho(\mathbf{r}) \tag{5.14}$$

The integral in the above expression is carried out over the domain where $\rho_0 > 0$. Eigenfunctions and eigenvalues of operator (5.13) are determined to investigate the stability of the BEC. The imaginary eigenvalues of Eq.(5.13) are related with the stable collective modes of the system [40] while the real eigenvalues shows that the instability grows. A polynomial ansatz for the perturbations in the coordinates x, y, and z of total degree N is considered to find imaginary eigenfunctions [84, 98]. The operator K can be determined for a general polynomial density perturbation $\delta\rho = x^p y^q z^r$, with p, q, and r being non-negative integers and $p+q+r \le N$ [40]. Thus, the perturbation evolution operator Eq.(5.13) can be written as a scalar matrix operator, acting on vectors of polynomial coefficients.

5.2 Dipolar BEC with a Single Vortex

5.2.1 Dipolar BEC with a Centered Vortex

Interparticle interaction potential in dipolar gases includes both van der Waals and dipole–dipole term. Because of the long-range character of the dipole–dipole interaction, scattering properties at low energies are significantly changed. In the case of a short-range interaction, only the s-wave scattering is important at

low energies. However, in the case of a long-range interaction, all partial waves contribute to scattering. Within the mean-field description of the condensate, the interaction potential is well described by the following model potential

$$V = g\delta(\mathbf{r}) + \frac{\mu^2}{r^3}\left(1 - 3\cos^2\theta\right) \tag{5.15}$$

The results are equally valid for electric dipoles.

Consider a dipolar BEC of N particles with mass m and magnetic dipole moment μ oriented in the z-direction by a sufficiently large external field. At sufficiently low temperatures, the description of the ground state of the condensate is provided by the solution of the Gross-Pitaevskii (GP) equation

$$i\hbar\frac{\partial\Psi(\mathbf{r},t)}{\partial t} = \left[-\frac{\hbar^2\nabla^2}{2m} + V_{ext} + g\left|\Psi(\mathbf{r},t)\right|^2 + \mu^2\Phi_{dd}(\mathbf{r})\right]\Psi(\mathbf{r},t) \tag{5.16}$$

where V_T is the trap potential $V_T = \frac{m}{2}\omega_x^2(\rho^2 + \gamma^2 z^2)$, and $\rho^2 = x^2 + y^2$. The equation (5.16) is an integro-differential equation since it has both integrals and derivatives of an unknown wave function. This equation can be solved analytically if the zero-point kinetic energy associated with the density variation is assumed to be negligible in comparison to both the trap energy and the interaction energy between atoms. The wave function is given by [99]

$$\Psi(\rho,\phi,z) = \sqrt{n_0}\sqrt{1 - \frac{\rho^2}{R_x^2} - \frac{z^2}{R_z^2}}\sqrt{1 - \frac{\beta^2}{\rho^2 + \beta^2}}e^{i\phi} \tag{5.17}$$

In TF regime, the variational ansatz for the density profile of a condensate with a single vortex is [94]

$$n(\mathbf{r}) = \left|\Psi(\mathbf{r})\right|^2 = n_0\left(1 - \frac{\rho^2}{R_x^2} - \frac{z^2}{R_z^2}\right)\left(1 - \frac{\beta^2}{\rho^2 + \beta^2}\right) \tag{5.18}$$

$$= \mathrm{n}_{\mathrm{bg}}(\mathbf{r}) + n_v(\mathbf{r}) \tag{5.19}$$

This ansatz can be written as the sum of two terms: the background Thomas-Fermi parabolic profile $n_{bg}(\mathbf{r})$ which is given in Eq. (2.57) and the vortex profile $n_v(\mathbf{r})$

$$n_v(\mathbf{r}) = -n_0 \frac{\beta^2}{\rho^2 + \beta^2}\left(1 - \frac{\rho^2}{R_x^2} - \frac{z^2}{R_z^2}\right) \tag{5.20}$$

The variational ansatz (5.20) has the correct $\rho^{2\ell}$ dependence on the density as $\rho \to 0$ (with $\ell = 1$). This is necessary to satisfy the GP equation for a vortex of ℓ circulation quanta [13]. It has also the correct asymptotic form that the solution must have for $\rho \to \infty$. n_0 is the central density and is found by normalization to be

$$n_0 = \frac{15N}{8\pi R_x^2 R_z} \Bigg/ \left(1 + \frac{20}{3}\overline{\beta}^2 + 5\overline{\beta}^4 - 5\overline{\beta}^2\left(1 + \overline{\beta}^2\right)^{3/2} \arctan h\left[1/\sqrt{1+\overline{\beta}^2}\right]\right) \tag{5.21}$$

where $\overline{\beta} \equiv \dfrac{\beta}{R_x}$. The total energy for a dipolar gas can be written as

$$E_{tot} = E_{kin} + E_{trap} + E_{sw} + E_{dd} \tag{5.22}$$

where E_{kin} is the kinetic energy calculated by

$$E_{kin} = -\frac{\hbar^2}{2m}\int d^3 r \Psi^*(\mathbf{r})\nabla^2\Psi(\mathbf{r}) \tag{5.23}$$

In the Thomas-Fermi approximation the kinetic energy due to the slowly varying condensate $\sqrt{1-\rho^2/R_x^2 - z^2/R_z^2}$ is neglected [94]. The terms arising from the gradient of the vortex part of the wave function $\sqrt{1-\beta^2/\left(\rho^2+\beta^2\right)}$ which varies

rapidly in the $\hat{\mathbf{e}}_\rho$ direction must be taken into account. With these approximations, the kinetic energy is calculated to be [94]

$$E_{kin} = \frac{\hbar^2}{2m}\frac{n_0 \pi R_z}{3}\left(-11\bar{\beta}^2 - \frac{26}{3} + \frac{11\bar{\beta}^4 + 16\bar{\beta}^2 + 8}{\sqrt{1+\bar{\beta}^2}}\arctan\left(1/\sqrt{1+\bar{\beta}^2}\right)\right) \quad (5.24)$$

The second term E_{trap} in Eq.(5.22) is the trap energy due to the harmonic trap

$$E_{trap} = \frac{m}{2}\omega_x^2 \int d^3 r \left|\Psi(\mathbf{r})\right|^2 (\rho^2 + \gamma^2 z^2) \quad (5.25)$$

This energy is evaluated to be

$$E_{trap} = \frac{2\pi}{3} n_0 m \omega_x^2 \frac{R_x^5}{\kappa}\left(\frac{4}{35} - \frac{2}{5}\bar{\beta}^2 - \frac{8}{3}\bar{\beta}^4 - 2\bar{\beta}^6 + \frac{2\gamma^2}{5\kappa^2}\left(\frac{1}{7} + \frac{23}{15}\bar{\beta}^2 + \frac{7}{3}\bar{\beta}^4 + \bar{\beta}^6\right)\right.$$
$$\left. + 2\bar{\beta}^2\left(\bar{\beta}^2 - \frac{\gamma^2}{5\kappa^2}(1+\bar{\beta}^2)\right)\left(1+\bar{\beta}^2\right)^{3/2}\arctan h\left(1/\sqrt{1+\bar{\beta}^2}\right)\right) \quad (5.26)$$

with the wave function given in Eq.(5.17).

E_{sw} is the energy due to the short range interaction

$$E_{sw} = \frac{g}{2}\int d^3 r \left|\Psi(r)\right|^4 \quad (5.27)$$

$$E_{sw} = \frac{8\pi}{15} g n_0^2 \frac{R_x^3}{\kappa}\left(\frac{2}{7} + \frac{107}{15}\bar{\beta}^2 + 16\bar{\beta}^4 + 9\bar{\beta}^6 - \right.$$
$$\left.\bar{\beta}^2\left(4 + 13\bar{\beta}^2 + 9\bar{\beta}^4\right)\sqrt{1+\bar{\beta}^2}\arctan h\left(1/\sqrt{1+\bar{\beta}^2}\right)\right) \quad (5.28)$$

Finally, the last term E_{dd} in Eq.(5.22) is the energy due to the dipolar interaction

$$E_{dd} = \frac{1}{2}\int d^3 r d^3 r' \left|\Psi(\mathbf{r})\right|^2 U_{dd}(\mathbf{r}-\mathbf{r}')\left|\Psi(\mathbf{r}')\right|^2 = \frac{1}{2}\int d^3 r n(\mathbf{r})\Phi_{dd}(\mathbf{r}) \quad (5.29)$$

where $\Phi_{dd}(\mathbf{r})$ is the dipolar mean field potential given in Sec.3.

The energies E_{kin}, E_{trap} and E_{sw} can be calculated analytically in a straightforward manner. To evaluate the dipolar energy, one can begin from substituting the density (5.17) in Eq. (5.29)

$$\begin{aligned} E_{dd} &= \frac{1}{2}\int d^3rd^3r' n_{bg}(\mathbf{r})U_{dd}(\mathbf{r}-\mathbf{r}')n_{bg}(\mathbf{r}') + \frac{1}{2}\int d^3rd^3r' n_{bg}(\mathbf{r})U_{dd}(\mathbf{r}-\mathbf{r}')n_{v}(\mathbf{r}') \\ &+ \frac{1}{2}\int d^3rd^3r' n_{v}(\mathbf{r})U_{dd}(\mathbf{r}-\mathbf{r}')n_{bg}(\mathbf{r}') + \frac{1}{2}\int d^3rd^3r' n_{v}(\mathbf{r})U_{dd}(\mathbf{r}-\mathbf{r}')n_{bg}(\mathbf{r}') \end{aligned} \tag{5.30}$$

Two cross terms between the vortex and background densities are identical so that the integral is invariant under exchange of the coordinates $\mathbf{r}$ and $\mathbf{r}'$. Thus, the dipolar energy functional can be written

$$\begin{aligned} E_{dd} &= \frac{1}{2}\int d^3rd^3r' n_{bg}(\mathbf{r})U_{dd}(\mathbf{r}-\mathbf{r}')n_{bg}(\mathbf{r}') + \int d^3rd^3r' n_{v}(\mathbf{r})U_{dd}(\mathbf{r}-\mathbf{r}')n_{bg}(\mathbf{r}') \\ &+ \frac{1}{2}\int d^3rd^3r' n_{v}(\mathbf{r})U_{dd}(\mathbf{r}-\mathbf{r}')n_{v}(\mathbf{r}') \end{aligned} \tag{5.31}$$

In these derivations it is assumed that the size of the vortex core is much smaller than the radius of the condensate. This is consistent with Thomas-Fermi approximation for the background parabolic density. The vortex-vortex part of the dipolar energy can be omitted since this has an extra factor of $\overline{\beta}^2$ in comparison to the cross term. The remaining two terms can be written as [94]

$$\begin{aligned} E_{dd} &\approx \frac{1}{2}\int d^3rd^3r' n_{bg}(\mathbf{r})U_{dd}(\mathbf{r}-\mathbf{r}')n_{bg}(\mathbf{r}') + \int d^3rd^3r' n_{v}(\mathbf{r})U_{dd}(\mathbf{r}-\mathbf{r}')n_{bg}(\mathbf{r}') \\ &= \frac{1}{2}\int d^3r n_{bg}(\mathbf{r})\Phi_{dd}^{bg}(\mathbf{r}) + \int d^3r n_{v}(\mathbf{r})\Phi_{dd}^{bg}(\mathbf{r}) \end{aligned} \tag{5.32}$$

The first term is the dipolar energy of the non-vortex condensate, while the second term is the dipolar interaction between the vortex and the background density profile. These terms have been reduced to single integrals of their own density

profiles. $\Phi_{dd}^{bg}(\rho,z)$ is the same potential as given by Eq. (3.25). The integrals are evaluated explicitly

$$\frac{1}{2}\int d^3 r n_{bg}(\mathbf{r})\Phi_{dd}^{bg}(\mathbf{r}) = -\frac{16\pi g n_0^2}{105\kappa}\varepsilon_{dd} R_x^3 f(\kappa) \tag{5.33}$$

and

$$\int d^3 r n_v(\mathbf{r})\Phi_{dd}^{bg}(\mathbf{r}) = -\frac{4\pi}{15} n_0^2 g\varepsilon_{dd}\frac{R_x^3}{\kappa}\bar{\beta}^2\left(\frac{122}{15}+\frac{68}{3}\bar{\beta}^2+14\bar{\beta}^4+\right.$$
$$\left.\frac{f(\kappa)}{15(\kappa^2-1)}\left[-62+245\kappa^2+30\bar{\beta}^2(2+15\kappa^2)+45\bar{\beta}^4(2+5\kappa^2)\right]-\right.$$
$$\left.(1+\bar{\beta}^2)^{3/2}\arctan h\left(\frac{1}{\sqrt{1+\bar{\beta}^2}}\right)\left[4+14\bar{\beta}^2+\frac{f(\kappa)}{\kappa^2-1}(-4+10\kappa^2+6\bar{\beta}^2+15\kappa^2\bar{\beta}^2)\right]\right) \tag{5.34}$$

The total energy $E_{trap}+E_{sw}+E_{dd}$ associated with the vortex-free Thomas-Fermi solution is given by [30]

$$E_0 = \frac{N}{14} m\omega_\perp^2 R_x^2\left(2+\frac{\gamma^2}{\kappa^2}\right)+\frac{15}{28\pi}\frac{N^2 g}{R_x^2 R_y}(1-\varepsilon_{dd} f(\kappa)) \tag{5.35}$$

E_0 is the ground state energy. E_{tot} is minimized with three variational parameters R_x, R_z and $\bar{\beta}$. Eberlein at. al. studied ^{52}Cr condensate with a single centered vortex case in Ref [94]. They found that in an oblate trap the dipolar interactions which are prodominantly repulsive raises the energy relative to the s-wave case. The dipolar interactions increases R_x and $\bar{\beta}$ sligthly above the pure s-wave value. But for large scattering lengths R_x and $\bar{\beta}$ of dipolar condensate get closer to the those of s-wave condensate since short range interactions are dominant. The aspect ratio of the condensate, κ, is reduced in the present of dipolar interactions because of magnetostriction effect.

5.2.2 Dipolar BEC with an Off-Axis Vortex

Consider a single straight vortex line at a position ρ_0 along the z-axis. In this case, the wave function, normalized to the total number of atoms $\int |\Psi(r)|^2 d^3r = N$, is given by

$$\Psi(\rho,\varphi,z) = n(r)e^{iS(\rho,\rho_0)} \tag{5.36}$$

where $n(r) = |\psi(r)|^2$ is the density. The expression of the phase $S(\rho,\rho_0)$ characterizing the circulating flow around the vortex line is given by [15]

$$S(\rho,\rho_0) = \arctan\left(\frac{y-y_0}{x-x_0}\right) \tag{5.37}$$

where $\rho_0^2 = x_0^2 + y_0^2$. The corresponding irrotational flow velocity is given by

$$\mathbf{v} = \frac{\hbar}{m}\nabla S(\rho,\rho_0) \tag{5.38}$$

There is a singularity on the vortex line, $\rho = \rho_0$, where the velocity diverges. However, the particle current density, $\mathbf{J} = n\mathbf{v}$, vanishes as $\rho \to \rho_0$. When a quantized vortex is present at the position ρ_0, the density drops to zero at the center of the vortex core whose size is determined by the parameter β. For a centered vortex in a BEC without dipole-dipole interaction, the parameter β is given by

$$\frac{\beta_{sw}}{R_x} = \left(\frac{d_\perp}{R_x}\right)^2 \tag{5.39}$$

where $d_\perp = \sqrt{\hbar/m\omega_\perp}$ is the mean oscillator strength. The TF limit holds when R_x is large compared to $d_\perp$. The TF length scale reads $\beta << d_\perp << R_x$. The vortex core size increases with ρ_0. The parameter $\beta_{sw}(\rho_0)$ characterizing the small vortex core at the position ρ_0 in a BEC without the dipole dipole interaction is [100]

$$\beta_{sw}(\rho_0) = \frac{\beta_{sw}}{\sqrt{1-\rho_0^2/R_x^2}} \tag{5.40}$$

Having written the expression of the phase, for a straight off-center vortex, the density $n(r)$ can be found. The repulsive interactions and the repulsive dipolar interaction (for oblate case) significantly expand the condensate, so that the kinetic energy associated with the density variation becomes negligible compared to the trap energy and interaction energies. In the TF regime, the density profile of a condensate with a straight off-axis vortex line at ρ_0 is given by [101]

$$n(\mathbf{r}) = n_0\left(1-\frac{\rho^2}{R_x^2}-\frac{z^2}{R_z^2}\right)\left(1-\frac{\beta^2}{|\rho-\rho_0|^2+\beta^2}\right) \tag{5.41}$$

where $n(\mathbf{r}) = 0$ when the right hand side is negative and β, R_x, and R_z are variational parameters that describe the size of the vortex core, and the radial and the axial sizes, respectively. Note that the density function (5.41) behaves like $|\rho-\rho_0|^2/\beta^2$ when $\rho << \beta$ and like $\left(1-\rho^2/R^2-z^2/L^2\right)$ when $\rho >> \beta$. These parameters will be calculated by minimizing the energy functional. The central density n_0 can be found using the normalization condition

$$n_0 = \frac{N\kappa\left[60R_x^2+25\overline{\beta}^2\left(4R_x^2\left(3In\left(\frac{2}{\overline{\beta}}\right)-4\right)+9\rho_0^2\left(3-2In\left(\frac{2}{\overline{\beta}}\right)\right)\right)\right]}{32\pi R_x^5} \tag{5.42}$$

An image vortex is not included because the form of the TF condensate density ensures that the particle current density vanishes at the surface.

Let the total angular momentum for a singly quantized vortex line along the trap axis at the position ρ_0 be L_z $\left(L_z = m\int rvn(r)d^3r\right)$. Then the corresponding energy of the system in the rotating frame is $E' = E - \Omega L_z$, where E is the energy in the non-rotating frame. By denoting the energy of the BEC in its ground state without a vortex by E_0 and the extra energy needed to generate a vortex by ΔE, then $E = E_0 + \Delta E$. The energy of the vortex state in the rotating frame can be written as

$$E' = E_0 + E_v - \Omega L_z \tag{5.43}$$

The critical rotational velocity is given by

$$\Omega_c = \frac{E_v}{N\hbar} \tag{5.44}$$

It should be noted that a vortex lattice starts to appear when the rotation frequency is further increased.

The total energy can be minimized with respect to the three variational parameters, R_x, R_z and β. The kinetic, trap, s-wave and dipole-dipole interactions energies are calculated separately for the density Eq.(5.42). Since β is small, the terms of order β^3 and higher can be neglected. The energy integral can be evaluated analytically up to the second order of ρ_0. Below the analytical energy expressions for small ρ_0 are given. When $\rho_0 = 0$, the results given in the previous section are found. Therefore, only the energy terms which depend on vortex displacement ρ_0 are given below. In the following section, numerical calculations for large ρ_0 will be performed in the TF limit. The kinetic energy due to the vortex displacement is

$$\Delta E_{kin} = \frac{\hbar^2 \pi n_0 R_x}{9\kappa m} 18\left(2 - \left(1 + 2\overline{\beta}^2\right) In\left(\frac{2}{\overline{\beta}}\right)\right)\overline{\rho}_0^2 \tag{5.45}$$

where

$$\overline{\rho}_0 \equiv \frac{\rho_0}{R_x} \tag{5.46}$$

Using the Eq.(5.25), the trapping energy is straightforwardly evaluated to be

$$\Delta E_{trap} = \frac{4\pi m n_0 \omega_\perp^2 R_x^5}{15\kappa^3} \frac{5\overline{\beta}^2}{12}\left(28\kappa^2 - 11\gamma^2 + 6In\left(\frac{2}{\overline{\beta}^2}\right)\left(\gamma^2 - 2\kappa^2\right)\right)\overline{\rho}_0^2 \tag{5.47}$$

In the similar way, the formula (5.27) yields the s-wave interaction energy

$$\Delta E_{sw} = -\frac{8\pi g R_x^3 n_0^2}{15\kappa} \frac{5\overline{\beta}^2}{6}\left(25 - 12In\left(\frac{2}{\overline{\beta}}\right)\right)\overline{\rho}_0 \tag{5.48}$$

The dipole-dipole interaction energy is calculated using Eq. (5.29). The density of an off axis vortex state is

$$n_v(\mathbf{r}) = -n_0 \frac{\beta^2}{\left|\rho - \rho_0\right|^2 + \beta^2}\left(1 - \frac{\rho^2}{R_x^2} - \frac{z^2}{R_z^2}\right) \tag{5.49}$$

Hence, the extra dipolar interaction energy with the second term of Eq. (5.29) becomes

$$\Delta E_{dd} = \frac{2\pi g \varepsilon_{dd} R_x^3 \overline{\beta}^2 n_0^2}{9\kappa}\left(50 - 24In\left(\frac{2}{\overline{\beta}}\right) + \frac{f(\kappa)}{\kappa^2 - 1}\left(6 + 69\kappa^2 - 36\kappa^2 In\left(\frac{2}{\overline{\beta}}\right)\right)\right)\overline{\rho}_0^2 \tag{5.50}$$

The energy expressions are obtained up to the second order of fractional vortex displacement, $\bar{\rho}_0$. Note that the central density n_0 in these expressions also includes $\bar{\rho}_0^2$ (5.42). Up to the order of $\bar{\beta}^2$, they agree with the results [94] in the limit $\rho_0 \to 0$.

As can be seen, the kinetic energy decreases with $\bar{\rho}_0$. The kinetic energy goes to zero as $\bar{\rho}_0 \to R$ since TF density vanishes at the surface. Note that the description of a vortex close to the boundary is outside the scope of the present approach, since TF approach doesn't work close to the surface. The dipole-dipole interaction increases with $\bar{\rho}_0$ for an oblate trap while decreases with $\bar{\rho}_0$ for a prolate trap. The kinetic energy depends on $\bar{\rho}_0^2$ while the dipolar, trap and the s-wave interaction energies depend on $\bar{\beta}^2\bar{\rho}_0^2$.

Before embarking on a specific example, the energy expressions should be studied qualitatively for an oblate trap. Firstly, it is investigated roughly how the total energy is distributed among kinetic, dipolar, trap and s-wave interaction energies. The ratio between the kinetic energy and the trap energy is of order $\bar{\beta}^2$; $E_{kin} \approx \bar{\beta}^2 E_{trap}$. The trap and the s-wave interaction energies are comparable to each other; $E_{sw} \approx E_{trap}$. The ratio between dipolar and the s-wave interaction energies is of order ε_{dd}; $E_{dd} \approx \varepsilon_{dd} E_{sw}$.

To investigate how the excess energy ΔE needed to generate a vortex is distributed consider first a central vortex, $\rho_0 = 0$. The excess energy for the trap, dipolar and s-wave interaction energies vary as $\bar{\beta}^2$. However the excess kinetic energy is of order the kinetic energy, $\Delta E_{kin} \approx E_{kin} \approx \bar{\beta}^2 E_{trap}$. Hence, $\Delta E_{kin} \approx \Delta E_{trap}$. The excess energy for dipole-dipole and s-wave interaction energies are negative. Hence, the effect of increasing dipole moment and scattering length is to decrease the critical angular velocity Ω_C. The relations between the excess energies for dipolar, trap and s-wave terms are given by $\Delta E_{dd} \approx \varepsilon_{dd} \Delta E_{sw}$ and $\Delta E_{trap} \approx -\Delta E_{sw}$.

The energy changes with the position of an off-axis vortex, $\bar{\rho}_0$. The kinetic energy and the trap energy decrease with $\bar{\rho}_0$ while the dipole-dipole and the s-wave interaction energies increase. Furthermore, the total energy decreases with $\bar{\rho}_0$.

If vortex bending effect is neglected, one can use the above energy expressions for a prolate trap with a straight vortex line. In this case, the dipolar interaction energy is negative. However, the excess energy for the dipolar interaction is positive. Hence, the effect of increasing dipole moment for a prolate trap is to increase the critical angular velocity Ω_C. Finally, the dipole-dipole interaction energy decreases with increasing $\bar{\rho}_0$. As a result, the effect of dipolar interaction is to repel an off axis vortex away from the trap center for a prolate trap while attract it to the trap center for an oblate trap.

In what follows, an explicit example for a straight off-axis vortex for an oblate trap will be given.

5.2.3 Results

In this section, a dipolar BEC with a single vortex in an oblate trap including 150000 ^{52}Cr atoms is examined. The numerical values are taken from the reference [94] to compare the off-center vortex to the central vortex. The trap frequencies are $\omega_\perp = 2\pi \times 200\,\text{rad/s}$ and $\omega_z = 2\pi 1000$ rad/s for $\gamma = 5$. The harmonic oscillator length of the trap along the radial direction is $d_\perp = 0.986\mu m$. The magnitude of the magnetic dipole interaction for ^{52}Cr is $C_{dd} = \mu_0 (6\mu_B)^2$. For small values of ρ_0, the analytical results obtained in the previous section is used. For large values ρ_0, numerical computation within the TF limit will be performed.

Three variational parameters, β, κ and R_x are analyzed firstly. The density of the condensate drops to zero at the center of the vortex core whose size is equal to β. It is very small compared to the radial size of the condensate. The smallness of $\bar{\beta}$ ensures that the vortex affects the density only the immediate

vicinity of the core. Fig.5.1 depicts the fractional vortex core size, $\overline{\beta} = \beta / R_x$, versus the scattering length. The solid curve corresponds to a central vortex, while the dashed curve to an off-center vortex with $\rho_0 = 0.4R_x$. The parameter $\overline{\beta}$ is bigger in the presence of an off-axis vortex. As can be seen from the figure, the fractional vortex core size decreases with increasing scattering length. This can be understood as follows. The radial size increases as scattering length is enlarged. The vortex core size is inversely proportional to radial size. So, it is concluded that $\overline{\beta}$ decreases with a_s.

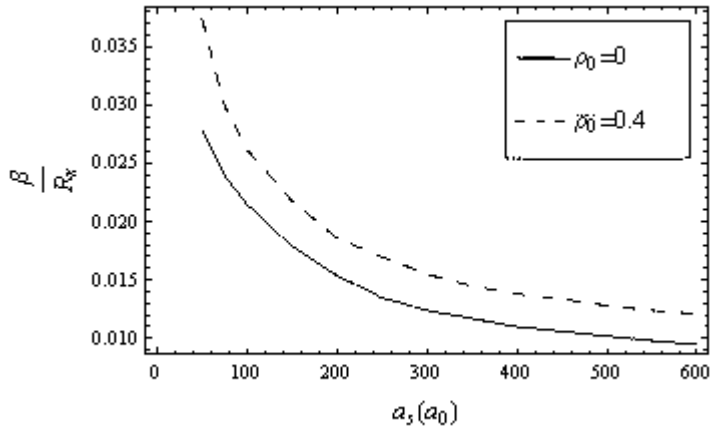

Fig. 5.1. The fractional vortex core size for cental $(\overline{\rho}_0 = 0)$ and off-axis $(\overline{\rho}_0 = 0.4)$ vortices versus the scattering length for a dipolar BEC. The scattering length is measured in units of Bohr radius, a_0, and $\gamma = 5$.

Similarly, Fig.5.2 and Fig.5.3 show the aspect ratio κ and the radial size (right) of the condensate R_x versus the scattering length, respectively for $\rho_0 = 0$ and $\rho_0 = 0.4R_x$. Contrary to the case of vortex core size β, the parameters κ and R_x don't change appreciably with ρ_0 when $a_s > 50a_0$, where a_0 is Bohr radius. Hence, the curves lie on top of each other in figures.

Figures 5.4 and 5.5 show the total energy as a function of vortex position for fixed $a_s = 100a_0$ and scattering length for fixed $\overline{\rho}_0 = 0.2$ in a non-rotating oblate trap $(\Omega = 0)$, respectively. The solid curve corresponds to a condensate with s-wave plus dipolar interactions while the dashed line corresponds to a

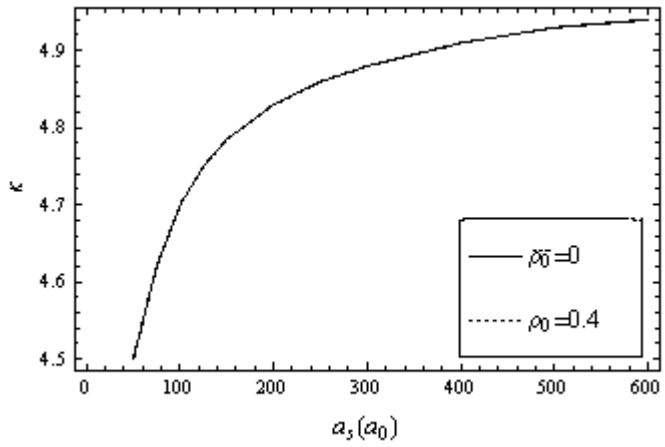

Fig. 5.2. For $\bar{\rho}_0 = 0$ and $\bar{\rho}_0 = 0.4$, the aspect ratio of a condensate with a vortex in an oblate trap as a function of the scattering length. The scattering length is measured in units of Bohr radius, a_0, and $\gamma = 5$.

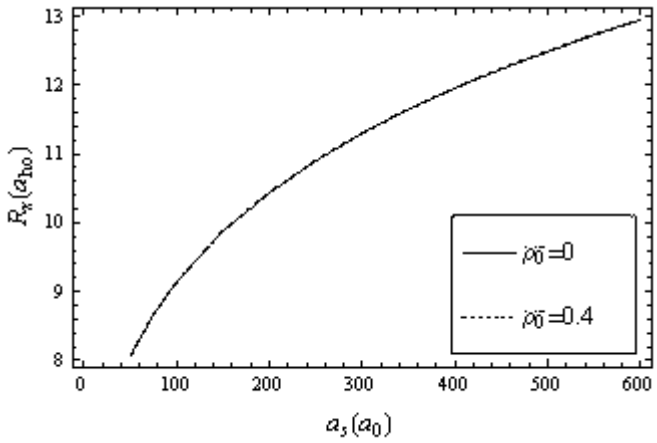

Fig. 5.3. The radial size of a dipolar BEC with a vortex in an oblate trap for $\bar{\rho}_0 = 0$ and $\bar{\rho}_0 = 0.4$ as a function of the scattering length. R_x is measured in units of d and the scattering length is measured in units of Bohr radius, a_0, and $\gamma = 5$.

condensate with pure s-wave interaction. The total energy is bigger when $\varepsilon_{dd} \neq 0$. This is because the dipole-dipole interaction energy is positive in an oblate trap. The total energy of the system attains a maximum when $\rho_0 = 0$ for both cases. As the off-axis vortex moves to the edge of the condensate, the total energy decreases. More specifically, the kinetic and trap energies decrease with $\bar{\rho}_0$ while

the dipolar and s-wave interaction energies increase with $\bar{\rho}_0$. In fact, higher than a specific value of ε_{dd}, dipolar interaction becomes more dominant, so total energy increases with $\bar{\rho}_0$. We calculate that this happens when $\varepsilon_{dd} > 1$. As mentioned in [94], however, the condensate enters an instability region when $\varepsilon_{dd} > 1$. As can be seen from the Fig.5.5, the energy differences between the two cases decreases when the scattering length is increased. This is because ε_{dd} is decreased with increasing scattering length.

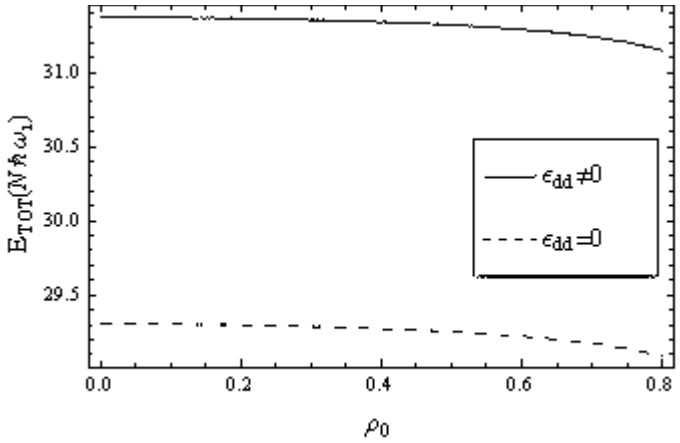

Fig. 5.4. The total energy of a non-rotating dipolar BEC with a vortex in an oblate trap as a function of vortex displacement. $\gamma = 5$ and the scattering length is $a_s = 100a_0$. The solid curve indicates the s-wave interaction.

For the investigation of the vortex generation, not the total energy but the excess energy ΔE associated with the presence of an off-axis straight vortex is more important. Fig.5.6 compares the excess energy of the condensates with $\varepsilon_{dd} = 0.15$ (solid curves) and $\varepsilon_{dd} = 0$ (dashed curves) as a function of a fractional vortex displacement. Different curves represent different fixed values of the external angular velocity Ω. The top solid and dashed curves correspond to $\Omega = 0$, where increases as one moves towards the lowest curve with $\Omega = 0.08\omega_\perp$ and $\Omega = 0.14\omega_\perp$. Note that the critical rotation frequency is $\Omega_C = 0.124\omega_\perp$

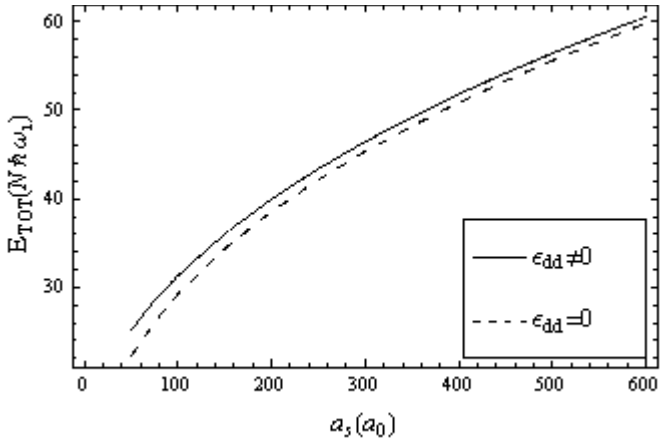

Fig. 5.5. The total energy of a non-rotating dipolar BEC with a vortex with $\bar{\rho}_0 = 0.2$ as a function of the scattering length. The solid (dashed) curve is for the condensate with both dipolar and s-wave interactions (only s-wave interaction), and $\gamma = 5$.

$\left(\Omega_C = 0.119\omega_\perp\right)$ when $\varepsilon_{dd} = 0$ $\left(\varepsilon_{dd} = 0.15\right)$. As can be seen from the figure, the dipolar interaction lowers ΔE compared to the pure contact interaction. It is of great importance to note that although dipolar interaction is positive for an oblate trap, the excess dipolar energy is negative. As $\bar{\rho}_0$ is increased, the curves for $\varepsilon_{dd} = 0.15$ and $\varepsilon_{dd} = 0$ start to coincide. The top two curves show that the excess energy ΔE decreases monotonically with increasing $\bar{\rho}_0$, with negative curvature at $\bar{\rho}_0 = 0$. So, a central vortex is unstable to infinitesimal displacements. The presence of dissipation will move an off-axis vortex toward the edge of the condensate. If the trap is rotated with angular velocity, Ω, then the energy of a vortex decreases. Inspection of Fig.5.6 reveals that with increasing rotation speed, the function ΔE flattens. At a special value of rotation frequency, Ω_m, curvature of the function ΔE becomes zero at $\bar{\rho}_0 = 0$. Hence, above an angular velocity Ω_m, the vortex attains a local minimum. The central position is not globally stable but locally stable. One of the results of this paper is that the presence of dipolar interaction lowers Ω_m for an oblate trap. Consider the lowest curves in Fig.5.6. In this case, appearance of a vortex becomes energetically favorable since $\Delta E < 0$. The central vortex is both locally and globally stable relative to the vortex-free

state. A vortex initially placed off-center will follow a path of constant energy under the action of the Magnus force, which is proportional to the gradient of the energy in the radial direction. The precession velocity of a displaced vortex of a nonrotating trap increases with the vortex displacement. Hence, a vortex near the surface precesses more rapidly than one near the center. Another result of this study is that the precession velocity of a displaced vortex is lowered in the presence of the dipolar interaction in an oblate trap. On the contrary, it is raised in a prolate trap (ignoring vortex bending effect). Note that the precession velocity around the center for a nonrotating trap, ω, can be calculated using $\omega = \frac{\partial E}{\partial L} = \frac{\partial E/\partial \overline{\rho}_0}{\partial L/\partial \overline{\rho}_0}$, where E is the energy and L is the angular momentum [15, 105]. For a condensate in rotational equilibrium at angular velocity, the original precession frequency is altered to $\omega \to \omega - \Omega$ [15].

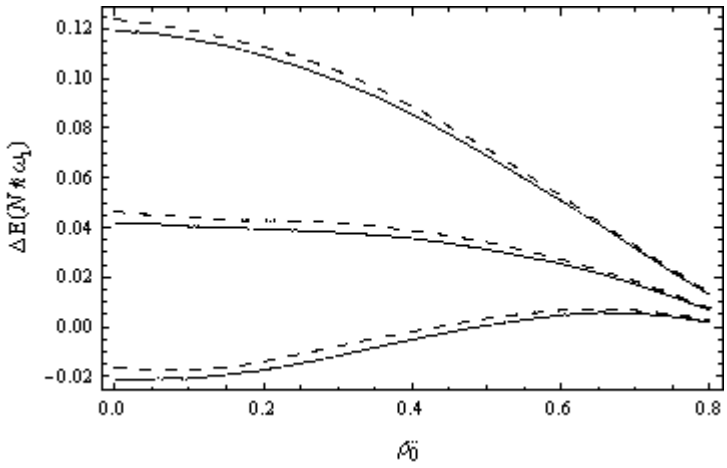

Fig. 5.6. The increased energy ΔE in units of $N\hbar\omega_\perp$ in the rotating frame as a function of a fractional vortex displacement in an oblate trap. The solid (dashed) curves correspond to $\varepsilon_{dd} = 0.15$ $(\varepsilon_{dd} = 0)$. Different curves represent different fixed values of the external angular velocity Ω. The top solid and dashed curves corresponds to $\Omega = 0$, where Ω increases as one moves towards the lowest curve with $\Omega = 0.08\omega_\perp$, $\Omega = 0.14\omega_\perp$.

Fig.5.7 shows the critical angular velocity of the condensate for $\gamma = 5$ and $\gamma = 10$. The critical angular velocity above which a vortex state is energetically favorable depends on γ. As can be seen, Ω_C increases with decreasing γ. For stirring frequencies below Ω_C, no vortex can be nucleated. The presence of dipole dipole interaction decreases Ω_C for an oblate trap.

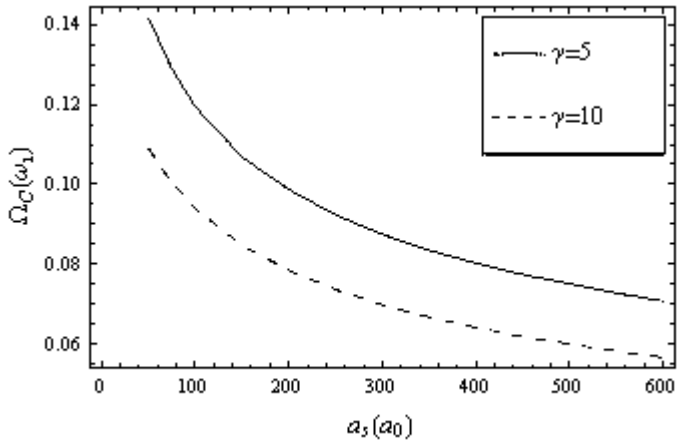

Fig. 5.7. The critical angular velocity of a condensate with a vortex for $\gamma = 5$ and $\gamma = 10$ as a function of the scattering length. Ω_c is measured in units of $\omega_\perp$.

It is found that Ω_C, Ω_m and precession velocity decrease (increase) in an oblate (a prolate) trap. This can be understood simply as follows. The dipolar mean field potential has a parabolic profile $\Phi_{dd}^{bg}(\rho,z) = \frac{n_0 C_{dd}}{3R_z^2}\left(1.21R_z^2 - 0.04\rho^2 - 1.83z^2\right)$ when $\varepsilon_{dd} = 0.15$ and $\gamma = 5$ [102]. This potential has the same inverted parabola shape as in the case of contact interactions. So, we conclude that there is a similarity between dipolar and non-dipolar BEC in the TF regime. The difference is in the expressions for the radial and axial size. It is well known that the contact interaction with positive scattering length decreases the critical angular frequency Ω_C ($\Omega_C = \omega_\perp$ for a noninteracting trapped gas). In the similar way, $\Omega_m/\omega_\perp$ and precession velocity decrease with increasing scattering length. So, the inclusion of dipolar interaction in an oblate trap reduces Ω_C, Ω_m, and precession velocity in the TF regime. Furthermore, if

vortex bending effect is ignored, the mean field dipolar potential for a prolate trap has the same form as the mean field contact potential with negative scattering length. In contrast to the case for repulsive interactions, Ω_C, Ω_m and precession velocity increase in the presence of attractive contact interactions.

5.3 Vortex Dipole

A vortex dipole is a pair of vortices of equal and opposite circulation situated symmetrically about the origin. Under linear motion of a localized repulsive Gaussian potential, a vortex pair formation with opposite circulation is possible if the potential is moved at a velocity above a critical value [103]. In the experiments [104, 105], a laser beam focused on the center of the cloud was scanned back and forth along the axial dimension of the cigar shaped condensate. Vortices were not observed directly, but the strong heating only above a critical velocity was measured. It was shown that the measurement of significantly enhanced heating is due to energy transfer via vortex formation [106]. Recently, experimental observations of singly and multiply charged quantized vortex dipoles in a highly oblate BEC with ^{87}Rb were reported by Neely et al. [107]. In the experiment, vortex dipoles were created by forcing superfluid around a repulsive Gaussian obstacle using a focused blue-detuned laser beam. The beam was initially located on the left of the trap center and the harmonic potential was translated at a constant velocity until the obstacle ends up on the right of the trap center. At the same time, the height of the obstacle is linearly ramped to zero, leading to the generation of a vortex dipole that is unaffected by the presence of an obstacle or by heating due to moving the obstacle through the edges of the BEC where the local speed of sound is small. Vortex dipoles were observed to survive for many seconds in the condensate without self-annihilation. The experiment also provided evidence for the formation of multiply charged vortex dipoles. The authors in [107] noted that the theoretical predictions of critical velocity for vortex pair formation in [108] are in good agreement with the experimental results. The critical velocity is given by the minimum of the ratio of the energy to the momentum of the vortex dipole

$$v_C = \min\left(\frac{E(I)}{I}\right) \tag{5.51}$$

where E(I) is the energy of an elementary excitation with linear momentum (or impulse) I [109]. When the object moves at a velocity above a critical value, the superfluid flow becomes unstable against the formation of quantized vortices, which give rise to a new dissipative regime [68, 110, 111]. Pairs of vortices with opposite circulation are generated at opposite sides of the object. The vortex and antivortex (vortex dipole) propel each other in a direction perpendicular to the line joining them [112, 113]. For vortex dipole in a trap, mutually driven or inhomogeneity-driven motion can dominate depending on the distance between the vortices. This causes to the fact that a vortex dipole with the same dipole direction can propagate in one of the two opposite directions, depending on the vortex separation [114]. Recently, instead of removing the trapping potential and expanding the condensate to make the vortex cores optically resolvable, Freilich et al. experimentally observed the real-time dynamics of vortex dipoles by repeatedly imaging the vortex cores [115]. Other vortex cluster configurations which are stationary in nonrotating BEC, such as vortex tripole and quadrupole, have been predicted in [116-118]. Vortex tripoles have also been observed experimentally [119]. Several theoretical investigations have been reported for the generation [120-128], stability [129, 130], and stationary configurations of vortex dipoles [116, 131]. In Ref. [126], vortex dipole dynamics in the weak interaction region has been studied and conditions under which a vortex pair annihilates and is created again have been reported. In addition, fully analytic expressions of the angular momentum and energy of a vortex dipole in a trapped two dimensional BEC were obtained [132].

GP equation can be written in scaled harmonic oscillator units (h.o.u.) for simplicity. In this system, the units of length, time, and energy are $\sqrt{\frac{\hbar}{2m\omega_\perp}}$, $\frac{1}{2m\omega_\perp}$ and $\hbar\omega_\perp$ respectively. Hence the GP equation in h.o.u reads [108]

$$\left(-\nabla^2 + V_T' + g'\left|\psi'(\mathbf{r})\right|^2\right)\psi'(\mathbf{r}) = \mu'\psi'(\mathbf{r}) \tag{5.52}$$

where $\mu' = \mu/\hbar\omega_\perp$, and the dimensionless interaction parameter g' is given by

$$g' = 2\sqrt{\frac{2m\omega_\perp}{\hbar}}\frac{mN}{\hbar^2}g \tag{5.53}$$

The normalization of $\psi'(\mathbf{r})$ chosen here is $\int|\psi'(\mathbf{r})|^2 d^3r = 1$. For large g' the solution to the GP equation without vortices is well approximated by the TF limit. In TF limit, the wave function in h.o.u. is given by

$$\psi'(\mathbf{r}) = \frac{1}{g'}\left(\mu' - \frac{\rho'^2 + \kappa^2 z'^2}{4}\right)^{1/2} \tag{5.54}$$

Substituting the wave function $\psi(\mathbf{r}) = \sqrt{n(\mathbf{r})}e^{i\varphi}$ into the GP equation and equating imaginary and real terms leads to the following hydrodynamics equations in h.o.u.:

$$\left(-\nabla^2 + (\nabla\varphi)^2 + \frac{\rho'^2 + \gamma^2 z'^2}{4} + g'n\right)\sqrt{n} = \mu'\sqrt{n} \tag{5.55}$$

$$-\sqrt{n}\nabla^2\varphi - 2\nabla\sqrt{n}.\nabla\varphi = 0 \tag{5.56}$$

In TF approximation, firstly the continuity equation Eq. (5.56) is solved for $\varphi(r)$, and then using that solution in Eq. (5.55) $n(r)$ is determined, neglecting the $\nabla^2 n(r)$ term. The energy function of the condensate is

$$E = \int d^3r\left(\left(\nabla\sqrt{n}\right)^2 + \left(\sqrt{n}\nabla\varphi\right)^2 + \frac{\rho'^2 + \kappa^2 z'^2}{4}n + \frac{g'}{2}n^2\right) \tag{5.57}$$

The total expression of impulse using the momentum of the condensate

$\mathbf{P} = \frac{i\hbar}{2}\left[(\nabla\psi^*)\psi - \psi^*\nabla\psi\right]$ is

$$I = \int d^3r|\mathbf{P}| = \hbar\int d^3rn(\mathbf{r})|\nabla\phi| \tag{5.58}$$

The critical velocity for vortex pair creation using the Landau criterion is defined as [108]

$$v_c = \frac{E_1 - E_0}{I_1} \tag{5.59}$$

Here E_1 and I_1 are the energy and impulse of vortex state whereas E_0 is the energy of non-vortex state.

5.3.1 The Critical Velocity in Nondipolar BEC

Analytical evaluation of these energy, impulse and critical velocity functions were performed by Crescimanno et al. in two dimensions for a nondipolar condensate [108]. They adopted the ansatz that the two vortices are far enough from each other, but near enough to the trap center. The total phase advance about the vortex pair is the sum of the phase advances of each vortices. This ansatz is equivalent to the condition $\frac{1}{\mu'} < d^2 < \mu'$ in h.o.u, where d is the distance between the vortex cores. The phase function $\varphi(r)$ satisfies $\varphi(r) = 0$ everywhere outside the vortex cores, which implies from the continuity expression Eq.(5.56) that $\nabla\sqrt{n}.\nabla\varphi$ must be zero in this region. $n(r)$ should satisfy the continuity equation near the vortex cores and far away from the vortices, because radial gradients of the phase vanish as $1/R^2$. In addition, the spatial integral of the continuity equation vanishes identically. The ansatz for the phase wave function of the vortex pair is [108]

$$\phi(r) = l\left(\arctan\left(\frac{\sin\theta - \frac{d}{2\rho'}}{\cos\theta}\right) - \arctan\left(\frac{\sin\theta + \frac{d}{2\rho'}}{\cos\theta}\right)\right) \tag{5.60}$$

where l is the vorticity. The condensate velocity is given by $v(\mathbf{r}) = \frac{h}{m}\nabla\varphi(\mathbf{r})$. The condensate wave function envelope is found to be [108]

$$n(\mathbf{r}) = \frac{1}{g'}\left(\mu' - \frac{\rho'^2}{4} - \frac{d^2 l^2}{\rho'^2 d^2 \cos^2\theta + \left(\rho'^2 - d^2/4\right)^2}\right) \tag{5.61}$$

The last term in this equation is the kinetic energy contribution. Excluding the vortex core regions from the domain complicates the analytic evaluation of energy and impulse precisely where the TF approximation fails. To prevent this difficulty, $\eta = \frac{l^2 d^2}{\mu'}$ is added to the denominator of Eq.(5.61) [108]. Thus, $n(\mathbf{r})$ is written as

$$n(\mathbf{r}) = \frac{1}{g'}\left(\mu' - \frac{\rho'^2}{4} - \frac{d^2 l^2}{\rho'^2 d^2 \cos^2\theta + \left(\rho'^2 - d^2/4\right)^2 + \eta}\right) \tag{5.62}$$

This regulated expression is confirmed by the observation that for vortex pair not too far from the trap center $\left(d^2 < \mu'\right)$, the contribution to $\sqrt{n(\mathbf{r})}$ from the kinetic energy term $\left|\nabla\varphi\right|^2$ is never larger than μ' [108].

The normalization of Eq. (5.54) for non-vortex case in two dimensions gives

$$\mu = \mu_0 = \left(\frac{g'}{2\pi}\right)^{\frac{1}{2}} \tag{5.63}$$

The integration is performed to the maximum radius $R_{TF} = 2\sqrt{\mu}$. Inserting Eq. (5.63) into normalization expression gives

$$\frac{g'}{2\pi} = \mu^2 - l^2 In\left(\frac{1+\frac{\mu d^2}{l^2}}{1+\frac{d^2}{8\mu}}\right) + ... \tag{5.64}$$

where the spatial integration is performed out to the Thomas-Fermi condensate edge, which for large g' is $R_{TF} = 2\sqrt{\mu} - \left(l^2 d^2\right)/16\mu^{5/2} + ...$. For the energy of non-vortex state, Eq.(5.54) is inserted into Eq.(5.57) and found

$$E_0 = \frac{4\pi\mu_0^3}{3g'} \tag{5.65}$$

To find the vortex pair energy, the Eq. (5.61)-(5.63) are substituted into energy equation. The result is

$$E_n = \frac{\pi}{g'}\left(\mu^2 R_{TF}^2 - \frac{R_{TF}^6}{48}\right) - \frac{d^2 l^2}{8g'}\left(\frac{8\mu^2}{1+d^2\mu/l^2} + In\left(\frac{R_{TF}^4 \mu^2\left(1+d^2/2R_{TF}^2\right)}{l^4\left(1+d^2\mu/l^2\right)}\right)\right) + ... \tag{5.66}$$

To find the impulse of the system Eq.(5.61) and the gradient of phase function Eq. (5.60) is inserted into Eq. (5.57) for large g'

$$I_n = \frac{ld\mu_0\pi}{g'} In\left(\frac{64\mu_0}{ed^2}\right) \tag{5.67}$$

It is found in Ref [108] that the largest contribution to the spatial impulse integral comes at large *R*, and is thus dependent on the condensate size as well as the vortex pair charge magnitude and separation. The impulse for vortex pair creation vanishes in the small *d* limit like energy, and is proportional to the vortex charge. The results for the energy and impulse gives the critical velocity v_c of the vortex pair

$$v_c = \frac{2}{d}\frac{In\left(d^2\mu_0\right)}{In\left(\frac{64\mu_0}{ed^2}\right)} \tag{5.68}$$

Crescimanno et al. [108] showed that the critical velocity expression given above was in good agrement with the experimental results of Ketterle *et al.* [104, 105].

5.3.2 The Critical Velocity in Nondipolar BEC

For dipolar condensate, dipolar interaction energy should be added to GP equation in h.o.u:

$$\left(-\nabla^2 + V_T' + g'\left|\psi'(\mathbf{r})\right|^2 + \Phi'_{dd}\right)\psi'(\mathbf{r}) = \mu'\psi'(\mathbf{r}) \tag{5.69}$$

where $\Phi'_{dd} = \Phi_{dd}\left(g \to g'\right)$. In h.o.u, the dipolar mean-field potential inside the condensate in the TF approximation is given by [39]

$$\Phi_{dd}(\mathbf{r}) = n_0 g' \varepsilon_{dd}\left(\frac{\rho'^2}{R_x'^2} - \frac{2z'^2}{R_z'^2} - f(\kappa)\left(1 - \frac{3}{2}\frac{\rho'^2 - 2z'^2}{R_x'^2 - R_z'^2}\right)\right) \tag{5.70}$$

where $n_0 = \mu'/g'$ and the scaled lengths $R_x' = \sqrt{2m\omega_\perp/\hbar}R_x$ and $R_y' = \sqrt{2m\omega_\perp/\hbar}R_y$ are the radial and axial sizes of the condensate in h.o.u., respectively. The solution of this integro-differential equation was presented by Eberlein et al. in TF regime [39] and a parabolic density is an exact solution for GP equation as discussed in the Section [4.4].

The hydrodynamic equation in dipolar condensates are written as

$$\left(-\nabla^2 + (\nabla\varphi)^2 + \frac{\rho'^2 + \gamma^2 z'^2}{4} + g'n + \Phi_{dd}\right)\sqrt{n} = \mu'\sqrt{n} \tag{5.71}$$

$$-\sqrt{n}\nabla^2\varphi - 2\nabla\sqrt{n}.\nabla\varphi = 0 \tag{5.72}$$

where the continuity equation is the same as nondipolar condensate. The phase function is also same function given by Eq.(5.60). It is reasonable to approximate the TF density in h.o.u. by

$$n(\mathbf{r}) = \frac{1}{g'}\left(\mu' - \frac{\rho'^2 + \kappa^2 z'^2}{4}\right) \tag{5.73}$$

The expression of total energy of the condensate in h.o.u is given by

$$E = \int d^3 r \left(\left(\nabla\sqrt{n}\right)^2 + \left(\sqrt{n}\nabla\varphi\right)^2 + \frac{\rho^2 + \kappa^2 z^2}{4} n + \frac{g'}{2} n^2 + \frac{1}{2}\Phi'_{dd} n \right) \tag{5.74}$$

In the following subsection, the critical velocity of a dipolar condensate in an oblate trap is calculated. As the resulting equations for v_c are complicated due to dipoar term, it is necessary to obtain them numerically for given as, ε_{dd}, κ. A comparision the critical velocities of dipolar and non-dipolar condensates is made.

5.3.3 Results

In this section, within the TF regime we numerically calculate the critical velocity for a vortex pair formation in a dipolar BEC. A dipolar gas containing 150000 ^{52}Cr atoms is examined in an oblate trap with trap frequencies $\omega_\perp = 2\pi \times 200$ rad/s, $\omega_z = 2\pi \times 1000$ rad/s, so the trap aspect ratio is $\gamma = 5$. The magnitude of the scattering length for ^{52}Cr is $105a_B$ (a_B is the Bohr magneton). Hence the dipolar interaction strength for ^{52}Cr atoms is $\varepsilon_{dd} \approx 0.15$. The vortex separation d satisfies the condition $\frac{1}{\mu'} < d^2 < \mu'$, where the scaled chemical potential, μ', decreases very sligthly with d. The scaled chemical potential depends alson on ε_{dd}. For example, it is 38, 42 in h.o.u. for $\varepsilon_{dd} = 0$ and $\varepsilon_{dd} = 0.15$, respectively. Hence, d is taken within the range between 0.5 and 6, $0.5 < d < 6$, for both dipolar and non-dipolar condensates. The dipole-dipole interaction decreases the chemical potential. Below, the numerical integrations of

energy and impulse functional (5.57, 5.58) is performed to find the critical velocity of vortex pair formation (5.59).

It is well known that condensate aspect ratio, κ, decreases with increasing ε_{dd} in an oblate trap [38]. Minimizing the energy functional of the dipolar condensate, it is found that κ increases slightly with d. For example, κ is between 4.73 and 4.76 when *d* is between 0.5 and 6, respectively for $\varepsilon_{dd} = 0.15$.

Before embarking on a specific example, it is convenient to study the energy expressions qualitatively for an oblate trap. The trap and the s-wave interaction energies are comparable to each other; $E_{sw} \approx E_{trap}$. The ratio between dipolar and the s-wave interaction energies is of order ε_{dd}; $E_{dd} \approx \varepsilon_{dd} E_{sw}$. Secondly, consider the distribution of the excess energy $\Delta E = E_l - E_0$ needed to generate a vortex. For fixed *l*, the main contribution to the excess energy comes from the kinetic energy due to the phase variation. The excess kinetic energy, ΔE, is of order the kinetic energy since E_0 is zero in TF limit. The first two terms in (5.57) are the kinetic energy due to the density variation and the phase variation. The first term is neglected in TF approximation while the second term changes significantly with vortex separation *d*. The other terms in the energy expression change slightly with *d* since the correction to the density is very small.

To find the critical velocity v_c, the ratio of excess energy to the impulse is needed. The impulse of vortex state *I* depends strongly on *d* and ε_{dd} since it scales as d/R^2 (5.58). It decrease with ε_{dd}, since the dipolar interaction decreases *d* and stretches the cloud radially in an oblate trap.

The critical velocity v_c decreases with increasing separation *d* for a non-dipolar condensate [108]. This is because the TF density is a maximum at the trap center and reduces with the distance away from the trap center. The critical velocity is expected decreases also with *d* for a dipolar BEC since parabolic form of density retains in the case of dipolar interaction. Fig.5.8 plots the critical velocity v_c as a function of vortex separation for $\varepsilon_{dd} = 0$ (solid curve) and for $\varepsilon_{dd} = 0.15$ (dashed curve). The critical velocity is between 2.15-1.25 mm/s for $\varepsilon_{dd} = 0.15$, and 2.24-1.27 mm/s for $\varepsilon_{dd} = 0$ in the range 0.5 < d < 6.

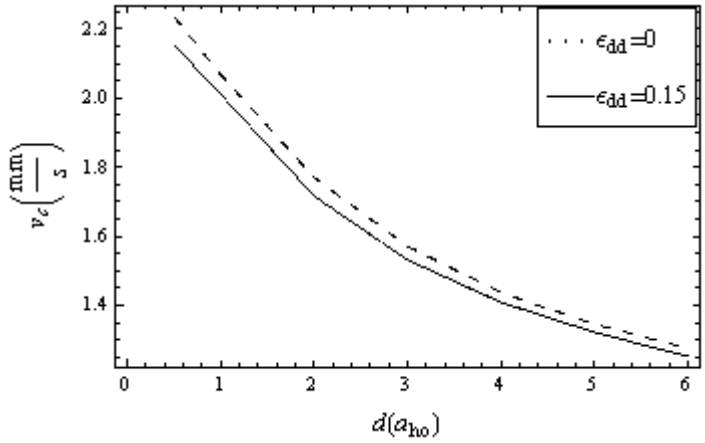

Fig. 5.8. The critical velocity, v_c (mm/s), for $\varepsilon_{dd} = 0$ (solid) and $\varepsilon_{dd} = 0.15$ (dashed) as a function of d in units of h.o.u. for an oblate trap with $\gamma = 5$

Fig. 5.9 shows the critical velocity as a function of ε_{dd} for fixed $d = 1$. The solid curve shows singly quantized vortex dipole while the dashed curve shows doubly quantized vortex dipole. The effect that v_c is decreased with increasing ε_{dd} in an oblate trap is the first main result of this study. It is energetically less expensive to nucleate a vortex in an oblate dipolar Bose-Einstein condensate than in a condensate with only contact interactions. At first sight, this might seem counterintuitive since the dipole-dipole interaction energy is positive in an oblate trap. It is remarkable to note that although dipolar interaction is positive for an oblate trap, the excess dipolar energy is negative. This situation is similar to thermodynamical critical angular velocity, Ω_c, for the onset of a vortex. Even though the interaction is positive for $a_s > 0$, Ω_c decreases with a_s. Qualitatively, increasing a_s and ε_{dd} increases the radial dimension R and the corresponding interaction energies decreases since they vary as R^{-3}.

The nucleation of multiply charged vortex dipoles was observed for trap translation velocities well above v_c in the experiment [107]. Furthermore, it was observed that the vortices exhibit periodic orbital motion and vortex dipoles may exhibit lifetimes of many seconds, much longer than a single orbital period [107]. Fig.5.9 compares the critical velocity for singly and doubly quantized vortex dipole. As expected, v_c is bigger for doubly quantized vortices.

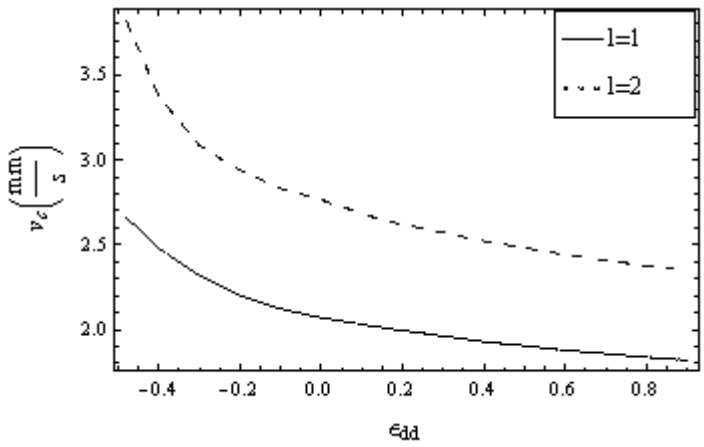

Fig. 5.9. The critical velocity, v_c (mm/s), for d = 1 in units of h.o.u. as a function of ε_{dd} for an oblate trap. The solid (dashed) curve is for singly (doubly) quantized vortex dipole, and $\gamma = 5$.

On the investigation of a vortex dipole, not only v_c, but also the ratio v_c/c is of importance. Here c is the speed of sound [133]

$$c = \sqrt{\frac{n_0}{m} g\left(1 + \varepsilon_{dd}\left(3\cos^2\alpha - 1\right)\right)} \tag{5.75}$$

where α is the angle between directions of the wave vector and the dipoles. This relation can be derived using $c^2 = \frac{1}{m}\frac{\partial p}{\partial n}$, where $n \approx N/V$ is the condensate density for a uniform system in a box of volume V and $p = -\left(\frac{\partial E}{\partial V}\right)_N$ is the pressure and E is the total energy [134]. Suppose the direction of the phonon wave vector is perpendicular to the orientation of the dipoles $(\alpha = \pi/2)$. In this case, the speed of sound becomes $c = \sqrt{\frac{n_0}{m} g\left(1 - \varepsilon_{dd}\right)}$. Remarkably, both v_c and c decrease with ε_{dd}. However, the ratio v_c/c increases with ε_{dd}. As ε_{dd} goes to one, the critical velocity approaches to the speed of sound. In Fig.5.10, v_c/c versus ε_{dd} is plotted for singly (solid curve) and doubly quantized vortex

dipoles (dashed curves) for fixed $d = 1$. The effect that v_c/c is increased with increasing ε_{dd} in an oblate trap is the second main result of this study. The ratio v_c/c for singly quantized vortices are found to be between 0.16−0.31 for dipolar condensate with $\varepsilon_{dd} = 0.15$ and 0.15−0.28 for non-dipolar condensate in the range $6 > d > 0.5$.

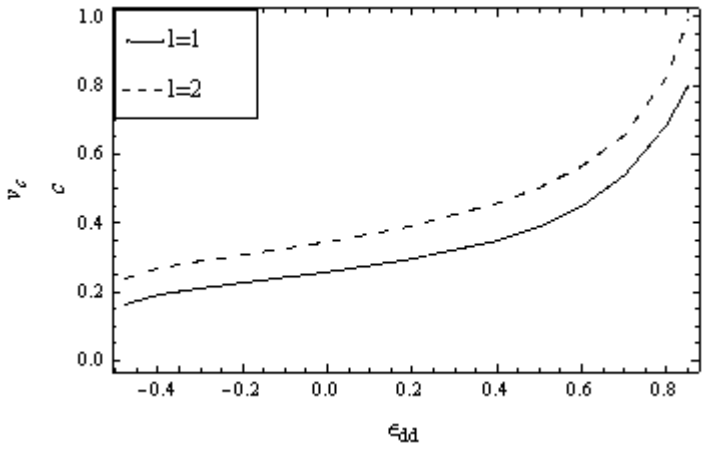

Fig. 5.10. The ratio of critical velocity to the speed of sound, v_c/c , for d = 1 in units of h.o.u. as a function of ε_{dd} for an oblate trap with $\gamma = 5$. The solid (dashed) curve is for singly (doubly) quantized vortex dipole.

6. CONCLUSIONS

In this thesis, the propeties of dipolar interactions have been examined and the different effects of dipolar and s-wave interactions on BEC have been discussed. The main effect of the dipolar interactions on the ground state of the system is the deformation of the condensate. The anisotropic character of dipolar interactions leads to this deformation, and it depends on the specific trap that is considered. *Cr* atoms are very proper for studying dipolar condensates since they have very large magnetic dipole moments. Thus, the condensate of ^{52}Cr atoms has been considered in this study.

To investigate the effect of the dipolar interactions on the vortex properties dipolar condensate with a single has been studied. The critical angular velocity is dependent of the interaction parameters, such as scattering length and dipole moment, the number of atoms and the trap geometry. In the presence of dipolar interactions, Ω_c changes depending on the trap shape. In an oblate trap, the maximum density reduces with respect to the s-wave condensate, and it is eaiser to nucleate vortex. Therefore, Ω_c decreases in an oblate trap, while it increases in a prolate trap. Ω_m also decreases in a dipolar oblate trap. The critical angular velocity also depends on the trap aspect ratio, γ. Ω_c increaes with decreases γ.

For an off-centered vortex, energy changes with the distance between the vortex and trap center, ρ_0. The kinetic energy and the trap energy decreases with ρ_0, while the dipolar and s-wave energies increase. The total energy of the condensate decreases as the vortex moves to the edge of the condensate. In an oblate trap, the total energy of the dipolar condensate is higher than the s-wave case since dipolar energy is positive. In a prolate trap, the negative dipolar energy causes a smaller total energy compared with s-wave condensate. s-wave interaction is dominant for high scattering lengths. Therefore, as the scattering length increases, the total energies of dipolar and nondipolar cases close each other.

The parameters condensate aspect ratio, κ, and the radial size, R_x, do not appreciably change with ρ_0. The ratio is bigger in the presence of an off-axis vortex since the radial size increases with the scattering length. An other result of

this study that the precession velocity of a displaced vortex is lowered (raised) by dipolar interaction in an oblate (prolate) trap.

Dipolar interactions also effect the superfluid properties of BEC. In Sec.5, the critical velocity of vortex pair formation has been calculated in an oblate trap. The dependence of the cririca velocity on the dipolar interaction strength and vortex separation has been considered. It has been found that the critical velocity decreases both with increasing ε_{dd} and vortex seperation d. However, the ratio between the critical velocity and sound velocity increases in a dipolar BEC.

As a result, the effects of dipolar and s-wave interactions on rotating BEC have been compared. This study can be extended for different types of trap potentials such as optical lattices and different kinds of atoms.

KAYNAKLAR

[1] Gavroglu, K., *Fritz London: A Scientific Biography,* Cambridge University Press, Cambridge, 1995.

[2] Anderson, M. H., Ensher, J. R., Matthews , M. R., C. E. Wieman, Cornell, E. A., Science, **269**, 198, 1995.

[3] Davis, K. B., Mewes, M. O., Andrews, M. R., van Druten, N. J., Durfee, D. S., Kurn, D. M., and Ketterle , W., *Phys. Rev. Lett.,*, **75**, 22, 1995.

[4] Bradley, C. C., Sackett, C. A., Tollett, J. J., and Hulet, R. G., *Phys. Rev. Lett.,* **75**, 9, 1995.

[5] Fried, D. G., Killian, T. C., Willmann, L., Landhuis D., Moss S. C., Kleppner, D. and Greytak, T. J. ,*Phys. Rev. Lett.,* **81**, 3811, 1998.

[6] Modugno, G., Ferrari, G., Roati, G., Brecha, R. J., Simoni, A. and Inguscio, M., *Science,* **294**, 1320, 2001.

[7] Robert, A., Sirjean, O., Browaeys, A., Poupard, J., Nowak, S., Boiron, D. Westbrook, C. I. and Aspect, A., *Science,* **292**, 461, 2001.

[8] Weber, T., Herbig, J., Mark, M., Nagerl, H. C. and Grimm, R., *Science,* **299**, 232, 2003.

[9] Takasu, Y., Maki, K., Komori, K., Takano, T., Honda, K., Kumakura, M., Yabuzaki, T., and Takahashi, Y., *Phys. Rev. Lett.,* **91** , 040404, 2003.

[10] Ketterle, W., and van Druten, N. J., *Advances in Atomic, Molecular, and Optical Physics*, **37**, 181-236, 1996.

[11] Leggett, A., J. *Rev. Mod. Phys.*, **73**, 307, 2001.

[12] Kasamatsu K., Tsubota, M.**,** *Prog. Low Temp. Phys.,* **16**, 351-403, 2008.

[13] Pethick, C., Smith, H., *Bose-Einstein Condensation in Dilute Gases*, Cambridge University Press, Cambridge, 2002.

[14] Greiner, W., Neise, L., Stöcker, H., *Thermodynamics and Statistical Mechanics*, Springer-Verlac, New York, 1987.

[15] Fetter, A*., Rev. Mod. Phys.*, **81**, 647, 2009.

[16] Dalfovo, F., and Giorgini, S., Pitaevskii, L. P., Stringari, S., *Reviews of Modern Physics*, **71**, 3, 1999.

[17] Williams, C. J., Tiesinga, E., and Julienne, P. S., *Phys. Rev.* A, **53**, 4, 1996.

[18] Abraham, E.R. I., McAlexander, W. I., Sackett, C. A., and Hulet, R. G., *Phys. Rev. Lett.,***74**, 8, 1995.

[19] Griesmaier, A., Werner, J., Hensler, S., Stuhler, J. and Pfau, T., *Phys. Rev. Lett.,* **94**, 160401, 2005.

[20] Hensler, S., Werner, J., Griesmaier, A., Schmidt, P. O., Gorlitz, A., Pfau, T., Rzazewski, K. and Giovanazzi, S., *Appl. Phys. ,* **77**, 765, 2003.

[21] Goral, K., Rzazewski, K., and Pfau, T., *Phys. Rev.* A, **61**, 051601, 2000.

[22] Yi, S., and You, L., *Phys. Rev.* A, **61**, 041604, 2000.

[23] Santos, L., Shlyapnikov, G. V., Zoller, P., and Lewenstein, M., *Phys. Rev. Lett.,* **85**, 1791, 2000.

[24] Goral, K., and Santos, L., *Phys. Rev.* A, **66**, 023613, 2002.

[25] Santos, L., and Pfau, T., *Phys. Rev. Lett.,* **96**, 190404, 2006.

[26] Diener, R. B., and Tin-Lun, Ho, *Phys. Rev. Lett.,* **96**,190405, 2006.

[27] Kawaguchi, Y., Saito, H., and Ueda, M., *Phys. Rev. Lett.,* **96**, 080405, 2006.

[28] Cooper, N. R., Rezayi, E. H., and Simon, S. H., *Phys. Rev. Lett.,* **95**, 200402, 2005.

[29] Zhang, J., and Zhai, H., *Phys. Rev. Lett.*. **95**, 200403, 2005.

[30] Giovanazzi S., Gorlitz A. and Pfau T. *Phys. Rev. Lett.,* **89**, 130401, 2002.

[31] Menotti, C., Lewenstein, M., Lahaye, T., and Pfau, T., cond-mat/ arXiv:07113.422v1, 2007.

[32] Lahaye, T., Menotti, C., Santos, L., Lewenstein, M., and Pfau, T. arXiv:0905.0386v1, 2009.

[33] Baranov, M. A., Physics Reports, **464**, 71–111, 2008.

[34] Menotti, C., and Lewenstein, M., arXiv:0711.3406v1, 2007.

[35] Baranov, M. A., Osterloh, K., and Lewenstein, M., *Phys. Rev. Lett.,* **94**, 070404, 2005.

[36] Griesmaier, A., *J. Phys. B: At. Mol. Opt. Phys.*, **40**, R91–R134, 2007.

[37] Yi, S., and You, L., Phys. Rev. A, **63**, 053607, 2001.

[38] O'Dell, D. H. J., Giovanazzi, S., and Eberlein, C., *Phys. Rev. Lett.,* **92**, 250401, 2004.

[39] Eberlein, C., Giovanazzi, S., and O'Dell, D. H. J., *Phys. Rev. Lett. A,* **71**, 033618, 2005.

[40] van Bijnen, R. M. W., Dow, A. J., O'Dell, D. H. J., Parker, N. G., and Martin, A. M., *Phys. Rev. Lett.,* **80**, 033617, 2009.

[41] Morse, P. M., and Feshbach, H., *Methods of Theoretical Physics,* Vol. II, Sec. 10.3, McGraw-Hill, New York, 1953.

[42] Madison, K. W., Chevy, F., Wohlleben, W., and Dalibard, J., *Phys. Rev. Lett.* **84**, 806, 2000.

[43] London, F., *Nature,* **141**, 643, 1938.

[44] Onsager, L., *Nuovo Cimento ,***6**, *Suppl. 2*, 249, 1949.

[45] Feynman, R. P., in *Progress in Low Temperature Physics*, Vol. 1, Chapter 2, North-Holland, Amsterdam, 1955.

[46] Varmchuk, E. J., Gordon, M. J. V., and Packard, R. E., *Phys. Rev. Lett.,* **43**, 3, 1979.

[47] Matthews, M. R., Anderson, B. P., Haljan, P. C., Hall, D. S., Wieman, C. E., and Cornell, E. A., *Phys. Rev. Lett.,* **83**, 2498, 1999.

[48] Anderson, B. P., Haljan, P. C., Wieman, C. E., and Cornell, E. A., *Phys. Rev. Lett.,* **85**, 2857, 2000.

[49] Abo-Shaeer, J. R., Raman, C., Vogels, J. M., and Ketterle, W., *Science,* **292**, 476, 2001.

[50] Hodby, E., Hechenblaikner, C., Hopkins, S. A., Marag`o, O. M., and Foot, C. J., *Phys. Rev. Lett.,* **88**, 010405, 2002.

[51] Raman, C., Abo-Shaeer, J. R., Vogels, J. M., Xu, K., and Ketterle, W., *Phys. Rev. Lett.,* **87**, 210402, 2001.

[52] Anderson, B. P., Haljan, P. C., Regal, C. A., Feder, D. L., Collins, L. A., Clark, C. W., and Cornell, E. A., *Phys. Rev. Lett.,* **86**, 2926, 2001.

[53] Dutton, Z., Budde, M., Slowe, C., and Hau, L. V., *Science,* **293**, 663, 2001.

[54] Inouye, S., Gupta, S., Rosenband, T., Chikkatur, A. P., Gorlitz, A., Gustavson, T. L., Leanhardt, A. E., Pritchard, D. E., and Ketterle, W., *Phys. Rev. Lett.,* **87,** 080402, 2001.

[55] Fetter, A. L., and Svidzinsky, A. A., J. *Phys.: Condens. Matter* **13** R135–R194 , 2001.

[56] Griffin, A., *Excitations in Bose-Condensed Liquid,* Cambridge University Press, New York, 1993.

[57] Griffin, A., Snoke, D. W., and Stringari, S., *Bose–Einstein Condensation,* Cambridge University Press, 1995.

[58] Parker, N. G., Jackson, B., Martin, A. M., and Adams, C. S. arXiv:0704.0146v1

[59] Stringari, S. *Phys. Rev. Lett.*,**77,** 2360, 1996.

[60] Abo-Shaeer, J. R., Raman, C., Vogels, J. M., and Ketterle, W., *Science***, 292**, 476, 2001.

[61] Lundh, E., Martikainen, J. P., and Suominen, K. A., *Phys. Rev. A,* **67**, 063604, 2003.

[62] Parker, N. G. and Adams, C. S., *Phys. Rev. Lett.,* **95**, 145301 (2005)

[63] Williams, J. E., Zaremba, E., Jackson B., Nikuni, T., and Griffin, A., *Phys. Rev. Lett.,* **88**, 070401, 2002.

[64] Dalfovo, F. and Stringari, S., *Phys. Rev. A,* **63**, 011601(R), 2001.

[65] Raman, C., Abo-Shaeer, J. R., Vogels, J. M., Xu, K., and Ketterle, W., *Phys. Rev.Lett.,* **87**, 210402, 2001.

[66] Williams, J. E. , and Holland, M. J., *Nature,* **401**, 568, 1999.

[67] Leanhardt, A. E., Gorlitz, A., Chikkatur, A., Kielpinski, D., Shin Y., Pritchard, D. E., and Ketterle, W. *Phys. Rev. Lett.,* **89**, 190403, 2002.

[68] Ginsberg, N. S., Brand, J., and Hau, L. V. , *Phys. Rev. Lett.,* **94**, 040403, 2005.

[69] Komineas, S., and Papanicolaou, N., *Phys. Rev. A,* **68**, 043617, 2003.

[70] Lundh, E., Pethick, C. J., and Smith, H., *Phys. Rev.* A, **55**, 2126, 1997.

[71] Castin, Y. and Dum, R., *Eur. Phys. J.* D, **7,** 399, 1999.

[72] Wilkin, N. K., Gunn, J. M. F., and Smith, R. A., *Phys. Rev. Lett.,* **80**, 11,1998.

[73] Sinha, S. *Phys. Rev. A,* **55**, 4325, 1997.

[74] Stringari, S., *Phys. Rev. Lett.,* **77**, 2360, 1996.

[75] Ghosh, S., *Phase Transitions*, **77**, 625-676, 2004.

[76] Dalfovo, F., Giorgini, S., Pitaevskii, L. P., and Stringari, S., *Rev. Mod. Phys.* **71**, 463, 1999.

[77] Mathews, M. R., Anderson, B. P., Haljan, P.C., Hall, D.S., Weiman, C. E., and Cornell, E. A., *Phys. Rev. Lett.,* **84**, 2498, 1999.

[78] Bogoliubov, N. N., *J. Phys. (USSR)* **11**, 23 (1947), reprinted in D. Pines, *The*

Many-Body Problem, (W. A. Benjamin, New York, 1961), p. 292.

[79] Steinhauer, J., Ozeri, R., Katz, N., and Davidson, N., *Phys. Rev. Lett.,* **88**, 12, 2002.

[80] Lundh, E., Pethick, C. J., and Smith, H., *Phys. Rev. A,* **55**, 2126, 1997.

[81] Abo-Shaeer, J. R., Raman, C., Vogels, J. M. and Ketterle, W. *Science,* **292**, 476, 2001.

[82] Madison, K. W., Chevy, F., Wohlleben, W., and Dalibard, J., *Phys. Rev. Lett.* **84**, 806, 2000.

[83] Recati, A., Zambelli, F. and Stringari, S. *Phys. Rev. Lett.,* **86**, 377, 2001.

[84] Sinha, S. and Castin, Y., *Phys. Rev. Lett.,* **87,** 190402, 2001.

[85] Madison, K. W., Chevy, F., Bretin, V. and Dalibard, J., *Phys. Rev. Lett.,* **86**, 4443, 2001.

[86] Parker, N. G., and Adams, C. S., *Phys. Rev. Lett.,* **95**, 145301, 2005.

[87] Parker, N. G., and Adams, C. S., *J. Phys. B,* **39**, 43, 2006.

[88] Stringari, S., *Phys. Rev. Lett.,* **77**, 2360, 1996.

[89] Parker, N. G., van Bijnen, R. M. W., and Martin, A. M., *Phys. Rev. A*, **73**, 061603(R), 2006.

[90] Santos, L., Shlyapnikov, G.V., and Lewenstein, M., *Phys. Rev. Lett.,* **90**, 250403, 2003.

[91] Wilson, R. M., Ronen, S., and Bohn, J. L., *Phys. Rev. A,* **79**, 013621, 2009.

[92] Klawunn, M. and Santos, L. *New J. Phys.,* **11**, 055012, 2009.

[93] Klawunn, M., Nath, R., Pedri, P., and Santos, L., *Phys. Rev. Lett.*, **100**, 240403, 2008.

[94] O'Dell, D. H. J., and Eberlein, C. *Phys. Rev.* A, **75**, 013604, 2007.

[95] Abad, M., Guilleumas, M., Mayol, R., Pi, M., and Jezek, D. M., *Phys. Rev.* A, **79**, 063622, 2009.

[96] Yuce, C., and Oztas, Z., *J. Phys. B: At. Mol. Opt. Phys.,* **43**, 135301, 2010.

[97] Yi, S., and Pu, H., *Phys. Rev.* A, **73**, 061602, 2006.

[98] van Bijnen, R. M. W., O'Dell, D. H. J., Parker, N. G., and Martin, A. M., *Phys. Rev. Lett.,* **98**, 150401, 2007.

[99] Giovanazzi S., Gorlitz, A., and Pfau, *T., J. Opt. B*, 5, S208, 2003.

[100] Lundh, E., and Ao, P., *Phys. Rev.* A, **61**, 063612, 2000.

[101] Jackson, B., McCann, J. F., and Adams, C. S., *Phys. Rev.* A, **61**, 013604, 1999.

[102] Zhang, J-N, He, L, Pu, H, Sun, C-P, and Yi, S, *Phys. Rev.* A, **79,** 033615, 2009.

[103] Jackson, B., McCann, J. F., and Adams, C. S., *Phys. Rev. Lett.,* **80,** 3903, 1998.

[104] Raman, C., Kohl, M., Onofrio, R., Durfee, D. S., Kuklewicz, C. E., Hadzibabic, Z., and Ketterle, W. *Phys. Rev. Lett.,* **83**, 2502, 1999.

[105] Onofrio, R., Raman, C., Vogels, J. M., Abo-Shaeer, J., Chikkatur, A. P., and Ketterle, W., *Phys. Rev. Lett.,* **85**, 2228, 2000.

[106] Jackson, B., McCann, J. F., and Adams, C. S., *Phys. Rev. A,* **61**, 051603(R), 2000.

[107] Neely, T. W., Samson, E. C., Bradley, A. S., Davis, M. J., and Anderson, B. P., *Phys. Rev. Lett.*, **104**, 160401, 2010.

[108] Crescimanno, M., Koay, C. G., Peterson, R., Walworth, R., *Phys. Rev. A,* **62**, 063612, 2000.

[109] Landau, L., *J. Phys.* (Moscow), **58**, 71, 1941.

[110] Stiebberger, J. S., and Zwerger, W., *Phys. Rev. A,* **62**, 061601, 2000.

[111] Pavlov, N., *Phys. Rev. A,* **66**, 013610, 2002.

[112] Fetter, A. L., *Phys. Rev. A,* **138**, 429, 1965.

[113] Jones, C. A., Roberts, P. H., *J. Phys. A: Math. Gen.,* **15**, 2599, 1982.

[114] Li, W., Haque, M., and Komineas, S., *Phys. Rev. A,* **77**, 053610, 2008.

[115] Freilich, D. V., Bianchi, D. M., Kaufman, A. M., Langin, T. K., and Hall, D. S., *Science,* **6329**, 1182, 2010.

[116] Pietil, V., Isoshima, T., Huhtamki, J. A. M., and Virtanen, S. M. M., *Phys. Rev. Lett.,* **74**, 023603, 2006.

[117] Mottonen, M., Virtanen, S. M. M., Isoshima, T., Salomaa, M. M. , *Phys. Rev. A,* **71,** 033626, 2005.

[118] Middelkamp, S., Kevrekidis, P. G., Frantzeskakis, D. J., Carretero, G. R., and Schmelcher, P. *Phys. Rev. A,* **82**, 013646, 2010.

[119] Seman, J. A. et al., *Phys. Rev. A,* **82**, 033616, 2010.

[120] Martikainen, J. P., Suominen, K. A., Santos, L., Schulte, T., and Sanpera, A., *Phys. Rev. A,* **64**, 063602, 2001.

[121] Liu, M., Wen, H., Xiong, H. W., and Zhan, M. S., *Phys. Rev. A,* **73**, 063620, 2006.

[122] Geurts, R., Milosevic, M. V., and Peeters, F. M., *Phys. Rev. A,* **78**, 053610, 2008.

[123] Schumayer, D., Hutchinson, D. A. W., *Phys. Rev. A,* **75**, 015601, 2007.

[124] Kuopanportti, P., Huhtamaki, Jukka A. M., and Mottonen, M., *Phys. Rev. A*, **83**, 011603(R), 2011.

[125] Fedichev, P.O., Fischer, U. R., and Recati, A. *Phys. Rev. A,* **68**, 011602, 2003.

[126] Klein, A., Jaksch, D., Zhang, Y., and Bao, W., *Phys. Rev. A,* **76**, 043602, 2007.

[127] Okulov, A. Y., *Laser Physics,* **19**, 8, 2009.

[128] Andrelczyk, G., Brewczyk, M., Dobre, L., Gajda, M., and Lewenstein, M., *Phys. Rev. A,* **64**, 043601, 2001.

[129] Carr, L. D., and Clark, C. W., *Phys. Rev. Lett.,* **97**, 010403, 2006.

[130]Crasovan, L. C., Vekslerchik, V., Perez-Garcia, V. M., Torres, J. P., Mihalache, D. , and Torner, L., *Phys. Rev. A*, **68**, 063609, 2003.

[131] Li, W., Haque, M., and S., Komineas, *Phys. Rev. A,* **77**, 053610, 2008.

[132] Zhou, Q., and Zhai, H., *Phys. Rev. A,* **70**, 043619, 2004.

[133] Lahaye, T., Menotti, C., Santos, L., Lewenstein, M., Pfau, T., *Rep. Prog. Phys.,* **72**, 126401, 2009.

[134] Fetter, A. L., and Svidzinsky, A. A., *J. Phys.: Condens. Matter,* **13**, R135, 2001.